Laser peak power scaling and beam quality improvement with Ytterbium rod-type fiber amplifiers made by powder sinter technology

Dissertation

zur Erlangung des akademischen Grades
doctor rerum naturalium (Dr. rer. nat.)

vorgelegt dem Rat der Physikalisch-Astronomischen Fakultät
der Friedrich-Schiller-Universität Jena

von Yuan Zhu, M.Sc.

geboren am 07.04.1986 in Shanxi, China

Gutachter:

1. Prof. Hartmut Bartelt (Leibniz-Institut für Photonische Technologien)

2. Prof. Dr. Markus Pollnau (Photonics Advanced Technology Institute, University of Surrey)

3. Prof. Carsten Fallnich (Institut für Angewandte Physik)

Tag der Disputation: **05.12.2017**

Contents:

1. Introduction

Lasers have influenced every part of human life and revolutionized many scientific and industrial sections since T.H. Maiman attained laser light in 1960 [1]. Even though all kinds of lasers share several similar principles and features, their specific details, such as power scaling, laser performance, cost, size and so on, determine their specific application range. In comparison with other types of high power solid-state lasers, fiber lasers are the newest entrants in the laser technology arena [2]. In time, fiber lasers have attracted strong attention and experienced rapid development especially in the last 20 years due to their numerous advantages such as good thermal management owing to a large surface to volume ratio, high power efficiency and stability, capability for high average power with superior beam quality, fast turn-on-key operation, low cost and easy beam delivery.

At present, the operation regime of high power fiber lasers, which combines a nanosecond pulse width and a multi-kilohertz repetition rate, is a key for many industrial applications [2, 3], especially for laser material processing such as micromachining, precision marking, and cutting [4]. Many of these processes require high peak power and a diffraction-limited beam quality. The high peak power is required to overcome the material processing threshold, while the diffraction limited beam quality is required to enhance the level of precision and to extend the laser working distance (remote processes).

Even though significant scaling has been achieved of both the peak power and the average power levels with the use of the Yb^{3+}-doped fiber amplifier (YDFA) and the fiber Master Oscillator Power Amplifier (MOPA) concept which can provide well controlled pulses without spikes, there still exists a huge challenge for further power scaling with preservation of the desired pulsed seed laser properties during the amplification process. There exist various unwanted effects which can degrade the spectral, temporal, and spatial fidelities of the signal when scaling up the laser peak power. First of all, the scaling to higher power with standard fiber amplifiers is limited by parasitic nonlinear effects (e.g. Stimulated Raman Scattering (SRS) and Stimulated Brillouin Scattering (SBS)) [2~6] due to the small fiber core, which leads to strong light confinement and long interaction lengths. The second limitation is the fiber facet damage threshold. In practice, the fiber facet damage threshold is proportional to the effective mode diameter and roughly a factor of 2~10 lower than the bulk damage threshold [7, 8]. Therefore, the scaling to larger effective mode areas

is a promising solution to suppress nonlinear effects, to protect the fiber by increasing the material damage threshold and to shorten the required fiber length by enhanced absorption when keeping the rare earth doping level. However, increasing the effective mode area by increasing the fiber core size can severely degrade the fundamental mode (FM) operation and therefore the beam quality due to excitation of higher order modes (HOMs). Fibers with core diameters > 15µm are typically referred to as large mode area (LMA) fibers [9,10] and require well defined small index contrast in order to assure fundamental mode operation.

Several additional techniques have been adopted to maintain single-mode operation in LMA fibers [11-16]. The most common method employs reduction of the core numerical aperture (NA) and coiling of the fiber to strip the high order modes [17, 18] due to bend loss. However, homogeneous fibers with extremely small NA are difficult to fabricate, while fiber bending induces mode distortion and can introduce loss even to the fundamental mode. Other approaches with more elaborate fiber designs based on reduced gain and/or increased losses for HOMs are e.g. based on leakage channel fibers, chirally coupled cores [19], and photonic crystal fibers (PCF) including also large pitch fibers [20]. The latter two have already achieved record high peak powers up to the self-focusing limit (about 4 Megawatt) together with near diffraction limited beam quality [21, 22]. But they are difficult to manufacture due to the elaborate fiber design in combination with tight tolerances and are therefore quite expensive. Additionally, they are more difficult to process (e.g. cutting, splicing, tapering, etc.) especially if they employ an air hole structure.

Consequently, all-solid step-index LMA fibers become an economical and practical option to adopt. Several methods have been proposed to scale the peak power while optimizing the beam quality with all-solid LMA fibers. Cheng and co-workers [23] have achieved 2.4-MW peak power for 4ns pulses at 1064 nm with the use of 200µm core (NA=0.062) Yb-doped fiber amplifiers. They optimized the beam quality from M^2=25 (uncoiled fiber) to M^2=6.5 (properly coiled fiber). Bobkov et al. [24] have used a 2.2m long tapered monolithic fiber amplifier with a mode field area of 1000 μm^2 nearby the output. Over 0.7MW peak power was achieved at 1056nm using 20ps chirped pulses with a diffraction limited quality (M^2 ~ 1.124). All fiber designs discussed above require precise refractive index and homogeneity control, because any significant deviation with feature sizes larger than the wavelength (e.g. middle dips) will result in severe mode field deformations. In the last few years, a new reactive powder sinter technology (REPUSIL) [25~27] has been developed that allows to manufacture LMA fibers with high refractive index accuracy and

homogeneous dopant distribution. So far, this technology has been mainly applied to multimode high power fiber lasers with a continuous wave (CW) power of 4kW [28] or few-moded pulsed amplification in short non-tapered rod-type fibers with peak powers up to 360kW [29].

The objective of this thesis is to investigate such rod type all-solid Yb^{3+}-doped double clad fibers fabricated with the new REPUSIL technology for achieving very high peak power and near diffraction limited beam quality. Two main aspects have been considered such as (1) explore rod-type step-index fibers for power scaling. (2) explore local adiabatic tapers for optimizing the beam quality. The investigated high power fibers arrangement is based on a modulator power amplifiers setup (master oscillator power amplifier system (MOPA)) with a fiber-coupled semiconductor seed laser.

The dissertation is structured as follows: In the first two chapters (Chapter 2 and Chapter 3), the basic theoretical background about pulsed fiber amplifiers and LMA fibers for peak power scaling and beam quality improvement is introduced. The basic technologies for fiber component preparation and the simulation models for fibers and tapers as used in this thesis are introduced in Chapter 4 and Chapter 5, respectively. Chapter 6 is focused on introducing the MOPA system which was built to provide the seed laser beam for the main amplifier stage. The main properties of the designed Yb^{3+}-doped LMA fiber amplifiers are discussed with experimental results in Chapter 7. Finally, the thesis is concluded and a brief outlook is offered.

2. Fundamentals of pulsed laser beam amplification in optical fibers

In this chapter, some basic concepts of pulsed fiber amplifiers are discussed. In the first part, the Ytterbium-doped pulsed fiber amplifier is introduced. Ytterbium dopants for laser amplification are described in the second part and the properties of amplified laser beams are introduced in the third part. Then the Master Oscillator Power Amplifier (MOPA) system consisting of a seed laser and the optical fiber amplifier chain to boost the output power is discussed. A thorough understanding of the basic aspects of pulsed fiber amplifiers is the basis to optimize later the system and fiber design.

2.1 Pulsed fiber amplifier

At present, the operation regime of high power fiber laser system which combines a nanosecond pulse width and multi-kilohertz repetition rate is a crucial key for many industrial applications [2, 3], especially for laser material processing such as micromachining, precision marking and cutting. The most important properties of this pulsed fiber laser beam are typically high peak power and near diffraction-limited beam quality. The high peak power is required to overcome the material processing threshold. The near diffraction-limited beam quality is required to enhance the level of material processing precision and to extend the laser operation distance.

Fiber amplifiers are used to amplify the signal power of a (fiber laser) seed signal. A simple pulsed fiber amplifier therefore consists of a pulsed seeder, an active fiber, and a pump diode connected to the active fiber by a suitable coupler (figure 2.1). The amplifiers adopting doped fibers as active gain media and a pulsed laser beam as seed beam are pulsed fiber amplifiers.

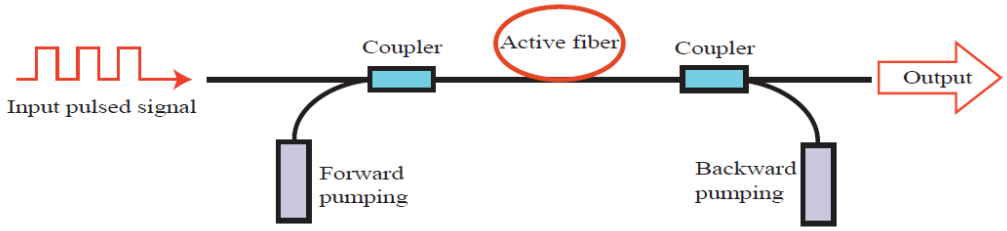

Figure 2.1 A simple pulsed fiber amplifier

As shown in the Figure 2.1, the central section of amplifier is the active fiber which is typically doped with rare earth ions such as Yb^{3+} or Er^{3+}. The active dopants can be pumped with continuous wave (CW) pumping or pulsed pumping. The pulsed pumping shows only advantage if the

repetition rate is lower than the inverse of the upper state lifetime (lifetime of population in excited state) which is a very rare case for fiber amplifiers. The pump laser beam can be injected inside the active fiber with forward pumping, backward pumping or bi-directional pumping which can be used to optimize the pumping efficiency. The peak power of a laser can be scaled up if the signal laser has relatively low repetition rate and short pulse width, provided that the seed power is still sufficient to saturate the amplifier. Then only a few pulses can extract the energy stored by active dopants and achieve quite high peak power at the output.

There exist several limitations for pulsed fiber amplifiers to further scale up the peak power and pulse energy with such a traditional pulsed fiber amplifier. The nonlinear effects (see chapter 3.1.1) [3,6,10] are the dominating limitations for high peak power due to the small active fiber core of a standard fiber amplifier which leads to strong light confinement and due to the long interaction lengths. The amplified spontaneous emission limits the population inversion for the active fiber which decreases the signal gain and leads to noise. The optical damage ultimately limits the peak power and can cause permanent damage of the fiber. Finally, the gain saturation effect which is discussed in chapter 2.3.1 can badly distort the pulse shape of high energy pulses.

2.2 Ytterbium dopants for laser amplification

The active medium which is doped with rare earth ions is the core component of a fiber amplifier and a fiber laser. The active dopants in the active medium can absorb the pump light and excite the atoms to a metastable level, then the stimulated photon emission is triggered by the seed photons which leads to light amplification. The core of an active fiber is usually doped with rare earth ions as active medium for fiber amplification. The figure 2.2 shows the rare-earth ions which are commonly used as active dopants and their possible lasing wavelength region [10].

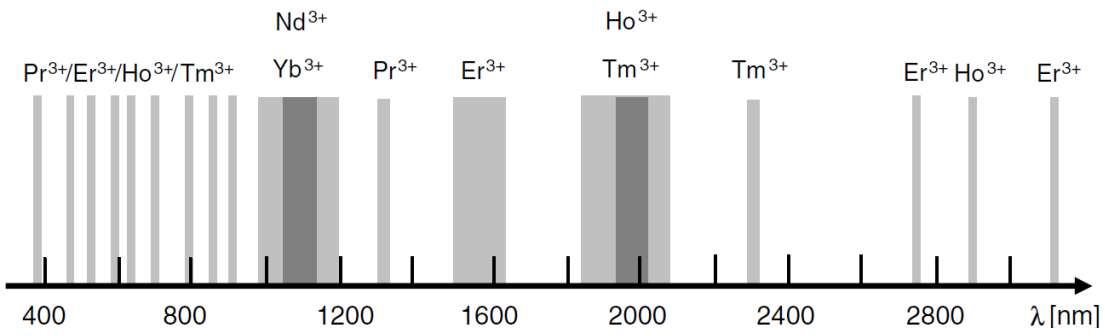

Figure 2.2. Rare earth ions with possible lasing wavelength region [10]

Er^{3+} and Yb^{3+} ions are the most important active dopants for fiber lasers and amplifiers. The Er^{3+} doped fiber laser has some limitations such as excited state absorption and concentration quenching. Therefore, the Er^{3+}-doped fiber laser does not have special advantages for high power fiber amplifiers [30,31]. Ytterbium-doped fibers [32,33] have proven superior properties in the high-power laser technology. They have become the best choice for power scaling due to advantages such as low quantum defect and high saturation fluence allowing high pulse energy. Excited state absorption and concentration quenching by interionic energy transfer do not occur due to Yb^{3+} simple energy level scheme. Yb^{3+} belongs to the lanthanides group and the common host media for Yb^{3+} is silica glass.

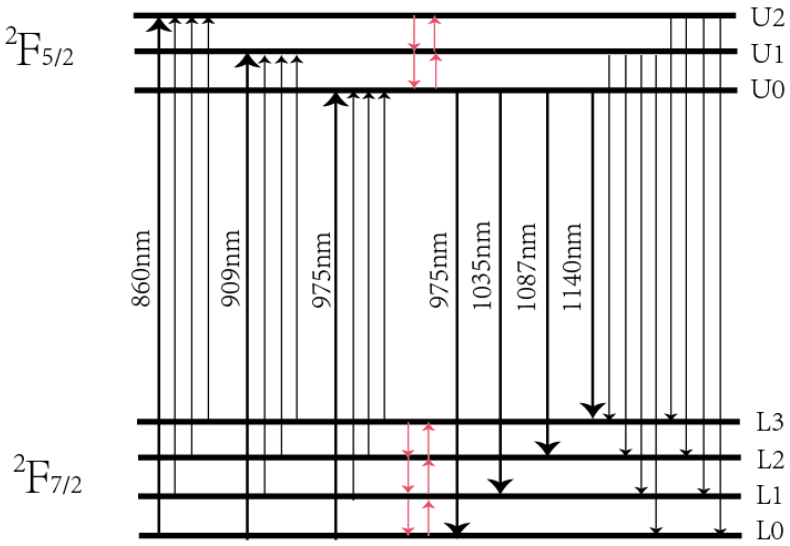

Figure 2.3 Possible photonic transitions of Yb^{3+}-ions in silica

The Figure 2.3 shows possible photonic transitions such as absorption and emission of the Yb^{3+} ions in silica as well as a typical energy level system for the ytterbium ions with sub-level Stark splitting [33,35]. The Yb^{3+}-ions energy-level structure is quite simple, consisting of a ground state $^2F_{7/2}$ with four Stark levels (L_0 L_1 L_2 L_3) as well as an excited state $^2F_{5/2}$ with three Stark levels (U_0 U_1 U_2). Therefore, there is no excited state absorption at pump or signal wavelength. The photon transitions of Yb^{3+}-ions can have several combinations which allow a wide range of pumping schemes (roughly from 860nm to 1064 nm) and a broad spectral emission (roughly from 975nm to 1200 nm) [34]. The bold arrows in absorption and emission parts correspond to pumping and lasing schemes, respectively. Generally, most of the excited atoms stay in U0 and the greatest possibility of lasing emission will occur from U0 into L1, L2 and L3 for Yb^{3+}-doped fibers.

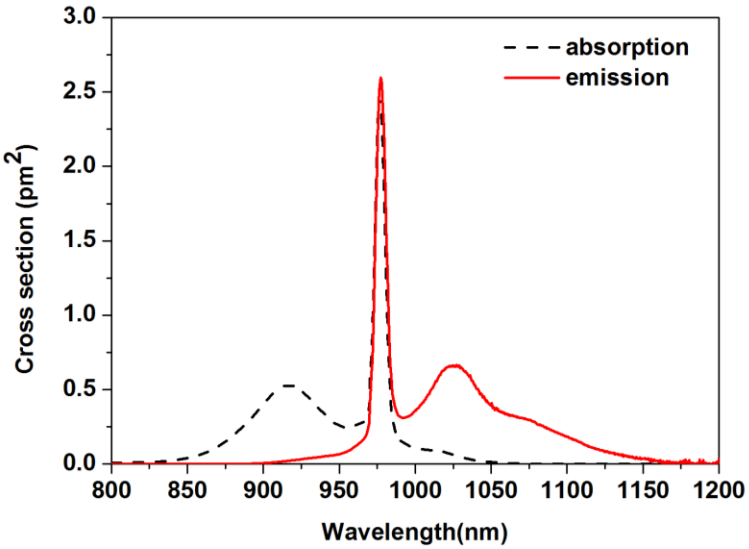

Figure 2.4 Typical emission and absorption cross-sections in ytterbium-doped fibers

The emission and absorption cross sections of a Yb^{3+}- aluminosilicate fiber is shown in Figure 2.4. It should be pointed out that different host glass compositions lead to a variation of the details of the emission and absorption cross-sections [36] and the pump wavelength can influence the emission cross section somehow. The Yb^{3+} shows quite broad absorption and emission spectra. This means that many wavelength options for pumping and lasing are possible. The quantum defect which is the energy difference between pump and laser photons is always small, therefore the potential thermal load is low and the optical to optical efficiency can be quite high for the laser amplification process. The Yb^{3+} has a relatively high energy storage capacity due to the long metastable state lifetime around 1ms. The Yb^{3+} doped active fiber has a relatively high saturation fluence which makes a high pulse energy and high peak power possible. The Yb^{3+}-doped active fiber allows a high doping concentration which can achieve high gain with a short fiber length.

Yb^{3+}-doped active fibers also have some drawbacks. The emission cross section and the absorption cross section of Yb^{3+}-doped fiber is overlapping partially as seen in the figure 2.4. However, the fiber amplifier features a low quantum defect when the pump and lasing wavelengths are quite close to each other. In Yb^{3+}-doped active fibers, some other co-dopants are used to improve the properties of the fiber. For example, Aluminum and Cerium co-dopants can reduce photo-darkening effects. Aluminum can also help to increase the rare-earth doping concentrations without quenching of the upper-state lifetime. Fluorine helps to decrease the refractive index of the fiber core to compensate the refractive index increase due to the Yb^{3+} dopants.

2.3 Amplification of pulsed laser beam

2.3.1 Rate equations and energy gain

The rate equations are a powerful tool to theoretically investigate the characteristics of Yb^{3+}-doped double clad fiber amplifiers. By solving rate equations, the output performance of fiber amplifiers can be analyzed numerically. Energy gain is also an important parameter of a laser amplifier and will be explained in the following.

(1) Rate equations of double clad fiber amplifiers

The schematic diagram of a double clad fiber amplifier with backward pumping is shown in figure 2.5. The fiber amplifier adopts a double-clad structure: the doped middle core is the signal waveguide, inner cladding is the pump waveguide, while the outer cladding has the lowest refractive index to assure light guiding. With this double-clad structure, high pump power can be coupled into the multimode inner cladding easily with low brightness pump light due to the large inner-clad size and the large pump NA. The absorption (or energy gain) exists only in signal core which results in a tremendous brightness enhancement.

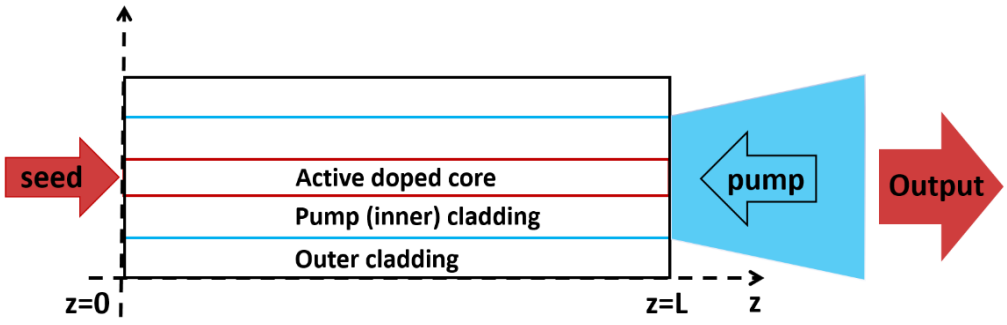

Figure 2.5 Illustration of double clad fiber amplifier with backward pumping

The performance of such a fiber amplifier can be expressed by the following space-dependent and time-independent steady rate equations [37, 38]:

$$\frac{N_2(z)}{N} = \frac{\frac{P_p^-(z)\Gamma_p\sigma_{ap}}{h\nu_p A} + \frac{P_S^+(z)\Gamma_S\sigma_{as}}{h\nu_S A}}{\frac{P_p^-(z)\Gamma_p(\sigma_{ap}+\sigma_{ep})}{h\nu_p A} + \frac{1}{\tau} + \frac{P_S^+(z)\Gamma_S(\sigma_{as}+\sigma_{es})}{h\nu_S A}} \tag{2.1}$$

$$N = N_1(z) + N_2(z) \tag{2.2}$$

$$-\frac{dP_p^-(z)}{dz} = -\Gamma_p\big(\sigma_{ap}N - (\sigma_{ap}+\sigma_{ep})N_2(z)\big)P_p^-(z) - \alpha_p P_p^-(z) \quad (2.3)$$

$$\frac{dP_s^+(z)}{dz} = \Gamma_s\big((\sigma_{as}+\sigma_{es})N_2(z) - \sigma_{as}N\big)P_s^+(z) - \alpha_s P_s^+(z) \quad (2.4)$$

Where N_1 and N_2 are the population densities of the ground state and the excited state, respectively, at the position z. The N is the doping concentration distribution which is assumed to be a constant value along the fiber core. $P_p^-(z)$ are the pump power at the z position in backward direction. $P_s^+(z)$ is the signal power in forward direction. A is the core area while the $A_{pumpclad}$ is the area for pump clad. Γ_p and Γ_s are the pump and signal filling factors. Γ_p can be calculated as $A/A_{pumpclad}$ if the pump power is homogeneously distributed in the pump clad. The Γ_s value depends on the excited modes number and the power distribution. σ_{ap} (σ_{as}) and σ_{ep} (σ_{es}) are the pump (signal) absorption and emission cross-sections, respectively. The parameter h is the planck constant and τ is the spontaneous lifetime of the excited state. The values of α_s and α_p represent loss coefficients of signal and pump light, respectively.

The equation 2.1 describes the population density of ground state N_1 and excited state N_2 at a speciefic position z. Equation 2.3 and equation 2.4 express the pump and signal power evolution along the fiber length. The initial boundary conditions are needed to solve the rate equations which are specified at the beginning and the end of fiber. The following is the boundary setting for a fiber amplifier with counter pumping:

$$P_p^-(L) = P_{p0} \quad (2.5)$$

$$P_s^+(0) = P_{s0} \quad (2.6)$$

Where the L is the fiber length, P_{p0} is the initial pump power and P_{s0} is the initial seed power. This simple model can be used to calculate the gain of a fiber amplifier and estimate the output power. The equation 2.3 and equation 2.4 can be modified to get:

$$P_p^-(z) = \mathrm{P_{p0}e^{(\Gamma_p\sigma_{ap}N_1-\Gamma_p\sigma_{ep}N_2+\alpha_p)(z-L)}} \quad (2.7)$$

$$P_s^+(z) = \mathrm{P_{s0}e^{(\Gamma_s\sigma_{es}N_2-\Gamma_s\sigma_{as}N_1-\alpha_s)z}} \quad (2.8)$$

Then, the pump absorption efficiency η (%) from z=L to z=0 (L is the fiber length) can be calculated

as

$$\eta(\%) = 1 - \frac{P_P^-(0)}{P_P^-(\mathrm{L})} = 1 - \mathrm{e}^{-(\Gamma_\mathrm{p}\sigma_\mathrm{ap}\mathrm{N}_1 - \Gamma_\mathrm{p}\sigma_\mathrm{ep}\mathrm{N}_2 + \alpha_p)\mathrm{L}} = 1 - \mathrm{e}^{-\kappa \mathrm{L}} \tag{2.9}$$

Here η corresponds to the percentage of pump power which is absorbed. κ can be used as pump absorption coefficient to identify the pump absorption whose unit is 1/m.

$$\kappa(\mathrm{m}^{-1}) = \Gamma_\mathrm{p}\sigma_\mathrm{ap}\mathrm{N}_1 - \Gamma_\mathrm{p}\sigma_\mathrm{ep}\mathrm{N}_2 + \alpha_p \tag{2.10}$$

The signal gain coefficient g in units of dB/m for the fiber amplifier can be calculated as

$$\mathrm{g} = \frac{10}{L}\log_{10}\frac{P_S^+(\mathrm{L})}{P_S^+(0)} = \frac{10}{ln10}(\Gamma_\mathrm{s}\sigma_\mathrm{es}\mathrm{N}_2 - \Gamma_\mathrm{s}\sigma_\mathrm{as}\mathrm{N}_1 - \alpha_s) \tag{2.11}$$

(2) Energy gain

In a laser amplifier, the amplification is a process to boost up the optical power at the signal wavelength while the gain is the ability of an amplifier to increase the optical power. The gain is an important characterization parameter to quantify the strength of an amplification process which can be expressed in a logarithm scale, especially for large gain. The unit for this logarithmic gain G is decibels (dB):

$$\mathrm{G} = 10\log_{10}\frac{\mathrm{P_{out}}}{\mathrm{P_{in}}} \tag{2.12}$$

The value of P_{out} is the output power after the amplification and the P_{in} is the input signal power at the beginning. The gain G normally depends on the pump absorption and the capability of energy storage of the active fiber. The stored energy E_{stored} in a fiber amplifier can be given by [39]:

$$\mathrm{E_{stored}} = h\nu_s \mathrm{A}\int_0^L N_2(z)dz \tag{2.13}$$

Here $n_2(z)$ is the population density in excited state at different positions z along the fiber amplifier. L is the fiber length. A is the doped area. $h\nu_s$ is the signal photon energy. The saturation energy is the optical short pulse energy when the gain is decreased to the 1/e-value of the initial small signal gain, especially in the case of a short pulse duration whose pulse duration is shorter than the upper state lifetime. For a fiber amplifier, the saturation energy E_{sat} [39] can be estimated by

$$E_{sat} = P_{sat} \cdot \tau = \frac{A h\nu_s}{\Gamma_s(\sigma_{es}+\sigma_{as})} \quad (2.14)$$

in which, σ_{es} and σ_{as} are the emission and absorption cross sections of the signal, respectively. P_{sat} is the saturation power. τ is the upper state lifetime. Γ_s is the signal filling factor for the active dopant. Saturation energy is an important parameter that determines the maximum pulse energy which is extracted from the stored energy in gain medium. The extractable energy E_{ext} is useful to estimate the difference between the stored energy E_{stored} and the bleach energy $E_{bleach.}$ The bleach energy is the required energy to bleach the signal reabsorption in a fiber (case of gain G = 0dB). The extractable energy can be given by [39]:

$$E_{ext} = E_{stored} - E_{bleach} = h\nu_s A \int_0^L n_2(z)dz - \sigma_{as} N \Gamma_s L E_{sat} \quad (2.15)$$

The equation 3.15 shows that the extractable energy E_{ext} is limited by the saturation energy E_{sat}. However, the extraction of high energy from a fiber amplifier always requires that the fiber amplifier operates beyond the saturation energy. This leads to a pulse-shape distortion for a pulsed fiber amplifier (see figure 2.6). The leading edge of the pulse depletes the inversion and achieves a high gain, while the trailing edge of the pulse does not get enough inversion to deplete and cannot get the same high gain as the leading edge. Hence, the leading edge experiences a higher gain than the trailing edge of the pulses in the pulsed fiber amplifier. For example, a rectangular seed pulse shape will be distorted and will show a very sharp peak in the leading edge region [40,41] as shown in figure 2.6.

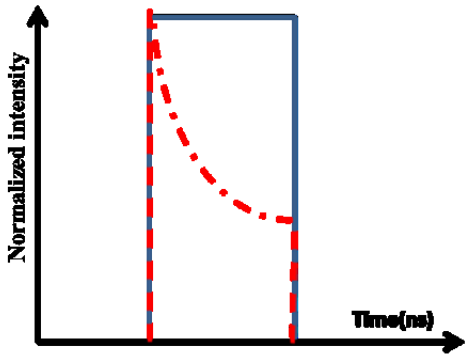

Figure 2.6 Distortion of pulse shape (Blue line: initial pulse shape. Red line: distorted pulse shape)

If the pulse energy is beyond the saturation energy, the gain of the fiber amplifier will generally

decrease to a saturation gain value G_{sat} given as:

$$G_{sat} \sim \frac{G}{e^{\left(\frac{E_P}{E_{sat}}\right)}} \tag{2.16}$$

in which the E_p is the pulse energy and E_{sat} is the pulse saturation energy. G is the normal gain and G_{sat} is the saturation gain of the pulsed fiber amplifier. Due to the energy storage capacity, an Ytterbium-doped pulsed fiber amplifier can achieve a relative high energy extraction.

2.3.2 Peak power and beam quality

The following properties of the laser pulse are very important to characterize the operation regime of a fiber amplifier.

(1) Peak power

Pulsed fiber amplifiers are different from continuous wave (CW) amplifiers. The optical power appears typically in periodical pulses with a certain repetition rate. The pulse shape may vary. In a simple case, the pulses may be described as rectangle shape (see figure 2.7).

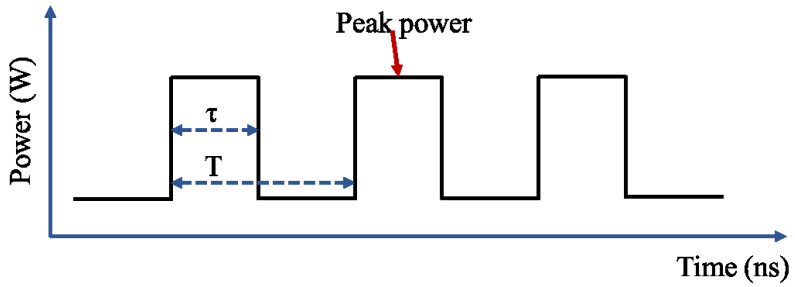

Figure 2.7 Pulsed laser beam signal with rectangle pulse shape

T is the period time and τ is the pulse duration time. If a regular repeating optical pulse with the constant time period T is considered, then the value of repetition rate f is 1/T. For a pulsed fiber laser, the average power and the peak power are two important parameters. The average power P_{ave} is the rate of energy flow which is averaged over one full period T:

$$P_{ave} = \frac{E}{T} = Ef \tag{2.17}$$

Here, E is the pulse energy in one period T. Peak power is the maximum optical power of a pulse. If the pulse format is a perfect rectangle shape, then the theoretical peak power value is

$$P_{peak} = \frac{E}{\tau} \tag{2.18}$$

In combination with the equation 2.17 and the equation 2.18, the following definition can be achieved:

$$P_{peak} * \tau = P_{ave} * T \tag{2.19}$$

If the equation 2.19 is rearranged, a new quantity Duty Cycle (DC) can be defined.

$$DC \equiv \frac{\tau}{T} = \frac{P_{ave}}{P_{peak}} \tag{2.20}$$

The Duty Cycle is the fraction of the time when the pulse is active. The Duty Cycle is related with the pulse peak power P_{peak} and the average output power P_{ave} (see equation 2.20) which ultimately influences the signal strength and the required power supply capacity. The peak power can be expressed by Duty Cycle which is shown as follows:

$$P_{peak} = \frac{P_{ave}}{Duty\ Cycle} = \frac{P_{ave}*T}{\tau} = \frac{P_{ave}}{\tau*f} \tag{2.21}$$

Equation 2.21 shows that the peak power of pulses can be scaled up for the same average output power (P_{ave}) level in case of shorter pulse duration t and smaller repetition rate f.

(2) Beam quality

For fiber lasers and amplifiers, the beam quality is defined by comparison with the ideal diffraction-limited Gaussian beam at the same wavelength. The propagation of a Gaussian beam in a homogeneous medium or in vacuum is show in Figure 2.8.

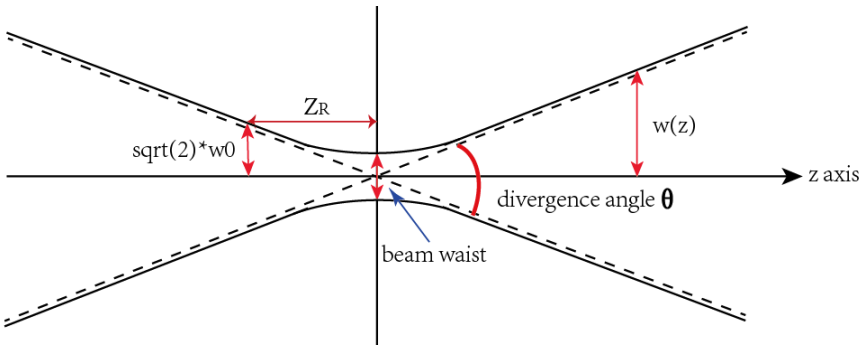

Figure 2.8 The propagation of a Gaussian beam

The complex electric field amplitude of a Gaussian beam in vacuum can be described as follows [42,43]:

$$\mathrm{E(r,z)} = E_0 \frac{w_0}{w(z)} \exp(-\frac{r^2}{w(z)^2}) exp\left(-i\left[kz - arctan\frac{z}{z_R} + \frac{kr^2}{2R(z)}\right]\right) \quad (2.22)$$

$$\mathrm{w(z)} = w_0\sqrt{1 + (z/z_R)^2} \quad (2.23)$$

$$z_R = \frac{\pi w_0^2}{\lambda} \quad (2.24)$$

in which w(z) is the beam radius variation along the propagation direction z. The beam radius w(z) of the Gaussian shape beam is the transverse beam axis value where the optical intensity drops to $1/e^2$ and the electric field strength drops to 1/e (37%). z_R is the Rayleigh length. The laser beam has two important parameters. The first parameter is the beam waist w_0. The beam waist w_0 of a Gaussian beam is the beam radius at the focus (here z=0) where the beam radius is the smallest (or where the intensity on axis is the highest). The second parameter is the beam far-field divergence angle which represents the level of expansion of the laser beam from the beam waist. As shown in Figure 2.8, the beam expands with a certain divergence angle when it propagates far away from the beam waist.

The beam quality of a laser beam is characterized by the M^2 parameter which is normally defined as the ratio between the measured beam parameter product (BPP, product of the beam radius and the far-field beam divergence) and the ideal Gaussian beam BPP for the same wavelength. If the divergence angle θ, the wavelength λ and the beam waist w_0 are known for a specific laser beam, then the M^2 factor can be described as [44]:

$$\mathrm{M^2} = \frac{\pi\theta w_0}{2\lambda} \quad (2.25)$$

The M^2 parameter is very helpful to quantify the degree of deviation of a laser beam from an ideal Gaussian beam. If only the single fundamental mode exists in a step-index fiber, the beam profile is nearly Gaussian shape and the corresponding M^2 value is nearly 1. If many higher order modes exist in a fiber beam, the M^2 value will be larger than 1. This means that for good beam quality higher order modes (HOMs) have to be avoided.

It is important to realize why a diffraction-limited single-mode laser beam is so important for fiber lasers and amplifiers. Generally, several reasons exist: First, a better beam quality means a possible

smallest beam spot size so that this light is much easier to couple into a delivery fiber, especially into a single-mode fiber. Second, a laser beam with good beam quality provides a smaller beam spot size on a working piece providing a better precision for material processing. Third, a laser beam with good beam quality allows a longer working range between the laser source and work piece due to possible beam with small divergence angle (figure 2.9). Fourth, a good beam quality laser beam has good spatial coherence which is important in some special applications, such as laser microscopy or laser interferometers. Fifth, excitation of HOMs can influence and distort the pulse shape for ultra-short pulsed fiber lasers. Therefore, a laser beam which is close to a diffraction-limited Gaussian beam is typically the best choice for many practical applications.

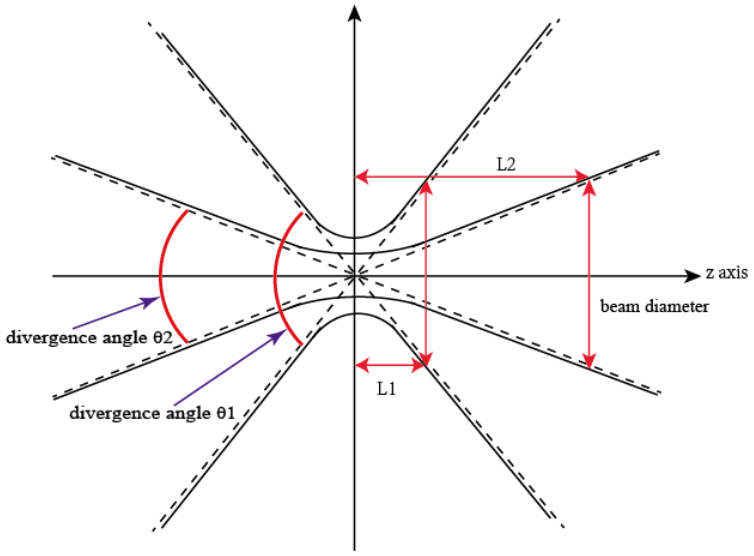

Figure 2.9 Different working range L1 and L2 with different divergence angle θ1 and θ2

The principle for beam quality determination is based on a fitting procedure with the measured the beam profile (i.e. beam diameter) at different positions for a given laser beam [45]. Since the laser beam typically does not have a clear edge, the laser beam diameter at different positions can be determined with several kinds of methods such as D4σ, knife-edge and full-width at half-maximum (FWHM). After several sample points (at least 10 samples) of the laser beam at different positions are measured within the near field and the far field region, the curve is fitted to show the real beam profile due to the measured sample data. Then the beam parameters which include the beam waist diameter, location of the beam waist and far field divergence angle of the laser beam can be known. For non-radially symmetric laser beams, two sets of beam parameters in X and Y axial directions are required. Finally, the beam quality (M^2 value) of laser beam can be derived with equation 2.25.

2.4 Master oscillator power amplifier (MOPA) system

The concept of a MOPA refers to an amplifier chain system which includes a seed laser and several optical amplifier stages to boost the output laser power (see figure 2.10) [2]. The master oscillator fiber amplifier is one special example for a MOPA where the amplifiers are fiber-based. The typical MOPA system is schematically shown in Fig 2.10.

Figure 2.10 Illustration of MOPA with an amplifier chain

Normally a low power laser is adopted as the seed in the MOPA system. Diode lasers are often used as seed laser for a pulsed fiber based MOPA system to provide flexible options for pulse formation and to optimize the spectral properties.

With the use of the fiber-based MOPA system, one can easily combine several fiber amplifiers as an amplifier chain to boost the output power. The significant advantage of the MOPA system is the staging gain. This design can employ different gain active fibers for different amplifier stages which can help to optimize the efficiency, minimize the non-linear effect and mitigate the Amplified Stimulated Emission (ASE) effect. Not all optical components must sustain the highest power levels which decreases the requirements for the optical components.

There are also some challenges with the use of fiber-based MOPA systems. The system is quite sensitive to back-reflections which can easily destroy the system. More components to avoid backwards travelling laser lights (e.g. isolators) increase the loss and the cost of the system. Due to the small core size of the fiber, it is easy to cause various kinds of nonlinear effects (see chapter 3.1.1) which make it difficult to achieve high peak power and to modify the optical spectrum.

In this research work, a three-stage MOPA system is investigated which is discussed in chapter 6. The two pre-amplifier stages boost the pulsed seed laser up to the limits of a standard single mode fiber amplifier according to the SRS limits which is discussed in chapter 3. Then the third amplifier stage is used to scale up the peak power to several hundred kilowatts level with use of a large mode area fiber.

3. Peak power scaling and beam quality improvement with Large Mode Area (LMA) fibers

Generally, the power scaling up of standard fiber amplifiers is limited by parasitic nonlinear effects due to the small fiber core diameter which leads to strong light confinement and long interaction lengths. Therefore, scaling up the fiber effective mode area is a promising solution to suppress the non-linear effect and to shorten the fiber length when keeping the rare earth doping level. In the following the main physical limitations affecting peak power scaling and beam quality improvement are identified. The concepts of using LMA fibers for peak power scaling and beam quality improvement are discussed in detail. The concepts of adiabatic taper and confined doping to improve the beam quality are specially introduced.

3.1 Physical limitations of pulse amplification

This section provides an overview of the physical limitations which must be considered to design the active LMA fiber to scale up the peak power and keep the beam quality for a pulsed LMA fiber amplifier. The key physical limitations such as non-linear effects, damage threshold and amplified spontaneous emission (ASE), are discussed.

3.1.1 Non-linear effects

Nonlinear effects are the dominant limitation for the performance of pulsed fiber amplifiers and lasers. This situation is the direct result of the strong confinement in the small guiding core and the long interaction length of fibers. Non-linear effects, i.e. optical phenomena involving a nonlinear response of the optical medium to intense laser radiation, are varied and can be summarized as follows [6,43]:

$$\mathrm{P(t)} = \varepsilon_0 \chi^{(1)} E(t) + \varepsilon_0 \chi^{(2)} E^2(t) + \varepsilon_0 \chi^{(3)} E^3(t) + \cdots \qquad (3.1)$$

The polarization density P(t) represents the power series of the medium under the influence of the applied electric field E(t). ε_0 is the electric permittivity of free space. The coefficients $\chi^{(n)}$ are the nth-order susceptibilities of the medium. $\chi^{(1)}$ is the linear susceptibility of the medium. $\chi^{(2)}$ is the second susceptibility of the medium which relates to effects such as frequency doubling, difference frequency generation and parametric amplification. These quadratic effects require a non-centrosymmetric medium which is typically not applicable in optical fibers based on silica glass. $\chi^{(3)}$ is the cubic component in the field and gives rise to some parametric nonlinear effects such as

Kerr effect, Stimulated Raman Scattering (SRS), Stimulated Brillouin Scattering (SBS), self-focusing, self-phase modulation, cross-phase modulation and four-wave mixing [6,43]. The non-linear effects, especially the cubic nonlinearity, have a strong effect for high power fiber lasers and amplifiers.

(1) Stimulated Raman scattering (SRS)

Stimulated Raman scattering (SRS) is an important inelastic nonlinear scattering process which can transfer a fraction of power from one wavelength region to a longer wavelength region. It can be described as the interaction between the laser beam and laser-induced vibrations associated with intramolecular bonds [47~49]. SRS is usually the dominant nonlinear effect for pulsed fiber amplifiers operating in the nanosecond region. The SRS effect was discovered by Raman in 1928 [47]. For high power fiber amplifiers, the SRS effect can transfer most of the laser power to longer wavelengths, decreasing the efficiency and introducing new spectral components that are not supported by the optical system. The threshold power P_{SRS} of SRS is described as follows [48]:

$$P_{SRS} = \frac{C_{direction} A_{eff}}{g_R L_{eff}} = \frac{\pi C_{direction}}{4 g_R} \cdot \frac{MFD^2}{L_{eff}} \tag{3.2}$$

Where g_R is the Raman gain coefficient which is typically in order of 10^{-13}m/W for silica glass. $C_{direction}$ is a constant value which depends on the propagation direction of the Stokes power, i.e. $C_{direction}$ is 16 for forward SRS and 20 for backward SRS. L_{eff} is the effective length of the fiber. A_{eff} is the effective mode area of the fiber and MFD is the effective mode field diameter of fiber.

(2) Stimulated Brillouin scattering (SBS)

Stimulated Brillouin scattering (SBS) is another inelastic nonlinear scattering process that exchanges energy between incident photons and acoustic phonons in the glass lattice [6,50,51]. SBS is normally encountered in amplifiers and lasers with narrow band signals. The threshold power P_{SBS} for SBS is shown as follows [6]:

$$P_{SBS} = \frac{21\pi}{4 g_B} \cdot \frac{MFD^2}{L_{eff}} \tag{3.3}$$

where g_B is Brillouin gain coefficient which is typically in order of 5×10^{-11}m/W for silica glass. The SBS threshold power increases significantly for broad-band signals.

(3) Self-focusing

Self-focusing is an important non-linear effect which is induced by the change of the material refractive index under high optical intensity. The medium whose refractive index is modified acts as a focusing lens [7,52,53]. The laser light will be focused on the axis with decreasing beam area and increasing intensity. This phenomenon typically continues until the medium damage interrupts this process. Such effect occurs when the optical power is higher than the critical power P_{self} [52]:

$$P_{self} = \frac{1.8362*\lambda^2}{4\pi n_0 n_2} \tag{3.4}$$

Where n_0 is the refractive index of the core material, n_2 is the nonlinear index and λ is the wavelength. Interestingly, self-focusing does not depend on the modefield and can therefore not be overcome by the fiber design. For silica fibers, the critical peak power of a pulsed laser due to the self-fousing is approximately 4MW around 1000nm wavelength.

3.1.2 Laser induced damage

The typical laser induced damage mechanism for continuous-wave lasers is chemical degradation of the active fiber which can cause severe damage of the fiber end-facet, when the material is overheated. For nanosecond pulses, the dielectric breakdown is the main reason [8,54~56]. The thermal effects also might occur for high pulse repetition rates.

Laser induced damage can happen not only on a bulk piece of the material, but also on the material surface. Normally the laser induced damage threshold for a material surface is lower than for the bulk material due to the high electric fields at the interface. Also, the material surface has usually more microscopic defects and impurities than bulk material. Tiny defects and impurities can reduce the laser induced facet damage threshold considerably. In order to increase the laser induced facet damage threshold and to protect the fiber amplifier, several methods can be considered: 1) Use an endcap to enlarge the beam size and decrease the power density at the interface [57,58]. 2) Well-cleaved end facet or well-polished end facet. 3) Avoiding dust on the fiber facet.

Regarding dielectric breakdown due to the high peak power density, many investigations have been done to estimate laser induced damage threshold in different pulse duration regimes [8,56]. For normal short pulse duration τ between about 0.01ns and 10ns, the laser induced damage threshold expressed as peak power density PD_{peak} is proportional to $\tau^{-1/2}$ MFD^{-1} where the τ is the pulse

duration and MFD is the effective mode field diameter [8]. Then the maximum peak power P_{max} below the dielectric breakdown for pulsed fiber lasers and amplifiers has a relationship with MFD and pulse duration according to:

$$P_{max} \propto \frac{MFD}{\sqrt{\tau}} \tag{3.5}$$

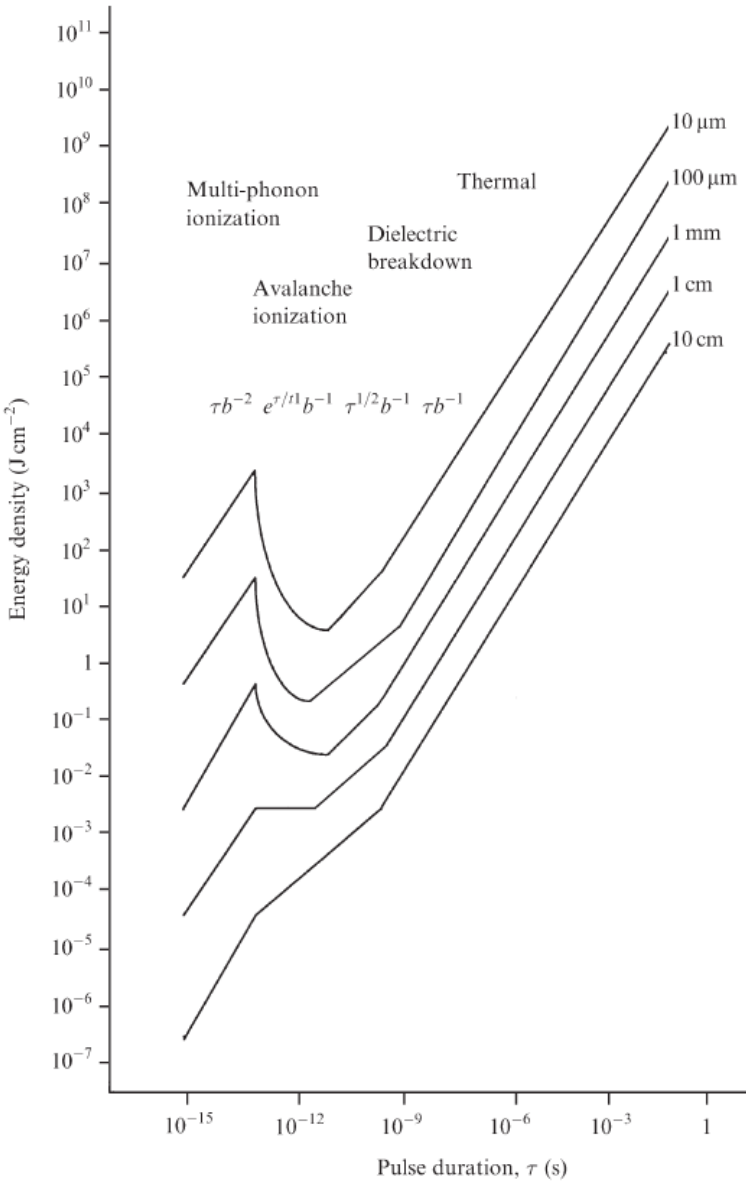

Figure 3.1 Laser induced damage threshold with different pulse durations and spot diameters at 1064nm wavelength for fused silica (b is mode field diameter) [8]

The figure 3.1 shows the critical energy density as a function of the pulse duration and spot diameter for fused silica.

3.1.3 Other limitations

(1) Amplified spontaneous emission (ASE)

In a fiber amplifier, the ions in excited states can spontaneously decay to the ground states or to some intermediate energy levels, releasing photons in random direction. A part of these photos can be captured by the fiber core and can propagate along the fiber in both directions. When the active fiber is pumped, the spontaneous emission light can be significantly amplified due to similar gain as the real signal [59]. This process is called amplified spontaneous emission (ASE).

Typically, the ASE is an unwanted phenomenon. The ASE can deplete the energy which is stored in the excited ions and can limit the extractable energy for signal generation. Especially for pulsed fiber amplifiers with low repetition rate, the ASE can degrade the pulse energy and pulse contrast, and can decrease the pump efficiency. Especially for fiber amplifiers, the ASE can also provide a broadband noise to the amplified signal [60].

Furthermore, the ASE can propagate in forward and backward direction. Especially the backward propagation ASE can be harmful for components in an amplifier system and can even be dangerous for the whole MOPA system. As the ASE is in general an unavoidable amplifier noise, some methods can be applied to minimize it. For example, (1) Spectral filtering devices can selectively transmit or reflect (or absorb) the light with different wavelengths in the optical path. Therefore, the ASE in different wavelengths compared to the signal light can be effectively filtered out by spectral filtering devices. (2) Temporal filtering devices can be used to control the spatial direction of a laser light and to “clean up” the ASE. For example, an Acousto-optic Modulator (AOM) gate based on the acousto-optic effect can periodically transmit or diffract the light with certain frequencies. For a pulsed fiber amplifier, the ASE among pulse intervals can be effectively filtered out by such an AOM gate.

(2) Photodarkening (PD)

Photodarkening is a phenomenon where the transmission losses due to induced absorption increase with time [61]. The mechanism of photodarkening is due to the formation of color centers with holes or electrons due to missing atoms in a fiber glass network structure [62]. The color centers are a damage which can absorb the pump and the signal light. Therefore, the power conversion efficiency of a fiber amplifier is reduced and excess heat is generated in the fiber. Due to

photodarkening, the Yb^{3+}-doped active fibers can suffer severe transmission losses in the 1µm spectral range. The photodarkening effect is more obvious when the fiber has a high Yb^{3+}-doping concentration and ion clusters are formed.

Several methods have been proposed to avoid photodarkening in a Yb^{3+}-doped fiber. It has been shown that heating of the fiber [63] or the irradiation of the fiber with ultraviolet light [64] can help to reverse the photodarkening effect. The Yb^{3+}-doped active fiber which has been co-doped with aluminum and phosphorus shows a photodarkening effect at a much lower level [65]. Also the co-doping with cerium can help to prevent photodarkening in Yb^{3+}-doped active fibers [66]. The figure 3.2 shows the mechanism of Ce^{3+}-ions for reduction of photodarkening which is attributed to their different valence states to trap the holes(h^-) and electrons(e^-).

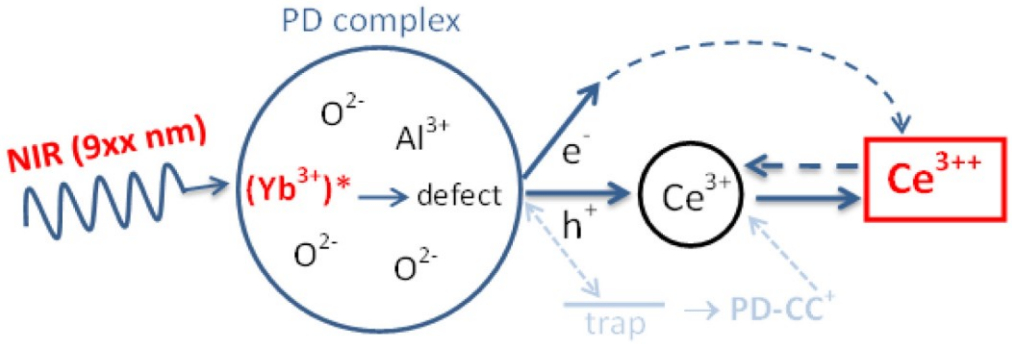

Figure 3.2 Schematic diagram of photo darkening inhibition in Yb^{3+} and Al^{3+} doped fibers with the use of Ce^{3+} co-doping (* means the excitation state of the Yb^{3+} ion, PD-CC^+ means a hole-related photo darkening color center) [66].

(3) Thermal effect

Even though fibers have an excellent performance to dissipate heat due to their large surface to volume ratio, a fiber can also be burned because of overheating, especially for high power applications. The best experimental results with high optical-to-optical conversion efficiency for Yb^{3+}-doped fiber lasers achieved 1.36kW continuous-wave output power with 83% slope efficiency [67]. Some amount of power at least will therefore be converted into heat, e.g. due to the quantum defect. Many scientific researchers have reviewed the thermal limits for power scaling of fiber lasers in detail [68~70]. In order to improve the heat dissipation in fiber lasers and amplifiers, cooling concepts, such as use of a metal holder, water cooling and fan cooling, can be adopted to efficiently remove excess heat from the fiber and to decrease the temperature of fiber.

3.2 Concepts for large mode area (LMA) fibers

Typically, fibers with a core diameter larger than 15μm are called large mode area (LMA) fibers [10] while fibers with core diameters > 50μm are typically referred to as very large mode area fibers (VLMA) [9]. For high power fiber amplification, the LMA fiber amplifier can effectively decrease nonlinear effects and can increase the damage threshold due to the reduction of the local power intensity (see chapter 3.1.2). The magnitude of signal distortions which is induced by nonlinear effects significantly decreases when compared to a standard single mode fiber amplifier with small core radius. For a double-clad fiber amplifier (see chapter 2.3.1) which has different waveguide structures for signal and pump laser light, the large core design also means a possibility of high average output power (or high peak power) and an optimization of the cladding pump absorption. The LMA fibers with a certain doping level allow the adoption of a relative short fiber length and provides also a higher energy storage capacity. At the same time, the short fiber design is helpful to suppress non-linear effects.

However, increasing the fiber core can also severely degrade the fundamental mode (FM) operation due to excitation of higher order modes (HOMs) which are the guided transverse modes of a multi-mode fiber except the FM itself. A straightforward method to design a single or few-modes fiber amplifier is to decrease the Numerical Aperture (NA) as part of the V parameter equation 3.6 and mode number M equation 3.7 as follows:

$$V = \frac{2\pi}{\lambda} r_{core}\, NA = \frac{2\pi}{\lambda} r_{core} \sqrt{n_{core}^2 - n_{cladding}^2} \tag{3.6}$$

$$M \approx \frac{V^2}{2} = 2\left(\frac{\pi r_{core}}{\lambda}\right)^2 \left(n_{core}^2 - n_{cladding}^2\right) \tag{3.7}$$

where r_{core} is the core radius, λ is the wavelength, and n_{core} and $n_{cladding}$ are the refractive indices of the core and cladding, respectively. The equation 3.7 can approximately estimate the supported number of modes M of a step-index fiber. A step-index fiber supports only the FM if the V parameter is smaller than 2.405. A LMA fiber with a large core radius value increases the V parameter proportionally to the core radius. Therefore, the number of modes M which can be supported in fiber, seriously increases with larger core radius fiber (see equation 3.7). The reduction of the core NA value, which means decreasing the refractive index difference between core and cladding for step index LMA fiber, can reduce the V parameter and achieve a single mode operation in a LMA fiber. However, there are several technological limitations for reducing the core NA: 1)

The precision of the refraction index control is practically limited to a value in the order of $5 \cdot 10^{-4}$ depending on the employed fiber technology [71,72]. Therefore, it is quite difficult to fabricate a fiber with NA values smaller than 0.06 [73]. 2) With the standard chemical vapor deposition methods, it is difficult to keep the refractive index of LMA fiber homogeneous with small core NA. 3) A fiber with very small NA is very sensitive to environmental disturbance such as fiber bending and flaws. The guidance of the fiber may be so weak that the loss of the fiber can significantly increase.

Several special techniques [74~89] have been proposed to maintain single-mode operation in LMA fibers while scaling up the output power based on reduced gain and/or increased losses for HOMs. Some of these important solutions are listed in the following section.

(1) Coiled multimode step-index fiber

For fibers with a limited number of HOMs, the HOMs may be stripped (i.e. coupled out of the core and possibly absorbed) by coiling the fiber and making use of the different modal bending loss [17]. Generally, the bending loss of the FM is smaller than that of HOMs. An optimum coiling radius can be chosen which provides high loss for HOM while keeping the loss of FM at a low level. However, fiber bending also induces mode distortions to the FM [18].

(2) Gain-guided index anti-guided fiber (GG IAG)

A gain-guided index anti-guided fiber is an optical fiber whose refractive index of the core is lower than that of the surrounding cladding [74]. Such kind of fiber cannot support the conventional index-guided modes, because the total internal reflection effect at the core–cladding interface will not occur and power can severely leak out of the fiber core. Only some small trapping can occur by grazing angle reflection. In principle, for the GG IAG fiber proposed first by A.E.Siegman [74], the loss of the fundamental mode light which leaks out of the core into the cladding, can be compensated by the amplification of the signal with a very large gain in the fiber core. Therefore, the fiber core size can be enlarged to over 100μm while still allowing single-mode operation.

Single-mode laser action with near Gaussian beam quality (M^2:1.2~1.5) in a Nd^{3+}-doped phosphate glass GG IAG fiber with 200um core diameter has been already demonstrated [11]. However, the GG IAG fiber has poor pump efficiency due to the large leaking loss of the pump light in the core. For side-coupling of the pump light, it is difficult to couple the pump light into the pump cladding

as well as inside the core due to the negative refractive index profile. For end-coupling of the pump light, the pump light will propagate out of the core, since there is no guiding effect for the pump light in the fiber core.

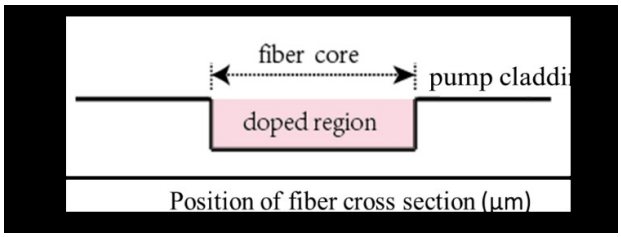

Figure 3.3 Refractive index profile of a GG IAG fiber

(3) Chirally coupled core fiber (CCC)

A CCC fiber [14,19] has a straight central core while one or several helical satellite cores with high loss wrap around the central core (see figure 3.4). The principle of a CCC fiber is to selectively couple the HOMs from fiber core into the satellite cores (or cladding) with high attenuation there, while maintaining the FM with a practically negligible loss by selecting suitable side-helix parameters. Therefore, the FM can propagate inside the central core while the HOMs suffer high losses by modal coupling and bend loss. Consequently, robust single-mode output in such CCC fiber with large core size can be realized.

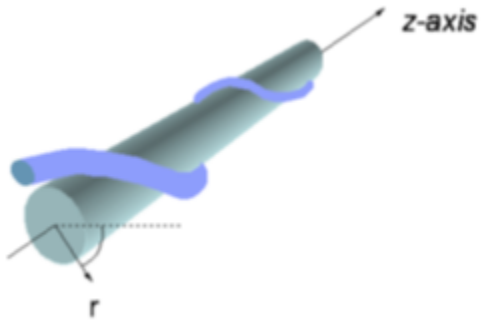

Figure 3.4 Structure of a CCC fiber [14]

(4) Photonic crystal fibers (PCF)

A PCF is a micro-structured fiber type with a center core which can be solid, liquid or gaseous, and a periodic array of structures in the cladding to confine the light. Different guiding mechanisms are possible, including effective index guiding (Figure 3.5) and Photonic Bandgap Guiding (PBG). The geometrical structure of a PCF employing effective index guiding can allow a flexible control of

the effective cladding index and can achieve a core NA such as 0.02 which permits FM propagation even in LMA fibers. The pump light can also be confined in the pump cladding with a dense hollow channel array (air clad) around the pump cladding region..

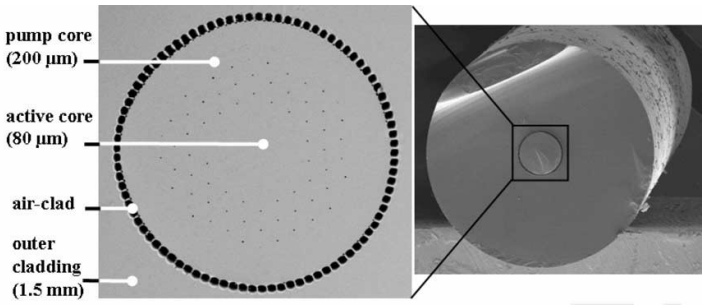

Figure 3.5 Cross section of rod type PCF [75]

Such PCF types achieved already record high peak powers up to the self-focusing limit (4 Megawatt) together with near diffraction limited beam quality [21,75]. But PCFs are difficult to manufacture due to the elaborate fiber design in combination with tight tolerances and therefore they are quite expensive. Additionally, they are more difficult to process (e.g. cutting, splicing, tapering, etc.) especially if they employ an air hole structure.

(5) Large pitch fiber (LPF)

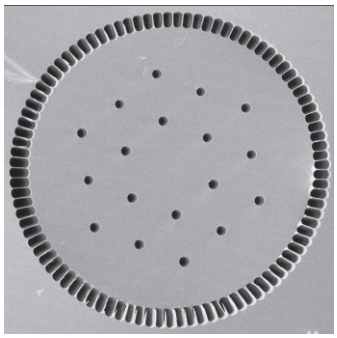

Figure 3.6 Cross section of LPF [76]

Large pitch fiber is a fiber type concept for single-mode operation by exploiting the delocalization concept [76,77]. The principle of the LPF is the delocalization of HOMs with use of a photonic structure which consists of a few hexagonally arranged air holes and large hole-to-hole distances [77]. The delocalization of HOMs in LPF helps to intrinsically improve the seed coupling, to get a preferred gain effect, and finally to achieve a robust single-mode operation in LMA fiber lasers and

amplifiers. The LPF has an excellent scalability by varying the hole-to-hole distance due to its non-resonant approach. Therefore, the delocalization effect of HOMs is maintained while the structure as well as the modal shape are scaled appropriately.

(6) Leakage channel fiber (LCF)

Leakage channel fibers make use of leakage channels between a few holes (leakage channels) around a solid core [20,78]. All modes in a LCF suffer a loss due to destruction of total internal reflection (TIR) induced by the holes, but a proper arrangement and design of the leakage channel (hollow holes) can achieve that the FM has low and negligible loss while the other HOMs suffer high losses. Even though the LCF is similar to the PCF, the LCF lacks of the repeated periodic structure and is therefore different from the concept of the PCF [20].

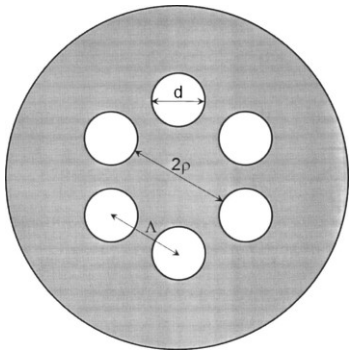

Figure 3.7 Cross section of LCF [20]

3.3 Concepts to improve the beam quality relevant for this work

3.3.1 Adiabatic taper

Step-index LMA fibers may support many HOMs to propagate together with the FM which badly degrades the achievable beam quality. It is known that the seed launching condition in fibers and in high power fiber amplifiers can decide how many HOMs are excited [90,91]. Therefore, optimization of the seed launching condition can help to achieve quasi single-mode performance with LMA fibers for high power amplification. An elegant proposal to solve the delicate mode launching problem is to use an adiabatic taper [92] to launch the FM in a multimode fiber as shown in figure 3.8. The LMA is tapered down at one end to ideally single-mode dimension. Then the taper waist in single mode region is directly spliced to a single mode fiber which is used to deliver the seed light. The single mode seed light is coupled from the delivery single mode fiber to the

LMA fiber with use of a local adiabatic short taper. Then the FM can smoothly evolve and expand without exciting other HOMs. The essence of this approach is utilizing of the local adiabatic short taper to provide a monolithic signal path and selectively excite the fundamental mode in a highly multimode fiber [86].

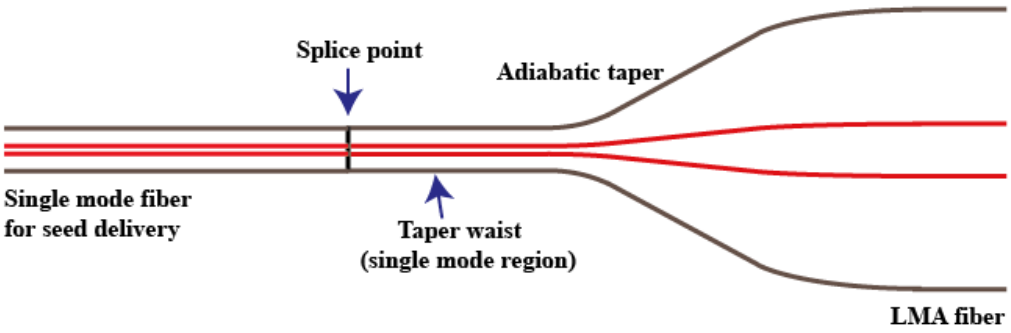

Figure 3.8 Seed coupling with adiabatic taper

Bobkov et al. [24] have adopted a 2.2m long tapered monolithic fiber amplifier and achieved over 0.7MW peak power in the quasi-single-mode regime using 20ps chirped pulses. This kind of long tapers are produced during the fiber drawing process with variation of the fiber drawing condition. However, it is difficult to produce such kind of long tapers with a LMA fiber. The LMA fiber with large outer diameter cannot be coiled or bended and the produced LMA fiber length is limited by the space of the fiber drawing tower which is normally shorter than 3m. Therefore, there is not enough space to produce long tapered LMA fibers. It is also difficult to precisely control the fiber drawing condition to achieve the long tapers with homogeneous shape and smooth geometry variation. The adiabatic taper shown in figure 3.8 is a local short taper which is normally shorter than 8cm due to the limitation of tapering device (i.e. Vytran GPX 3200 splicing system) and is much easier to handle and produce.

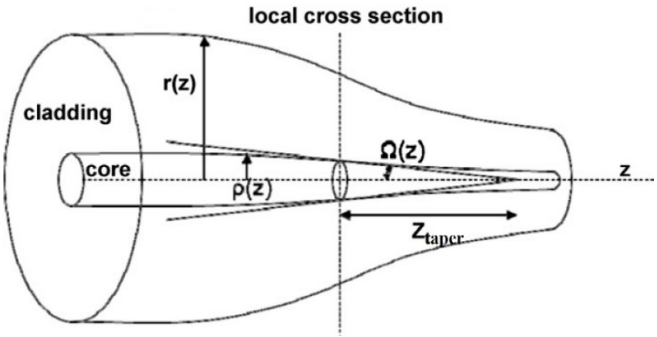

Figure 3.9 Schematic graphic of local short taper transition [93]

A taper can be called adiabatic if the taper geometry varies slowly enough everywhere that the power coupling between FM and the other HOMs can be neglected when propagating along the taper [93,94]. One important criteria to judge if the taper is adiabatic or not is the length scale criterion which is shown as follows [93]. According to the figure 3.9, the local taper length scale (z_{taper}) at different taper position z can be given:

$$Z_{taper}(z) = \frac{\rho(z)}{tan\Omega(z)} \tag{3.8}$$

Where the Ω(z) is the local taper angle and ρ(z) is the local fiber core radius at different positions z along the taper. The beat length (z_{beat}) is the local coupling length between FM and the other HOMs,

$$Z_{beat}(z) = \frac{2\pi}{\beta_{FM}(z) - \beta_{HOM}(z)} \tag{3.9}$$

Where the β_{FM} (z) and β_{HOM}(z) are local propagation constants of the FM and the other HOMs at different taper position z according to the local taper geometry. Theoretically, if no power coupling happens between FM and HOMs along the taper, the beat length (Z_{beat}) between FM and the other HOMs should be smaller than the local taper length scale (Z_{taper}) at different taper position z along the taper length

$$Z_{beat}(z) < Z_{taper}(z) \tag{3.10}$$

By calculation of equations (3.8), (3.9) and (3.10), the allowed local taper angle is given as:

$$\left|\frac{d\rho(z)}{dz}\right| = tan\Omega(z) < \frac{\rho(z)(\beta_{FM}(z) - \beta_{HOM}(z))}{2\pi} \tag{3.11}$$

If the condition 3.11 is satisfied, the taper will have a small local angle and the taper length is long enough to have negligible loss of the FM. In this case, the diameter of the taper varies so slowly that power coupling along the taper transition length is avoided.

3.3.2 Confined doping

Confined doping is a method by employing a special radial gain profile to discriminate the gain of different modes. By this way, the active dopants are distributed in part of the fiber core in order to provide a good overlap with the desired fundamental mode but a significantly lower overlap with undesired modes. In general, the FM profile has the largest overlap ratio with the active dopant

profile while the HOMs have a small overlap. Then the FM can have a large gain while the gain of HOMs is suppressed to improve the beam quality of the signal. A detailed calculation and analysis is shown in chapter 8.

Recently confining the active ion doping area has attracted much attention to favor the FM by preferential gain [95~101]. In particular, the LMA fiber can have a radially controlled distribution of the active ion concentration and possibly of the refractive index profile with the use of REPSUL technology which overcomes the limitation of the traditional doped fiber manufacturing technologies.

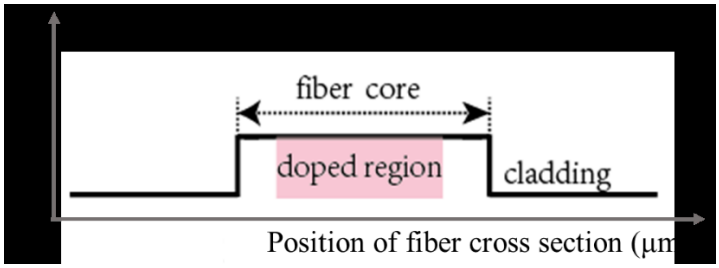

Figure3.11 Refractive index profile of confined doping fiber with partially doped core

The normal step-index LMA fiber can support the FM and many other HOMs. The mode profile of the FM features a nearly Gaussian profile with the highest amplitude in the center and a gradually decaying field along the fiber radius. At the same time, the amplitude profile of other HOMs can be divided into two cases: First, the amplitude peak of some HOMs (i.e. LP11, LP21, et al) is on the edge and not in the center. Second, some HOMs (i.e. LP02, LP03, et al) amplitude peak is in the center, but they have one or more sub-peaks outside the center which can distract power from the center. Therefore, confining the active dopants within the smaller part in the center of the fiber core can lead to modal discrimination, i.e. the FM has a better overlap with the gain region than the other HOMs. Consequently, the FM dominates the output power and the beam quality is improved. This technology is normally called confined doping or gain-filtering method.

Up to now, several groups have done theoretical investigations for the spatial distribution of the dopants in LMA fibers [95~99]. Mali Gong et al [99] have built up a numerical model to study the transverse mode competition under various conditions for confined doped fibers. Based on the numerical algorithm, individual transverse mode power distributions of output are simulated which demonstrate that the partially doped active LMA fiber can really suppress the HOM gain. John R.

Marciante et al [100] have also done numerical simulations with up to 100-μm-diameter core fibers. The results show that gain filtering is quite robust and can provide 99% of the output power in the fundamental mode output. The authors also find that most of the output power can be in the FM even with poor seed launch.

Although there are many promising numerical calculation results which show that the confined doping can really help to discriminate the gain between FM and HOMs, very few papers have shown the successful usage of this gain filtering method in an experiment. Up to now, the largest core diameter used in an experiment is 41 μm with an actively doped area diameter of 27μm. The output beam quality M^2 is improved to a value around 1.27 [101]. The difficulty for this confined doping method is to find a suitable material to match the refractive indices between the active region and the passive region.

4. Technologies for fiber component preparation

In this chapter, the technologies which have been used to fabricate the designed LMA fibers and tapered amplifiers are introduced. The powder sinter technology (REPUSIL) can provide LMA fibers with very homogeneous dopant distribution and refractive index profile which is essential for this research. The stack-and-draw method which is employed to produce the fibers is also briefly introduced. Then the preparation of the tapered fiber amplifier is discussed.

4.1 Powder sinter technology (REPUSIL)

In the past decades and even today, a combination of Modified Chemical Vapor Deposition (MCVD) and solution doping [102,103] has been the standard method to produce rare-earth-doped active fibers. This kind of preparation method has several drawbacks. First, the deposition process efficiency is not very high. Second, the geometrical size and the refractive index homogeneity of the preform is limited. Third, the refractive index of the preform has a deep dip in the preform center due to the required collapsing process, especially when using Germanium and Phosphorus as co-dopants.

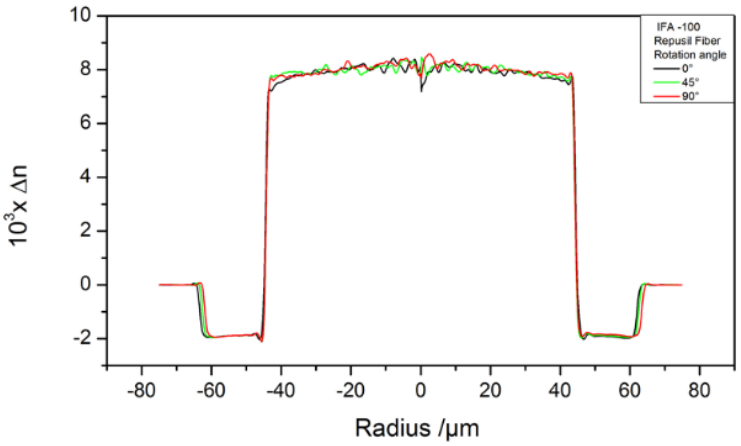

Figure 4.1 Homogeneous refractive index profile of a fiber which is made by REPUSIL method

In recent years, a new technique named reactive powder sinter technology (REPUSIL) which was developed by the IPHT and Heraeus Quarzglas to overcome the MCVD limitations. The most obvious feature of this REPUSIL method is its excellent material homogeneity (i.e. homogeneous refractive index profile and homogeneous dopants distribution) and less defects including bubbles and crystal parts. These characteristics make it possible to produce very large core fibers with good homogeneity and small numerical aperture (NA) which is very important for the production and

application of fiber lasers and amplifiers [25~27]. Up to now, the largest active rods achieve a diameter of 30mm, an order of magnitude larger than other typical MCVD core diameters in a preform.

Several steps are needed to prepare the doped rods with the REPUSIL method [25~27]. First, the defined amounts of the doping solution according the desired rod components are prepared and mixed into a silica suspension. The liquid suspension is stirred to make sure that all particles are mixed homogeneous. Second, the liquid suspension is dehydrated until the solid particles are all precipitated. This powder granulate normally is white and loosely structured (figure 4.2). Third, the power is compressed into a rod shape. Forth, the compressed rod is put inside a silica tube and purified to remove impurities. Finally, the rod is vitrified by a sintering technology at temperatures of up to 2200 °C.

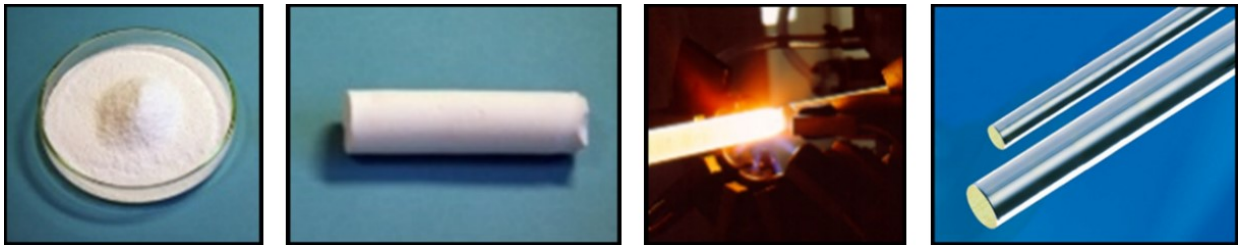

Figure 4.2 The process of producing preform with REPUSIL [25]: powder granulate, compressed rod, vitrification process and final rods.

4.2 Preform and LMA fiber fabrication

For the preform preparation, the Yb^{3+} doped active core rod and other passive inner cladding rods are prepared by the REPUSIL technology. Therefore, all desired doping elements (for example: Yb_2O_3, Al_2O_3, Ce_2O_3) for the active core rod are mixed with pure silica nano-particles to achieve a LMA fiber with a very homogeneous dopant distribution and a uniform refractive index profile [104,105]. Yb_2O_3 is the active dopant for amplifying the laser light, Al_2O_3 enhances the solubility of Yb^{3+} ions and helps to achieve a homogeneous Yb^{3+} dopant distribution by avoiding Yb^{3+} clusters and Ce_2O_3 is added to suppress the photo darkening effects.

The passive inner cladding rods, which are made of Al^{3+}-doped silica material can increase the refractive index of the inner cladding (Figure 4.3). By this way the core NA can be decreased to limit the number of HOMs. In addition, the pump NA of the inner cladding increases, which means that the acceptance angle for pump light also increases. This makes the pump coupling easier and

paves the way for increasing the pump power. The control of the refractive index of the inner cladding by using Al^{3+}-doped silica material enables the optimization of the core NA and pump NA at the same time. This is a new degree of freedom in the fiber design that is provided by the REPUSIL method. Figure 4.3 shows the comparison of the refractive index profile between fibers with pure silica cladding and Al^{3+}-doped cladding. The refractive index (RI) of the fiber core is quite high for highly Yb^{3+}-doped active fibers. For normal active fibers with silica cladding, the core NA is then large which leads to multi-mode operation. Also the pump cladding NA is small which leads to a low pump coupling efficiency. Therefore, the Al^{3+}-doped inner cladding is used to replace the pure silica cladding and to elevate the RI of the inner cladding to compensate the high refractive index of fiber core. This index-adjusted inner cladding method can decrease the core NA and increase the pump (inner) cladding NA at the same time.

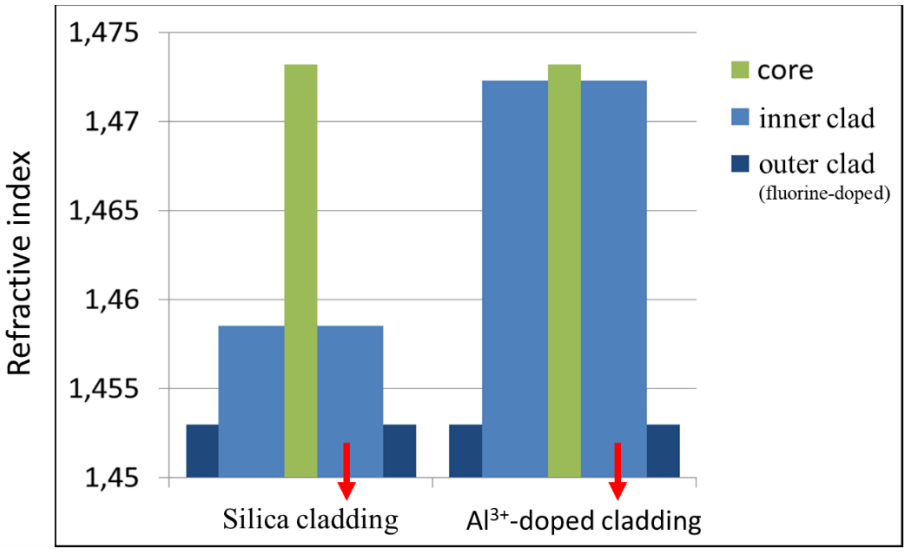

Figure 4.3 Comparison of refractive index structure for fibers with pure silica cladding (left) and Al^{3+}-doped cladding made by REPUSIL (right)

After finishing the preparation of the REPUSIL rods, they are stacked in a hexagonal shape as shown in figure 4.4. The active core rod is surrounded by passive inner cladding rods and all rods are over-cladded by a silica tube to form the initial preform package. The hexagonal shape of the inner cladding which stems from the rod stacking method is useful to facilitate good pump absorption. This initial preform package is collapsed to a solid rod without air holes inside. This solid rod is then over-cladded again with another tube (i.e. pure silica tube or fluorine doped silica tube) to extend the dimensions of the outer cladding and to obtain a straight fiber rod of the desired

geometry after the fiber final drawing. Fibers were made at the in-house fiber draw tower in IPHT with a temperature of approximately 2000 °C [104].

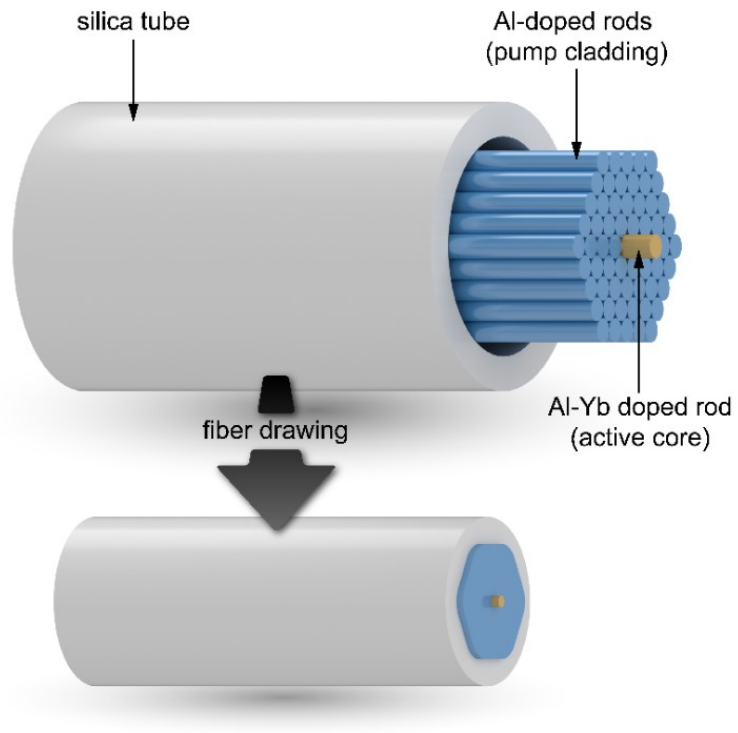

Figure 4.4 Stack-and-draw method: Preform preparation by stacking rods of core and inner pump cladding rods into a fluorine doped silica tube and drawing into a fiber.

4.3 Tapered fiber amplifier setup

Figure 4.5 shows a schematic tapered LMA double clad fiber amplifier. The seed light is delivered by a standard single mode fiber in which only the FM is propagating. The local adiabatic taper is directly spliced to a SM standard fiber for seed coupling. The local adiabatic taper provides a monolithic signal path and selectively excites the fundamental mode in a highly multimoded fiber. The LMA fiber adopts a double clad structure which allows high pump power with low brightness and high signal power with high brightness due to the different waveguide shapes of pump and signal light.

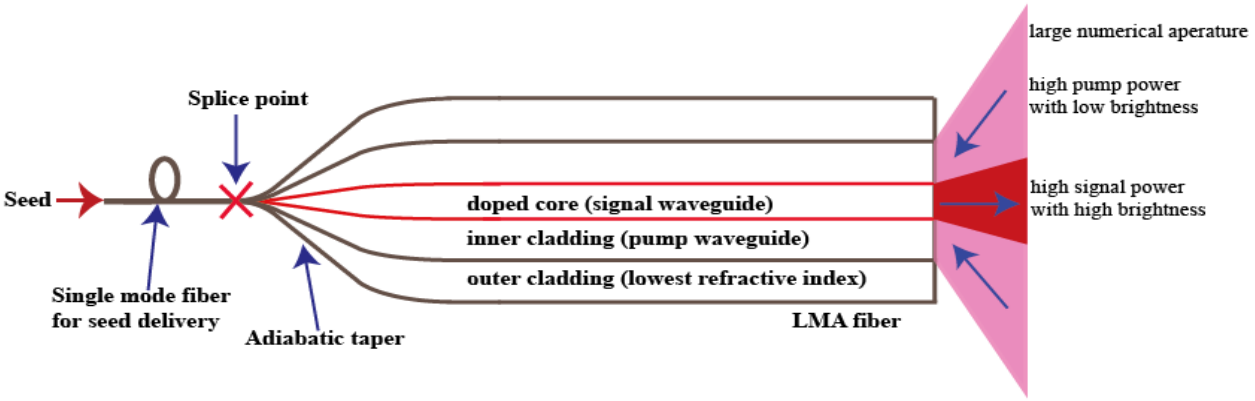

Figure 4.5 Tapered fiber amplifier setup with double clad fibers structure

The tapering of fiber can be performed by flame, filament heating, discharge arc, CO_2 laser or fiber furnace for drawing tower tapers. The filament heating is mainly adopted to produce short local adiabatic tapers for this research work. As is shown in figure 4.6, the fiber is held by two fiber holders which are fixed on two translation stages. Both translation stages can move forward and backward. A filament is used to heat the fiber to its softening temperature. During the tapering process, one translation stage moves with fast speed while the other one moves with constant low speed.

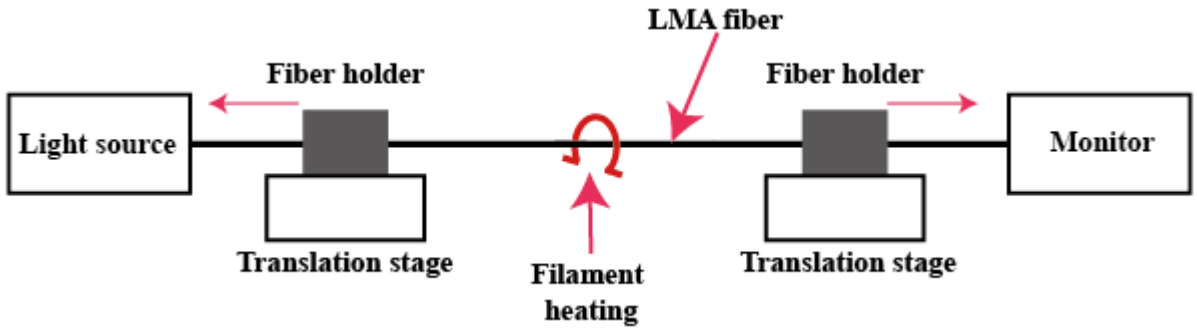

Figure 4.6 Schematic of the tapering process

In this research work, the rod fiber with large mode area was tapered down at one end to ideally single-mode dimension using a Vytran GPX 3200 splicing system (see figure 4.7) and was directly spliced to a standard single mode passive fiber (core diameter = 10μm, NA = 0.08, polarization-maintaining). While the number of guided modes in the rod fiber is rather large, the taper ratio can be chosen to lower the core diameter down to the single-mode limit of V=2.405.

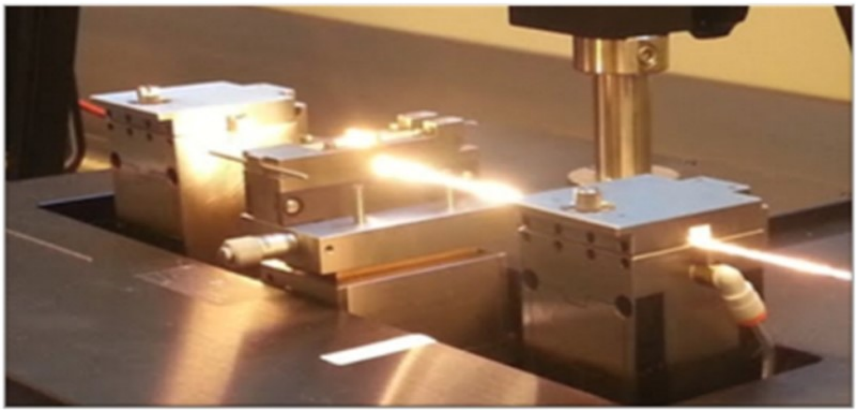

Figure 4.7 Tapering process with the use of a Vytran GPX 3200 employing a graphite filament for heat introduction.

5. Simulation models

In this chapter, several simulation models for large mode area (LMA) active fibers and adiabatic tapers are presented. First, the LMA fiber amplifier simulation with rate equations is introduced which can provide an estimation of the experimental results concerning power amplification. Second, a mode solver is introduced to calculate all guided modes of a LMA fiber core. Third, the adiabatic taper calculation according to the theory introduced in chapter 3 is described which results in a limitation boundary for an adiabatic taper. Forth, the calculation for a confined doped fiber is introduced which is based on the mode overlap coefficient calculation. The optimum doping radius and the tolerance for refractive index mismatch between active and passive regions of the fiber core can be estimated by this method. All simulations and calculations are done with simulation models which are scripted in MATLAB software.

5.1 Fiber amplifier simulation with rate equations

A model based on the rate equations is employed to simulate the expected performance of fiber amplifiers [37,38]. In this numerical calculation, the following assumptions are considered: (1) Only the ground state and the excited state of atoms are considered. (2) The pump power is assumed to be homogenously distributed over the cross section of the pump core. (3) The amplified spontaneous emission (ASE) and the non-linear effects are ignored.

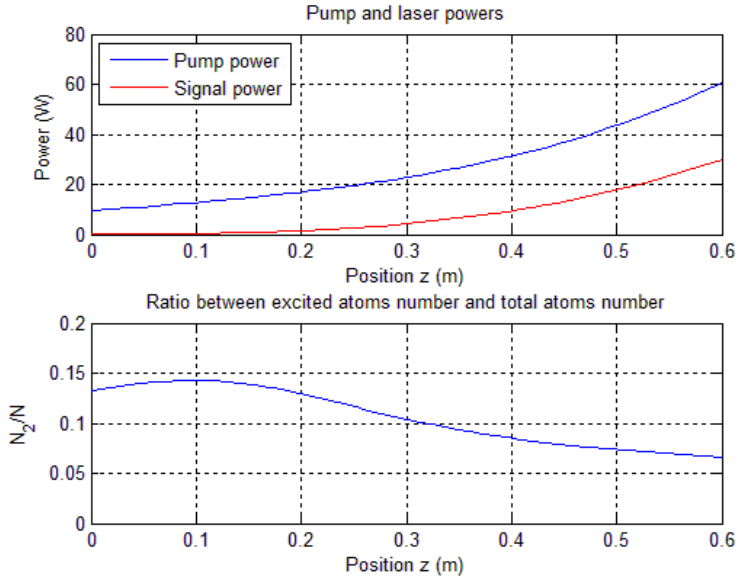

Figure 5.1 Example of a simulation of fiber amplifier properties as used in chapter 7.2.2

The model can be expressed by the space-dependent and time-independent steady rate equations which have been already discussed in chapter 2.3.1. The illustration of a double-clad fiber amplifier with backward pumping and the boundary conditions are also shown in chapter 2.3.1. The rate equations can be numerically solved with suitable fiber physical parameters and boundary conditions according to the practical fiber amplifier. Here the MATLAB function named bvp4c (a typical function to solve ordinary differential equations with two points boundary value) is used to solve the rate equations. This model provides information on the position dependent pump and signal power along an amplifier fiber and the relative number of excited atoms in the active core. In figure 5.1 an example is shown for a fiber amplifier with backward pumping and the fiber parameters are explained in chapter 7.2.2. Such model experiments provide information for optimized amplifier length and expected signal powers.

5.2 Mode solver for large mode area (LMA) fibers

A mode solver is used to calculate the electromagnetic eigenmodes and propagation constants of LMA fibers. In order to realize the LMA fiber with high peak power and good beam quality, it is necessary to investigate the specific mode transmission properties of the fiber. This mode solver is the foundation to investigate modal discrimination by differentiating the gain (or loss) between the fundamental mode and the other higher order modes to improve the beam quality.

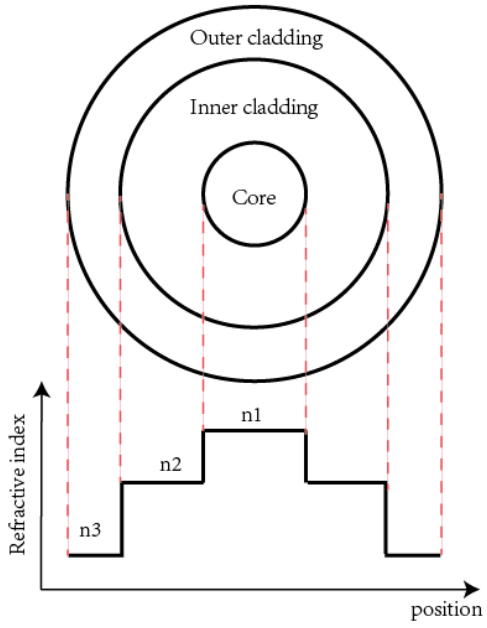

Figure 5.2 Three-layer structure of the LMA fiber model

In particular, a step index double clad fiber with three layers is considered whose geometry structure and refractive index profile are sketched in figure 5.2. In this model, it is assumed that the z axis is the propagation direction and the electromagnetic field has six field components ψ which are E_r E_θ E_z H_r H_θ H_z. According to the waveguide theory, the transverse field components have the relationship as follows [106~108]:

$$E_r = \frac{i\beta}{\omega^2\mu\varepsilon-\beta^2}\left(\frac{\partial}{\partial r}E_z + \frac{\omega\mu}{\beta}\frac{\partial}{r\partial\theta}H_z\right) \tag{5.1}$$

$$H_r = \frac{i\beta}{\omega^2\mu\varepsilon-\beta^2}\left(\frac{\partial}{\partial r}H_z - \frac{\omega\varepsilon}{\beta}\frac{\partial}{r\partial\theta}E_z\right) \tag{5.2}$$

$$E_\theta = \frac{i\beta}{\omega^2\mu\varepsilon-\beta^2}\left(\frac{\partial}{r\partial\theta}E_z - \frac{\omega\mu}{\beta}\frac{\partial}{r\partial\theta}H_z\right) \tag{5.3}$$

$$H_\theta = \frac{i\beta}{\omega^2\mu\varepsilon-\beta^2}\left(\frac{\partial}{r\partial r}H_z + \frac{\omega\varepsilon}{\beta}\frac{\partial}{\partial\theta}E_z\right) \tag{5.4}$$

The field components E_z and H_z satisfy the following equations:

$$\nabla_t^2 E_z + (\omega^2\mu\varepsilon - \beta^2)E_z = 0 \tag{5.5}$$

$$\nabla_t^2 H_z + (\omega^2\mu\varepsilon - \beta^2)H_z = 0 \tag{5.6}$$

By applying appropriate boundary conditions and solving the equations, all numerical solutions can be found for all transverse modes supported by the fiber. Here a matrix method is adopted to solve the wave equations and calculate the mode characteristics in LMA fibers [106,107]. The time average of the power flow is given by [108]

$$P = I \cdot A = S_z \cdot A = 0.5Re\{E \times H^* \cdot \hat{z}\} \cdot A = \frac{1}{4}Re\{\int_0^r \int_0^{2\pi}[E_r H_\theta^* - E_\theta H_r^*]rd\theta dr\} \tag{5.7}$$

Where S_z is the z-component of the Poynting vector, A is the area of the fiber cross section. The effective mode area is an important concept in fiber optics. Transverse modes have smooth profiles on the fiber cross section. The effective mode area A_{eff} [109] and the corresponding effective diameter d_{eff} can be derived using equations 5.8 and equation 5.9:

$$A_{eff} = \frac{(\int IdA)^2}{\int I^2 dA} = \frac{(\int |E|^2 dA)^2}{\int |E|^4 dA} \tag{5.8}$$

$$d_{eff} = 2\sqrt{\frac{A_{eff}}{\pi}} \tag{5.9}$$

5.3 Adiabatic taper calculation

One of the central intentions of this research work is the use of a local adiabatic taper to preserve near-diffraction limited beam quality. Therefore, the following model is employed to provide guidelines to design short and low loss adiabatic local tapers [86,110] according to the theory introduced in chapter 3.3.1. It is known that a taper is approximately adiabatic when the local taper angle is small enough along the taper. Then the power coupling between FM and HOMs is negligible as the FM propagates along the taper. Normally the real taper shape is not perfect linear shape. In order to calculate the local taper angle, the taper is separated into small length segments as shown in figure 5.3, each piece can be treated separately as a short cylindrical fiber. Then the local taper angle can be derived from the taper shape. This model is believed to be similar with the real taper when the number of mesh pieces is large enough.

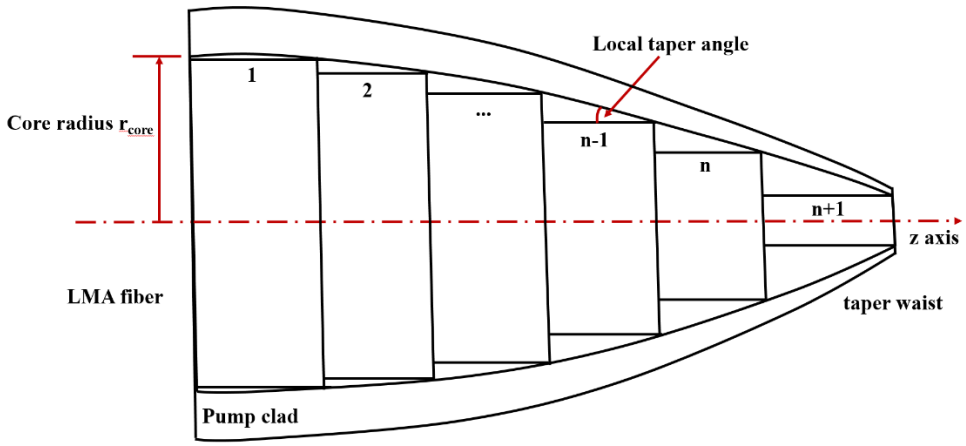

Figure 5.3 Illustration of a taper model

The modes solver can be used to calculate the modes of every short cylindrical fiber. According to the length scale criterion (equation 5.10) [93,111], the critical angle at the local position with different core radius of the taper can be calculated. Then the adiabatic region boundary according to critical angle with different core radius can be identified with equation 5.10:

$$\tan\Omega(r_{core}) = \frac{r_{core}\cdot\Delta n(r_{core})}{\lambda} = \frac{r_{core}\cdot(n_{FM}(r_{core})-n_{HOM}(r_{core}))}{\lambda} \qquad (5.10)$$

where Ω is the local critical taper angle, r_{core} is the core radius of the local fiber piece. λ is the wavelength, and the $\Delta n(r_{core})$ is the effective refractive index difference between FM and HOMs at different taper position with different core radius r_{core}.

5.4 Confined doping calculation with the overlap coefficient

The principle of confined doped fiber is to partially dope the LMA fiber core and get a preferred gain for FM (see figure 5.4). The corresponding model employs the mode solver (discussed in chapter 5.2) and the theory of overlap coefficient calculation [84,97,112] to find the optimum doping radius and the tolerances for refractive index mismatch between active and passive regions of the fiber core.

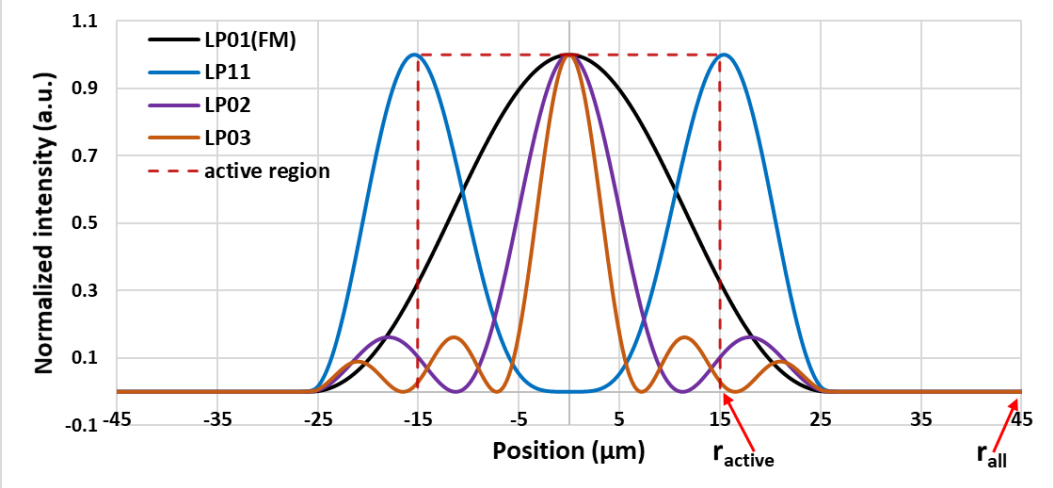

Figure 5.4 Illustration of overlap between modes and active region

The overlap coefficient η_{mn} between different modes (LP_{mn}) and the active Yb^{3+}-doped region can be calculated with the equation 5.11:

$$\eta_{mn} = \frac{\iint I_{mn} dA_{active}}{\iint I_{mn} dA_{all}} = \frac{\int_0^{r_{active}} \int_0^{2\pi} I_{mn} dr d\varphi}{\int_0^{r_{all}} \int_0^{2\pi} I_{mn} dr d\varphi} \tag{5.11}$$

In which, η_{mn} is the overlap coefficient between mode LP_{mn} and the active region in the fiber core. I_{mn} is the intensity distribution of mode LP_{mn}. A_{active} means the active area of the fiber core center, while the A_{all} is the whole fiber cross section area. The r_{active} means the radius of the active area of the fiber core and the r_{all} is the radius of the fiber outer-cladding. Once the active doping radius in fiber core center is determined, the overlap coefficient between the Yb^{3+}-distribution profile and the mode profile can be calculated. The optimum doping profile ratio can be found by achieving a high overlap value for the FM while keeping the overlap with HOM profiles small. Then, the FM can get high gain while the gain for the other HOMs is suppressed.

6. MOPA system setup and characterization

In order to test the designed LMA fiber, a three-stages MOPA system was built. In this chapter, the setup of all stages in the MOPA system is discussed and the amplified laser beams in first and second amplifier stage are characterized in detail.

6.1 MOPA system overview

In order to test the designed LMA fiber, a three-stages ns-pulse fiber master oscillator power amplifier (MOPA) system was built. It features a directly modulated seed diode to choose the pulse shape and the repetition rate independently. The gain of a single amplifier is typically limited to around 30dB. It is easier and more flexible to combine several fiber amplifiers together as an amplifier chain instead of developing a single amplifier with very high gain (e.g. 60dB). In case of several stages, not all components are exposed to very high beam intensities which reduces the power requirements especially for the first stage.

The schematic diagram of the complete MOPA system is shown in figure 6.1. In this system, a directly modulated semiconductor laser is used as the master oscillator which provides the initial seed signal. Pulsed operation is obtained by means of an external electronically controlled modulator. The two pre-amplifier stages are all-fiber structures. All passive and active fibers used in these two pre-amplifiers are based on polarization-maintaining (PM) single-mode fibers which can maintain a near diffraction limited beam quality. All components are connected with PM fusion splices. Several isolators are included to avoid backward propagation of laser light e.g. due to reflections. Several monitors are placed at different positions in the MOPA system to monitor the working condition of the system. An acousto-optic modulator (AOM) gate is inserted between the second and the third stage to protect the two pre-amplifiers against the possible external back-reflections of the laser beam. The AOM gate is a device which utilizes the acousto-optic effect to deflect a laser beam within a very short time when a pulse passes by. The rise-time and gate width of the AOM gate are important parameters to modulate the optical pulses travelling through the AOM gate.

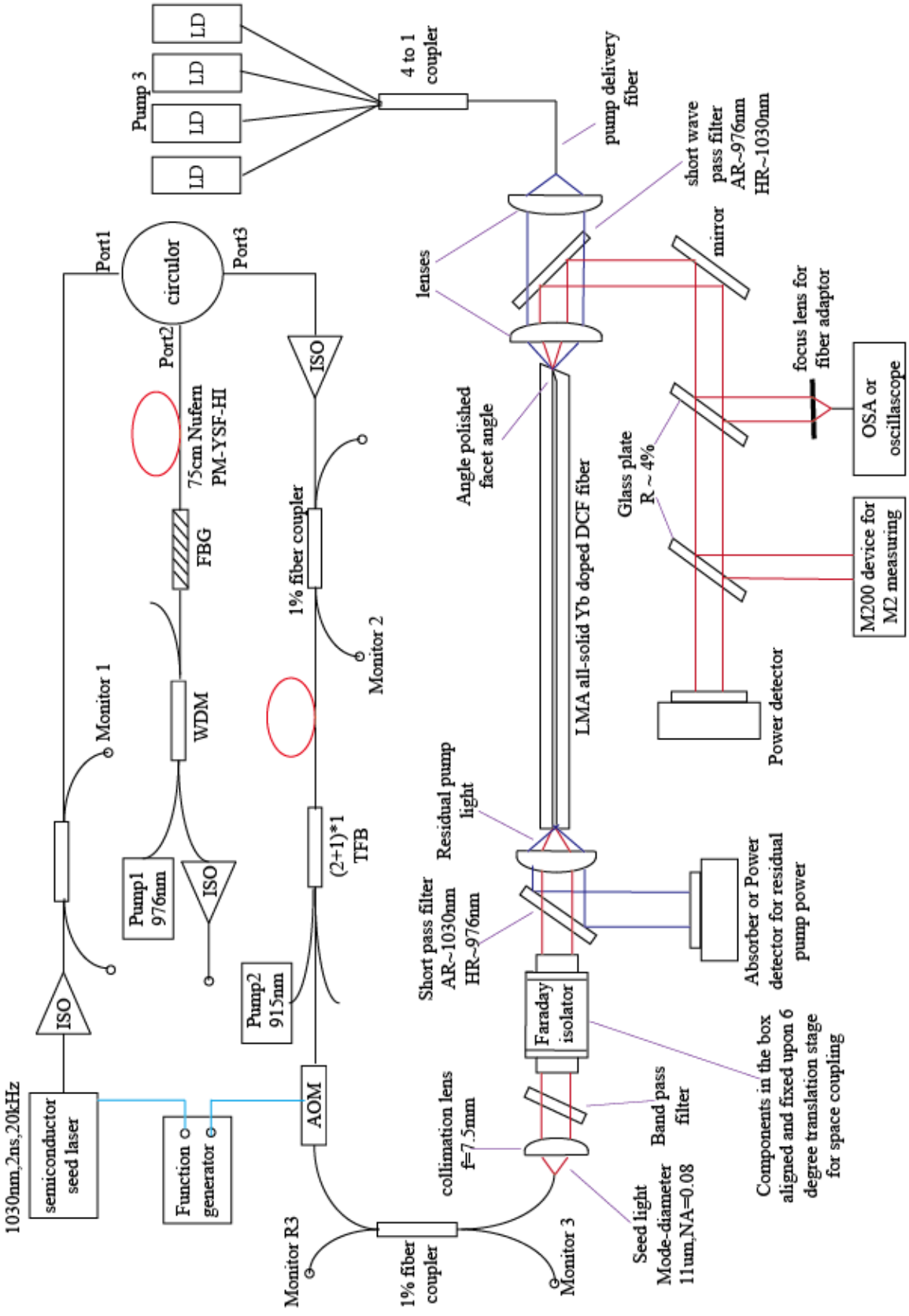

Figure 6.1 A sketch of the complete MOPA system

6.2 Pre-amplifier stages and the amplified laser beam

(1) The initial semiconductor seed laser

The initial semiconductor laser provides the initial seed laser pulse with a wavelength of 1030nm and allows adjustment of the pulse duration (1ns to 100ns) and the repetition rate (1kHz to 1MHz) in a flexible way. Even though various pulse formats are available, a combination with 2ns pulse duration and 20kHz repetition rate is mainly used. The pulse width of 2ns is the shortest pulse width with full pulse power which can be achieved by the semiconductor laser. Normally the repetition rate of the amplifier should be larger than the inverse of the upper state lifetime. If the lifetime of Yb^{3+}-population in excited state is assumed to be 1ms, the repetition rate of amplifier should be larger than 1kHz. The repetition rate of 20kHz is the lowest value to scale up the peak power and to supply enough seed power at the same time.

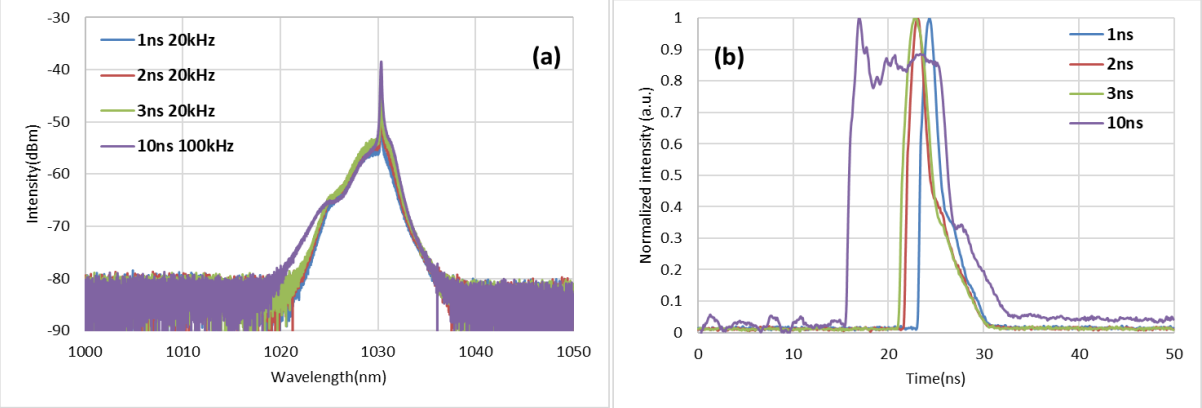

Figure 6.2 (a) Spectrum of the semiconductor seed laser with different pulse formats. (b) The measured pulse shape with different pulse widths.

The figure 6.2 shows the typical spectrum of different pulse formats and the pulse shape of different pulse widths of the laser which is measured using a spectrum analyzer and an oscilloscope, respectively. The center wavelength is 1030.3nm. The peak power of the pulse (2ns 20kHz) from the semiconductor laser is 1.32W.

(2) The first amplifier stage

The first amplifier uses the double path design which makes use of a Fiber Bragg Grating (FBG) to reflect the amplified laser beam back into the active fiber. Therefore, the laser beam is amplified twice by the active fiber and the amplifier efficiency is increased. One 75cm long Nufern

polarization maintaining Yb^{3+}-doped single mode active fiber (fiber type: Nufern PM-YSF-HI) is chosen to amplify the laser beam.

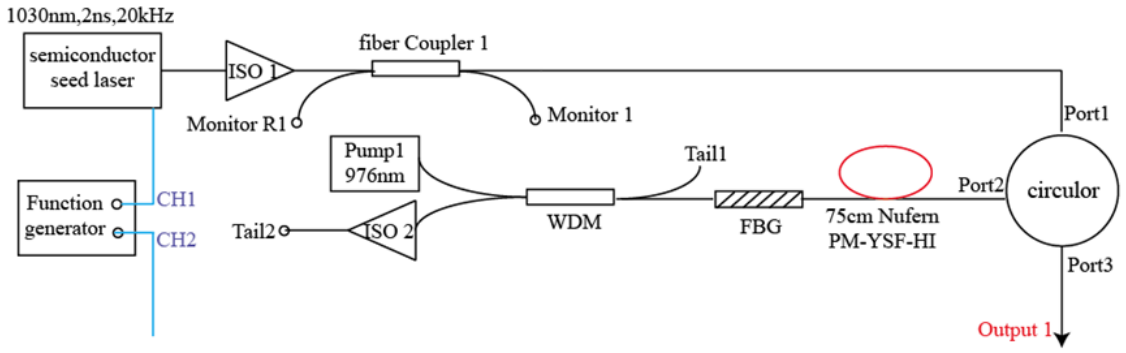

Figure 6.3 Setup of the first amplifier stage

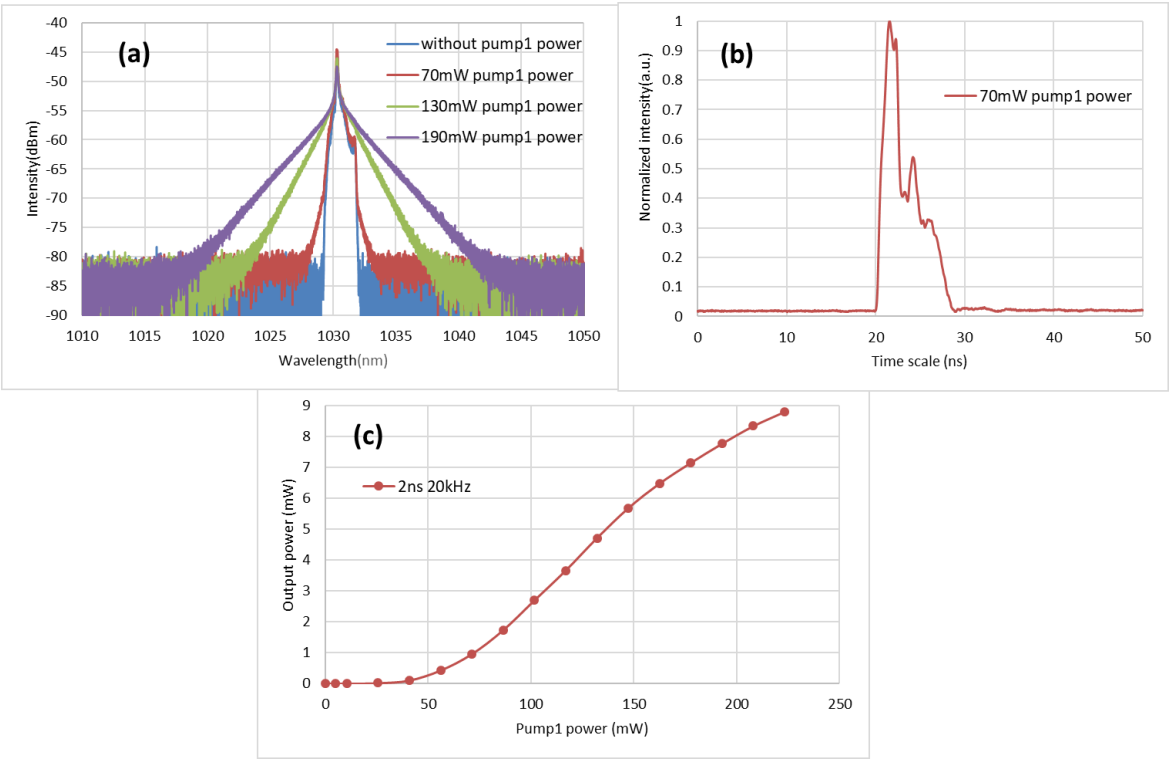

Figure 6.4 Characterization of the first amplifier (a) Emission spectrum. (b) Pulse shape. (c) Average output power (Output 1 of figure 6.3) at different power of pump1.

Figure 6.4 shows the characterization of the first amplifier with different pump powers under the 2ns 20kHz pulse format. The diagram 6.4(a) shows that part of the emission of the seed laser is filtered out and the spectrum becomes much more narrow with lower pump levels (compared to

figure 6.2(a)). The spectra become broader when increasing the pump power because of the nonlinear optical broadening. The pulse shape is slightly distorted due to the amplification saturation. In order to keep the output power as high as possible, the power of pump1 was chosen to be 70mW for all subsequent experiments. The average output power after the circulator (Output 1 of figure 6.3) is 1mW with 10W peak power.

(3) The second amplifier stage

The second amplifier stage uses a normal one loop amplifier structure which is shown in figure 6.5. The active fiber for the second amplifier stage uses a 5m length active fiber (fiber type: Nufern PM-YDF-10/125) whose core diameter is 10μm. The pump light is counter-propagating at a wavelength of 915nm.

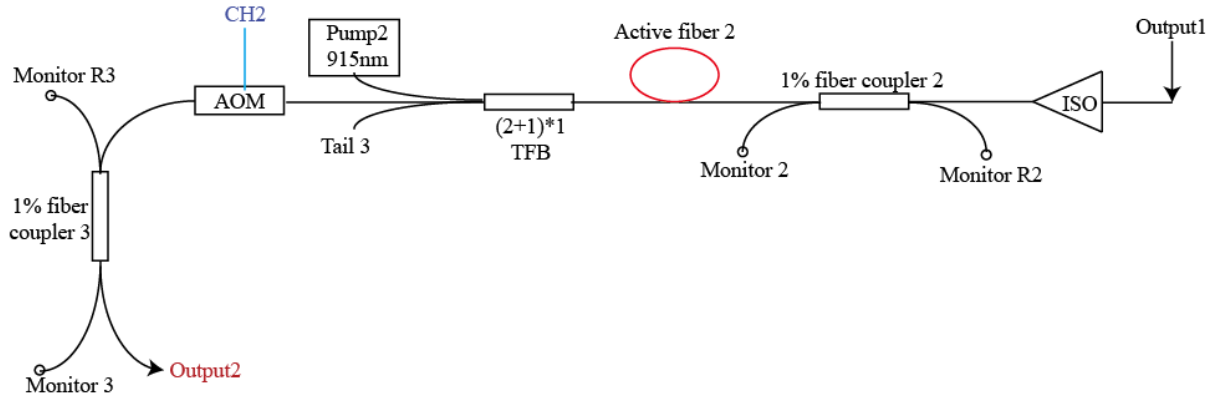

Figure 6.5 Setup of the second amplifier stage

When the output power increases with increasing power level of pump2, the spectral broadening increases significantly (see figure 6.6(a)). The average output power (before the AOM gate) is 470mW with a pump power of 4W of pump2, while the overall gain of the second amplifier is roughly 24dB.

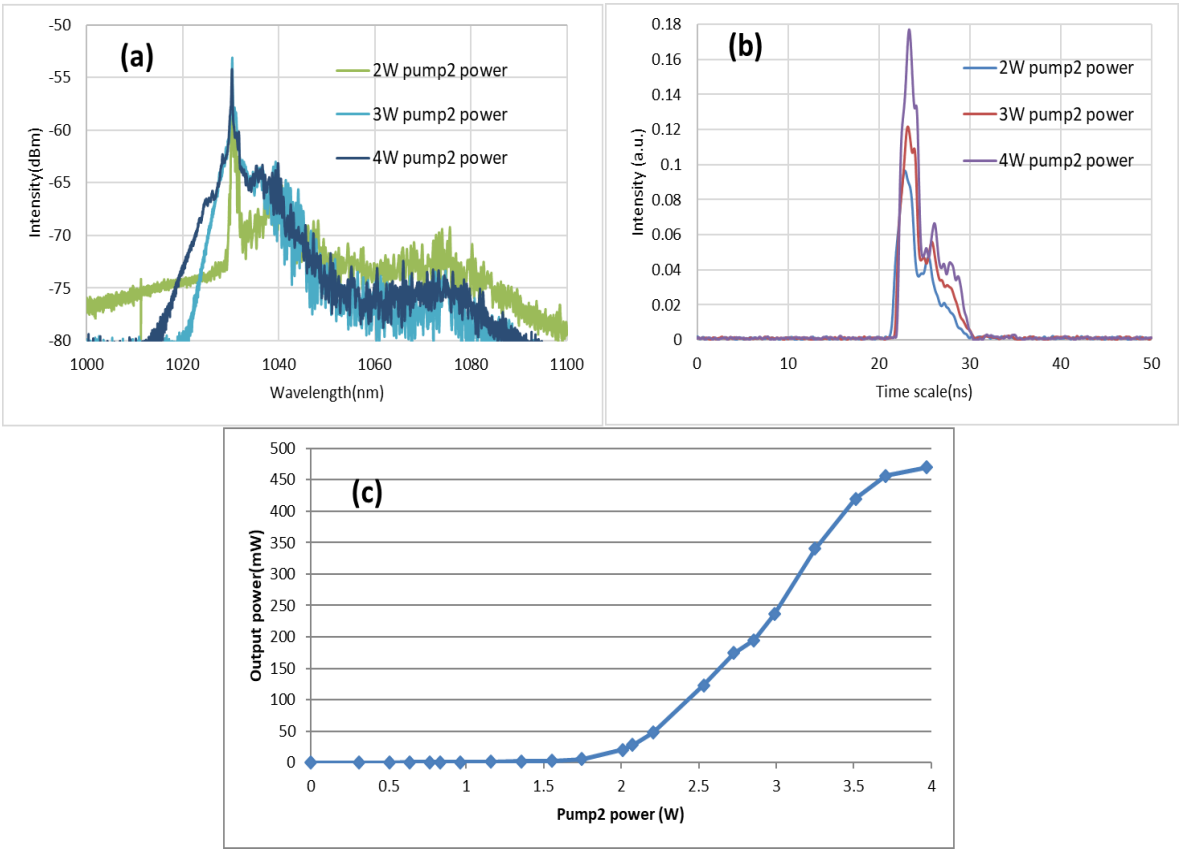

Figure 6.6 Characterization of the second amplifier (a) Emission spectrum. (b) Pulse shape. (c) Average output power with different power of pump2 (before AOM gate).

(4) Filtering of laser signal after second amplifier stage

An AOM gate is inserted between the second amplifier and main (third) amplifier stage which can filter out unwanted emission (e.g. ASE) between the pulses and which has a very high isolation for time-delayed back-reflections to protect two pre-amplifier stages. One coupler is also adopted to monitor the working situation of the pre-amplifier stages. The table 6.1 shows the output average and peak power after the AOM gate which seeds of the main amplifier stage.

Pump1	Pump2	Average output power	Peak power
70mW	4W	138mW	3kW

Table 6.1 The amplified laser light after the 2nd amplifier stage (Output 2 in figure 6.5)

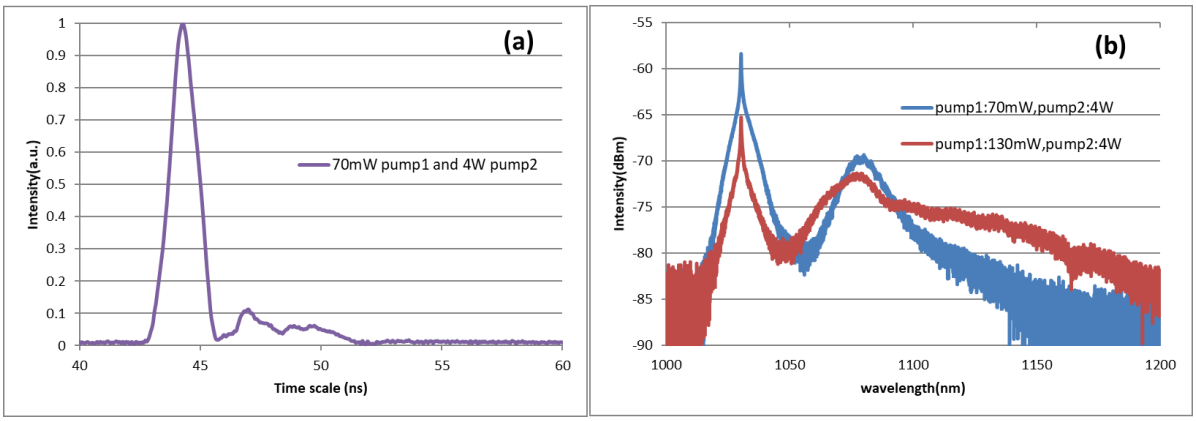

Figure 6.7 Properties of the amplified laser light after the 2nd amplifier stage

The characterization of this seed light for the main amplifier stage is shown in figure 6.7. The SRS effect is obvious around 1080nm wavelength. The average output power is 138mW with 3kW peak power (Output2 in figure 6.5) corresponding to 70mW pump1 power and 4W pump2 power. The difference between the main signal peak and the first Stokes peak is approximately 10dB with 70mW pump1 power. An almost diffraction-limited Gaussian beam with M^2~1.06 for the laser beam is measured. This amplified laser beam is the seed laser beam for the main(third) amplifier stage to scale up the peak power with the specially designed LMA rod-type fiber.

6.3 Main (third) amplifier stage setup based rod type fiber

The third stage in the MOPA system is the main stage to test the specially prepared rod-type fibers with 976nm wavelength counter pumping. The main sketch of the main amplifier is shown in figure 6.8. Here two different methods for seed coupling have been applied, one reference setup with a non-tapered rod fiber and one setup with the tapered rod fiber are illustrated in figure 6.8.

(a) For a non-tapered rod fiber, the free space coupling is adopted (Figure 6.8(a)). The seed laser beam from the two pre-amplifier stages is collimated by an aspheric lens with 7.5mm focus length. A Faraday isolator is inserted between the coupling lenses to avoid back-reflection laser light and to protect the pre-amplifiers. One long wave pass filter is placed in front of the focus lens to reflect the residual pump light outside while it is transparent to the signal light. The collimated laser beam is focused by the lens to the rod type fiber end. All these components are mounted and aligned in an aluminum box (seed box). The seed box is fixed on a platform of a translation stage which has six degrees of freedom to precisely couple the seed light into the rod fiber. Both end facets of the

rod fiber were angle-polished to avoid back reflections. The measured result, especially for beam quality (M^2 value), depends strongly on such seed coupling condition.

(b) For tapered rod fibers, the taper is directly spliced to the single-mode standard fiber (core diameter 10μm and core NA 0.08) and connected to the MOPA system with the purpose of providing a monolithic signal path and adiabatic excitation the fundamental mode in rod-type amplifiers (Figure 6.8(b)). The end facet of the tapered fiber was angle-polished to avoid back reflections. The fiber was placed on one aluminum holder, the taper and splice regions were embedded in index-matched acrylate to strip out the residual pump light from cladding.

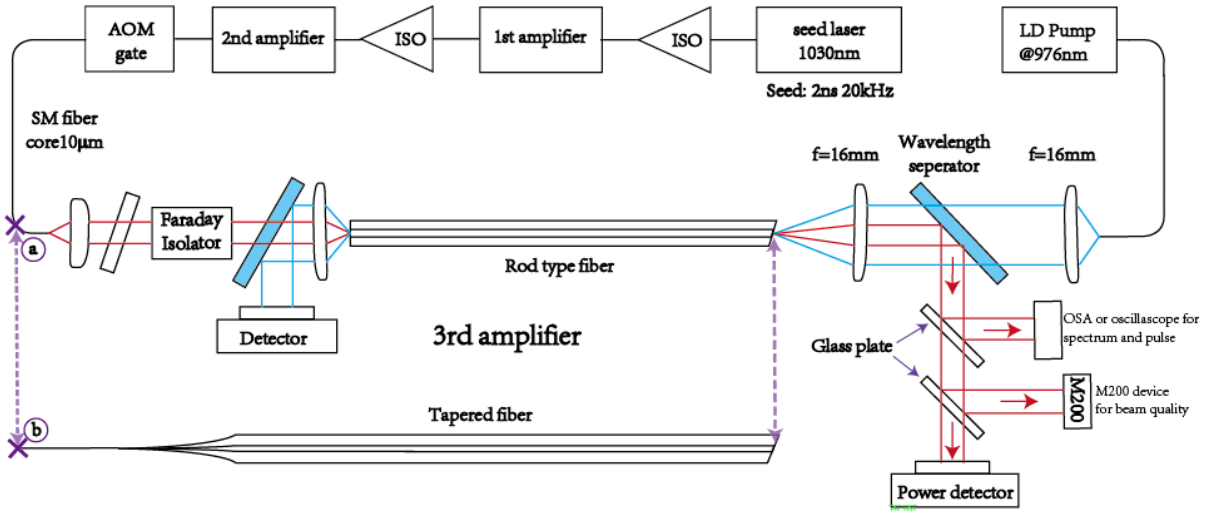

Figure 6.8 The third amplifier stage. (a) Free space coupling with rod type fiber. (b) Monolithic coupling with fusion splice and local adiabatic taper.

In the following, several important concepts for main amplifier stage are introduced.

(1) Free space coupling analysis

Free space coupling using a lens pair is the straightforward method to couple the laser beam between fibers with different mode field diameters. In order to find out the suitable lens combination to optimize the coupling efficiency, a theoretical calculation and analysis is necessary. As is shown in figure 6.9, a laser beam with radius w1 is collimated by lens1 and re-focused by lens2 into the laser spot with radius w2.

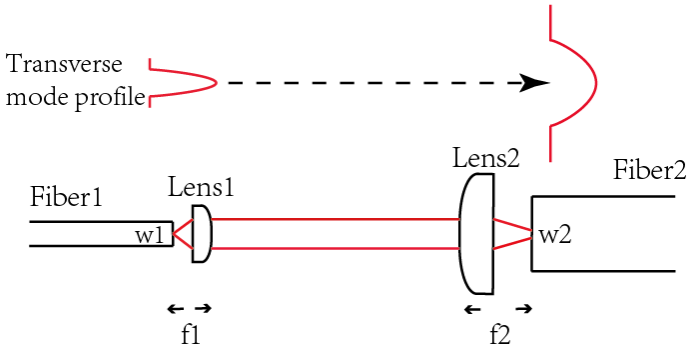

Figure 6.9 Illustration of free space coupling

Normally, a well collimated Gaussian beam with a sufficiently large waist diameter has the following approximate relationship [43]:

$$\frac{f_1}{f_2} = \frac{w_1}{w_2} = \frac{NA_2}{NA_1} \tag{6.1}$$

Where the f_1 and f_2 are the focus lengths of the lens pair, NA1 and NA2 are the numerical apertures for the two fibers, w1 and w2 are the effective mode radii (waist radius of Gaussian beam).

(2) Pump configuration

The pump configuration is backward pumping which is provided by four combined laser diodes at 976nm. The pump light is delivered with the pigtail fiber of a pump module. Here a single pump module with 105μm core diameter (NA=0.16) and a multi pump module with 200μm core diameter (NA=0.22) are used to choose from for different rod type fibers. Finally, the pump light is coupled into the pump cladding of the rod fiber with the use of a lens pair with two identical aspheric lenses. The lenses, the wavelength separator and the holder of the pump delivery fiber are all fixed in a one cage system and mounted on a plate of a translation stage with three free degrees of freedom to adjust. This can be used to align the laser beam and to efficiently couple the pump laser beam. The power of pump3 versus the current is shown in figure 6.10 and the parameters for these two different pump modules are shown in table 6.2.

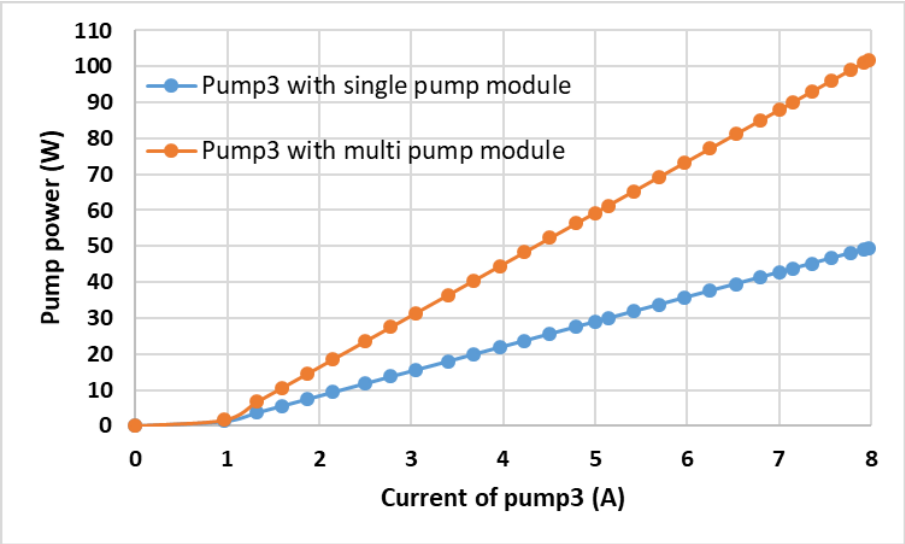

Figure 6.10 Pump power versus current of pump3 in the third amplifier stage

	Maximum power	**Delivery fiber core diameter**	**Delivery fiber core NA**	**Brightness (W rad^{-2} µm^{-2})**
Single pump module	50W	105µm	0.16	0.071
Multi pump module	102W	200µm	0.22	0.021

Table 6.2 Parameters of the single pump module and multi pump module

(3) Measurement system

The measurement setup for the analysis of the output of the main amplifier stage is shown in lower right part of figure 6.8. A wavelength separator is inserted between the two identical aspheric lenses where the laser beams are collimated. The pump laser light at 976nm can pass through the separator while the amplified signal laser beam at 1030nm is reflected outside at a certain angle. Two glass plates are adopted to couple out 4% of the signal laser beam. One 4% laser beam is used to measure the spectrum and pulse shape while the other is used to measure the beam quality (M^2 value). The signal power in the main path is measured by a thermal power detector.

7. Rod type fibers characterization and beam quality improvement

In this chapter, the characterization of the designed and prepared large mode area (LMA) fibers is presented and the local adiabatic tapers are experimentally demonstrated to improve the beam quality. The essence of the local adiabatic taper approach is to provide a monolithic signal path and selectively excite the fundamental mode in a highly multimode fiber. The design of the LMA fibers and adiabatic tapers is based on the models developed in chapter 5. Many Yb^{3+}-doped LMA fibers samples with different processing were tested in this research work, but only some of them which provided good and stable performance are presented here. In the last section, the optimized active core radius ratio and the tolerance of refractive index mismatch for confined doping fiber is analyzed.

7.1 Design aspects of rod type fiber amplifiers

In order to achieve reasonable rod fiber parameters such as mode field diameter, core NA, Yb^{3+}-doping concentration and fulfill the purpose of this research work, the design aspects of rod type fiber are discussed in the following.

(1) Core numerical aperture (NA) of rod fiber and the mode field diameter of taper waist

In order to achieve the maximum signal power coupling without higher order modes (HOMs) excitation using a local short adiabatic taper of a tapered rod fiber which is directly spliced inside the MOPA system with a seed delivery fiber (core diameter 10µm, core NA 0.08 and outer clad diameter 125µm), mode matching at the splice between the seed delivery fiber and the taper waist should be satisfied and the taper waist should be single mode to prevent HOMs excitation. The mode field diameter (MFD) is an important parameter to characterize the transverse extent of a laser beam and the mode matching between two fibers. The MFD of a step index single mode fiber can be estimated using Marcuse's equation [113] as shown in equation 7.1:

$$MFD \approx \mathrm{D} \cdot \left(0.65 + \frac{1.619}{\left(\frac{\pi DNA}{\lambda}\right)^{1.5}} + \frac{2.879}{\left(\frac{\pi DNA}{\lambda}\right)^{6}}\right) \tag{7.1}$$

The D is the fiber core diameter and the NA is the fiber core numerical aperture. The λ is the wavelength. Figure 7.1 shows the MFD as a function of fiber core diameter with different core NA. The MFD of the seed delivery fiber is 11µm with 10µm core diameter and 0.08 core NA. If the core NA of rod type fiber is too large e.g. NA=0.1, the taper waist of tapered rod fiber will operate

in the multi-mode region when it is tapered down to seed delivery fiber dimension. Then the HOMs can be excited at the splice. If the core NA of rod type fiber is too small e.g. NA=0.4, the MFD of the taper waist will be quite large and extend into the pump cladding, compared with the seed delivery fiber. Then the MFD of taper waist and the seed delivery fiber cannot match very well. The V parameter (see equation 3.6) of the taper waist should be below 2.405 to support only fundamental mode (FM). Due to the mode matching between seed delivery fiber and taper waist of rod fiber, the core NA of the rod type fiber should be around 0.08 and the MFD of the taper waist should be around 11μm to match the seed delivery fiber.

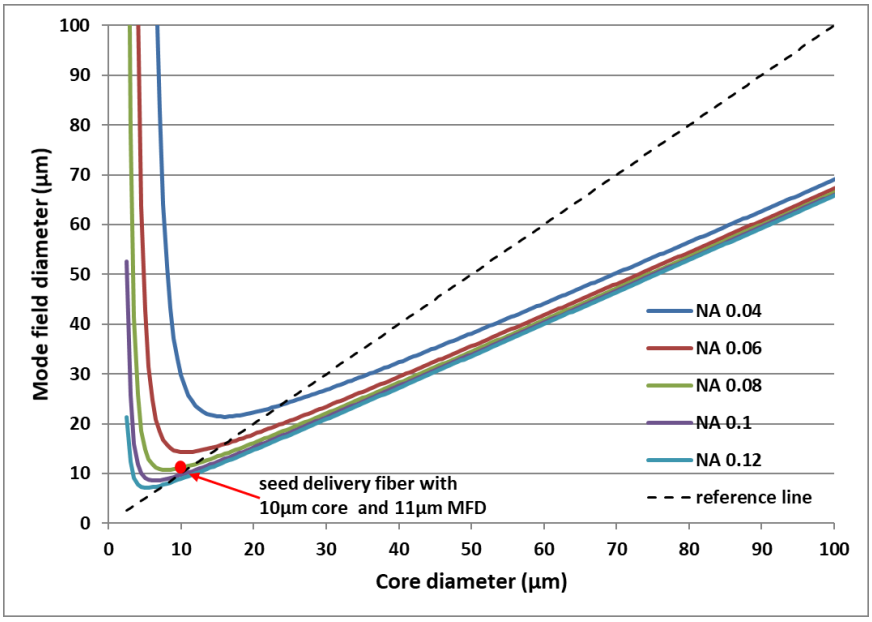

Figure 7.1 Mode field diameter for different core diameters D and core NA

(2) Pump beam product (Pump clad NA and the pump clad diameter)

In order to increase the pump coupling efficiency, the pump clad NA (NA_{pump}) and the pump clad diameter (D_{pump}) should be large enough to accept the pump brightness of the pump module. Normally the brightness B of pump can be estimated with the pump power P_{pump}, beam radius w and the divergence angle θ shown in equation 7.2:

$$B = \frac{P_{pump}}{\pi w^2 \pi \theta^2} \tag{7.2}$$

For the designed rod-type fiber, the pump power is coupled into the fiber with free space coupling. The pump cladding of the rod type fiber should accept the pump brightness of the pump module.

Therefore, the pump beam product ($NA_{pump} \cdot D_{pump}$) of the designed rod-type fiber should be slightly higher than the pump beam product of the pump module. The pump product of two different pump modules is discussed in chapter 6.3 are 16.8 and 44 (unit: μm), respectively.

(3) Clad absorption and rod fiber length

One of the most important aspects for the rod fiber design is to achieve sufficient clad absorption based on Yb^{3+}-doping concentration, core to clad ratio and the fiber length. As is known, the core absorption α_{core} coefficient of a Al^{3+}-doped silica active fiber with 1000ppm Yb^{3+}-concentration has an experimental value of 480dB/m at 976nm pump wavelength (unsaturated absorption). Then the clad absorption $\alpha_{pumpclad}$ can be estimated from the core absorption α_{core} as shown in equation 7.3:

$$\alpha_{pumpclad} = (\frac{r_{core}}{r_{pumpclad}})^2 \alpha_{core} \tag{7.3}$$

Where r_{core} is core radius and $r_{pumpclad}$ is the pump clad radius of the rod fiber. At first, the target value of clad absorption is 25dB in case of unsaturated pump clad absorption by considering the gain of peak power amplified from 3kW to 1MW. The clad absorption based on the first non-tapered rod type fiber discussed in chapter 7.2.2 (56μm/460μm core/inner cladding diameter, 0.6mol% (or 6000ppm) Yb^{3+}-concentration and 0.6m fiber length) is theoretically 25.6dB with equation 7.3. But the actual experiment value for clad absorption is much lower (8.6dB with the highest output power 28W) due to the helix modes and saturation effects. Therefore, the theoretical clad absorption of the designed fiber should be higher than 25dB (the base line for fiber design) according to the Yb^{3+}-doping concentration, core to clad ratio and the fiber length. Normally the fiber length of a rod type fiber should be shorter than 1m which would be easy to handle, and the fiber length should not be too short (e.g. 0.1m) to get enough pump absorption.

(4) Mode field diameter (MFD) of rod fiber

In order to estimate the required MFD of the rod fiber, the critical power threshold (discussed in chapter 3.1) is plotted in figure 7.2 as a function of the MFD where it is assumed that the effective fiber length is 0.2m, the pulse width is 2ns and the wavelength is 1030nm. The spectral broadening effect (figure 7.2) in dashed green line only influence the spectrum property and is not critical for nanosecond fiber amplifier. The black dashed line shows the power scaling is limited to 500kW

according to the damage threshold and 1MW according to the SRS limit of the fiber with a MFD of 40µm. And an end cap for fiber can be used to enhance the damage threshold. The critical power due to the self-fousing is approximately 4MW (see discussion in chapter 3.1).

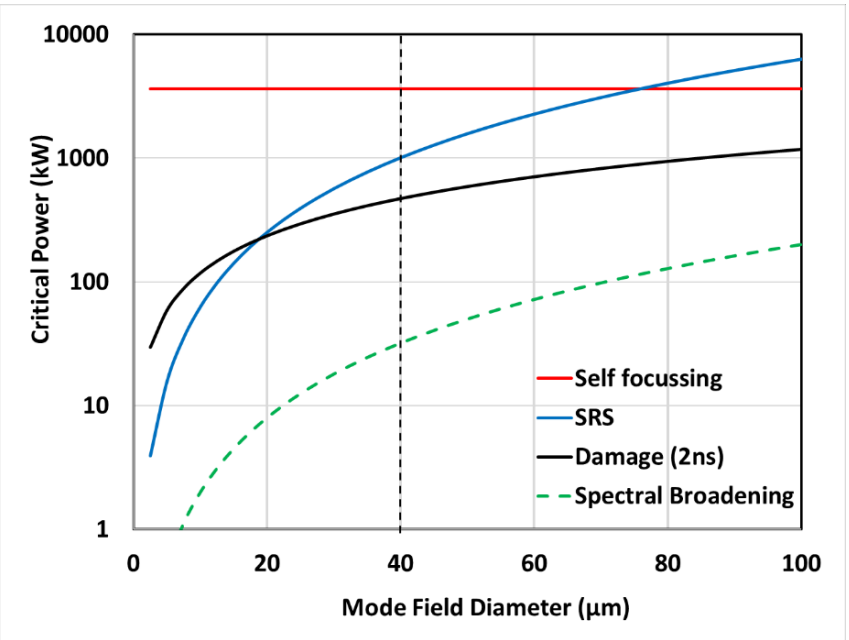

Figure 7.2 Critical power limited as a function of MFD

(5) Outer diameter of rod fiber

In order to match the seed delivery fiber in terms of MFD, core and clad, the outer diameter of the rod type fiber should be extended to a large size according to the core to outer clad ratio. Because the taper waist of tapered rod fiber should have a similar outer diameter with the seed delivery fiber (outer clad diameter 125µm) to get a good splice for seed coupling. For example, the core diameter of the first rod type fiber discussed in chapter 7.2.2 has a 56µm core diameter, the outer diameter of rod type fiber should be 700µm due to the ratio 1: 12.5 between core diameter and the fiber outer diameter. The preform for rod-type fiber is obtained by a second over-cladding process to increase the outer cladding dimensions.

7.2 Fully doped rod-type fiber with high Al^{3+}-concentration (999c)

7.2.1 Parameters of rod type fiber

This rod-type double-clad fiber (fiber code: 999c) has a 56µm core, a 460µm inner cladding (see figure 7.3) which were measured using a microscope. The shape of the core and the inner cladding

is hexagonal due to the stacking method of the REPUSIL preform rods which can help to improve the pump power absorption during the amplification process. The outer clad which is made from an F300 silica tube has a double D-shape, which however is not relevant for the optical function. The large diameter is 1250µm and the small diameter is 990µm. According to the calculation, the effective mode area diameter of FM of the core is 40µm.

The active core of the rod fiber has a doping concentration of 0.6mol% Yb_2O_3 and 7mol% Al_2O_3. The Yb^{3+} is the active dopant to amplify the laser light. The Al^{3+}-dopant is used to increase the solubility of Ytterbium and to suppress the photo-darkening effect. The passive inner cladding contains an Al_2O_3-concentration of 9mol%. The Al^{3+} in the passive inner cladding is used to elevate the refractive index of the inner cladding which can decrease the core NA and increase the pump inner-clad NA at the same time. The small core NA can suppress the HOMs number which can be excited in fiber core during the amplification while the bigger inner clad NA can help to increase the pump light coupling efficiency.

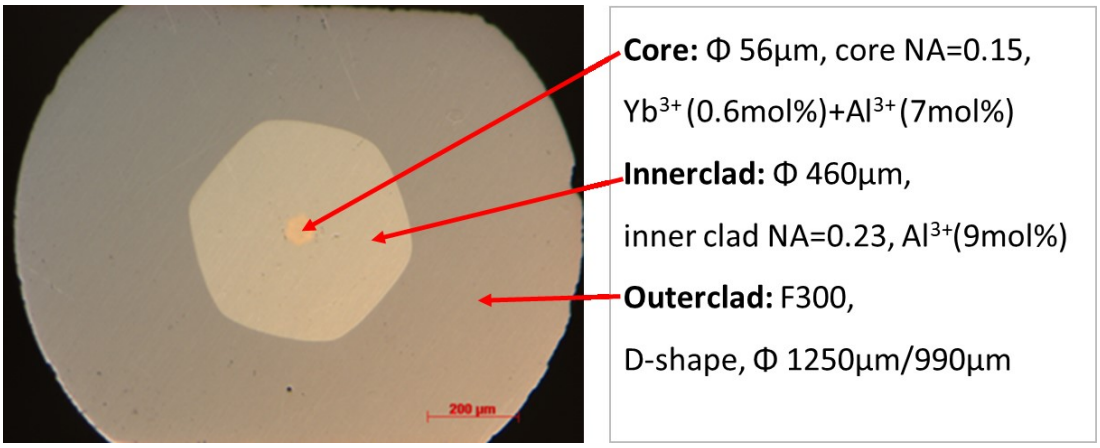

Figure 7.3. Cross-section of LMA fiber.

A thin fiber with an outer clad diameter of 120µm was drawn from the same preform of this rod type fiber for characterization purposes. The refractive index was measured with a commercial York S14 refractive index profiler. The refractive index profile of the 120µm thin fiber (figure 7.4) shows that the REPUSIL process delivers a homogenous step index profile with a core NA of 0.15 and a pump NA of 0.23. The rounded shape of the core refractive index profile is a result of the limited spatial resolution of the index profiler S14 and due to a certain amount of dopant diffusion during fiber drawing. The rod-type fiber which is produced from the same preform of thin fiber should have a similar refractive index profile and the same core/clad NA value.

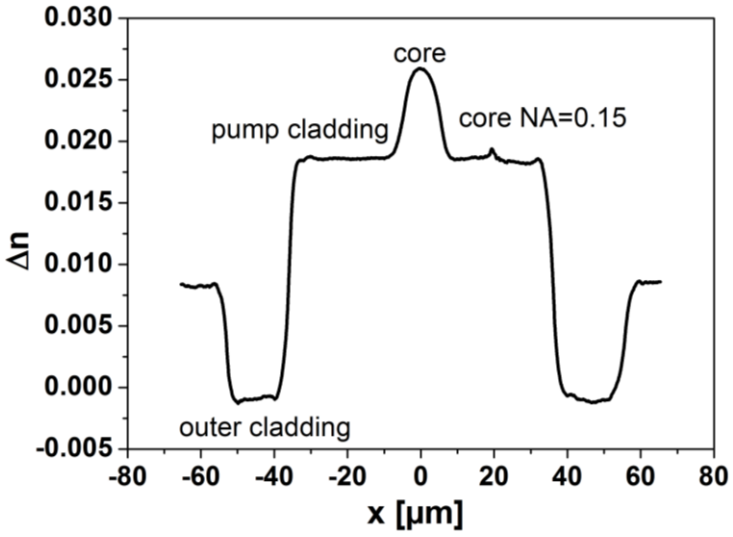

Figure 7.4 Refractive index profile of the 120μm outer diameter thin fiber.

The rod-type fiber core diameter is 56μm with a 40μm mode field diameter (MFD). The fiber core NA is 0.15 which is relatively high according to the targeted core numerical aperture (NA) of approximately 0.08. Even though this fiber is not perfect, it can be tapered to the right MFD, close to the value of the seed fiber. Therefore, our investigation and experiments begin with this fiber. After drawing the LMA fiber, the fiber parameters, such as fiber geometry parameters, refractive index profile, are characterized first. Then the fiber is carefully checked for defects and bubbles inside the fiber which are marked. Finally, the fiber is cut into several pieces as the fiber samples. Normally the fiber sample pieces should not contain detectable bubbles or defects.

7.2.2 Characterization of the non-tapered reference fiber

(1) Fiber sample parameters

As is shown in figure 7.5, the non-tapered reference fiber sample has a length of 60cm. One end facet of fiber (pump coupling) is polished with 8 degrees angle while the other side of fiber (seed coupling) is polished with 4 degrees. The pump with multi pump module (200μm core diameter and 0.22 core NA) is used to supply the pump power for fiber amplifier. The pump product of the rod fiber (460μm pump clad diameter and 0.23 pump clad NA) is 105.8 which is higher than the pump product of pump delivery fiber with the value of 44. Therefore, the pump clad of rod fiber can accept the pump brightness of the multi pump module. A pair of lenses with 7.5mm and 40mm focal length is used to couple the seed light while a pair of lenses with 30mm and 30mm focal length is used to couple the pump light inside the rod fiber with free space coupling method.

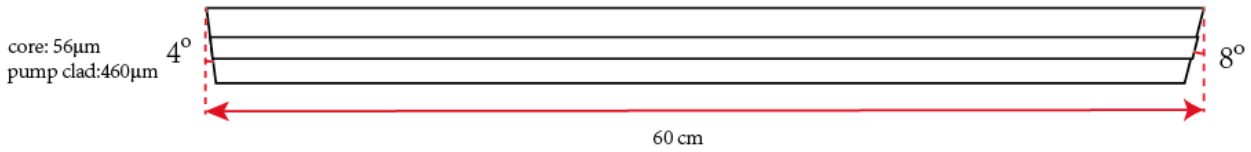

Figure 7.5 Schematic of non-tapered reference fiber

(2) Experiment results

The slope efficiency was characterized first (figure 7.6) and the output power is plotted vs. the absorbed pump power. This absorbed pump power was estimated based on assumed 90% pump coupling efficiency and the measured residual pump power from the non-tapered amplifier. The slope of the non-tapered amplifier displays a slope efficiency of 83% vs. the absorbed pump power. The highest output power reached 28W under 61W of coupled pump power, corresponding to a peak power of 544kW and a pulse energy of 1.4mJ. The single-pass gain based on average output power of this non-tapered rod fiber amplifier is 23dB. The launched pump power is the pump power before the focus lens which couples the laser light inside the fiber.

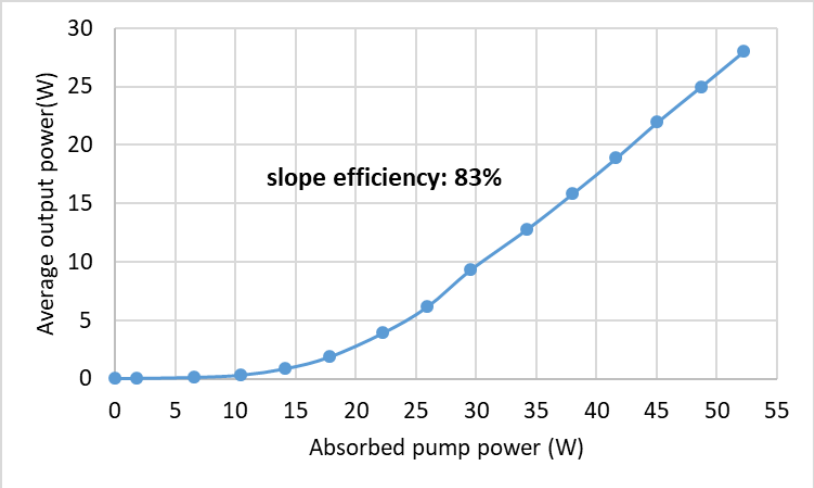

Figure 7.6 Average output power versus the absorbed pump power

The peak power is an important parameter for fiber amplifier, but one cannot easily measure the peak power. Therefore, the following strategy is developed to calculate the peak power based on the relationship between the peak power of pulses and the pulse energy: (1) measure the pulse shape and pulse peak value $Peak_{pulse}$ (unit: V) by photodetector several times (for example: 10 times) and get an average pulse shape. (2) integrate the pulse shape to get the pulse area $Area_{pulse}$ (unit: V·ns) and find out the peak power $Peak_{pulse}$ (unit: V). (3) calculate the average single pulse energy E_{pulse}

(unit: nJ or W·ns) by averaging the output power $P_{average}$ (unit: W) and the repetition rate f (unit: Hz). (4) then calculate the peak power P_{peak} (unit:W) according to the equation 7.4 which contains all discussed parameters above.

$$P_{peak}(W) = E_{pulse}(nJ) * \frac{Peak_{pulse}(V)}{Area_{pulse}(V \cdot ns)} = \frac{P_{average}(W)}{f(Hz)} * \frac{Peak_{pulse}(V)}{Area_{pulse}(V \cdot ns)} \quad (7.4)$$

The figure 7.7 shows the direct efficiency, the overall efficiency, and the pump absorption efficiency which are defined as follows. The direct efficiency is the signal power divided by the absorbed pump light. The overall efficiency is the signal power divided by the launched total pump power. The direct efficiency means the ratio of absorbed pump power which can converse to the signal power, while the overall efficiency is based on the total pump power which supports the amplification process. Both, the direct efficiency and the overall efficiency are increasing with the increasing launched pump power. The direct and overall efficiencies under 67W launched pump power were 54% and 42% respectively. The absorption of pump power drops from 85% to 78%. The clad absorption at 976nm based on the pump absorption efficiency in figure 7.7 varies between 21dB/m and 15dB/m which is lower than the theoretical calculation value of 40dB/m because of the pump power saturation and the pump modes with low core overlap.

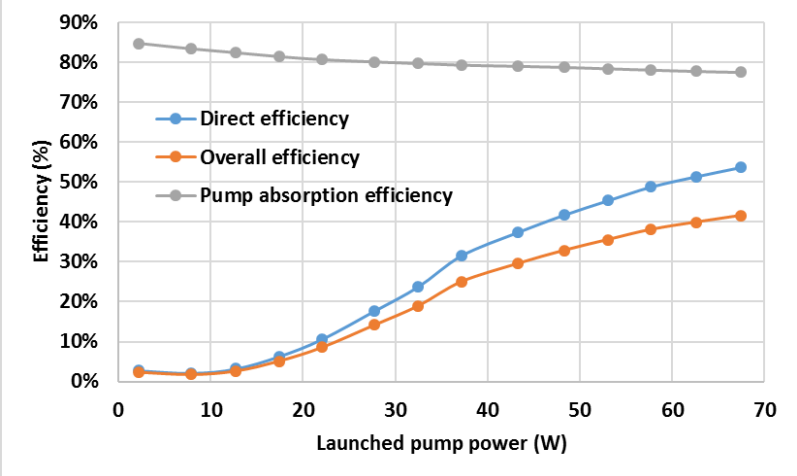

Figure 7.7 Direct efficiency, overall efficiency and pump absorption efficiency as a function of the launched pump power.

As the launched pump power and amplified signal power increase, the temperature of the rod fiber end facet increases at approximately 1K/W pump power which is measured by a thermal cameral. The heat accumulation mainly comes from the quantum defect.

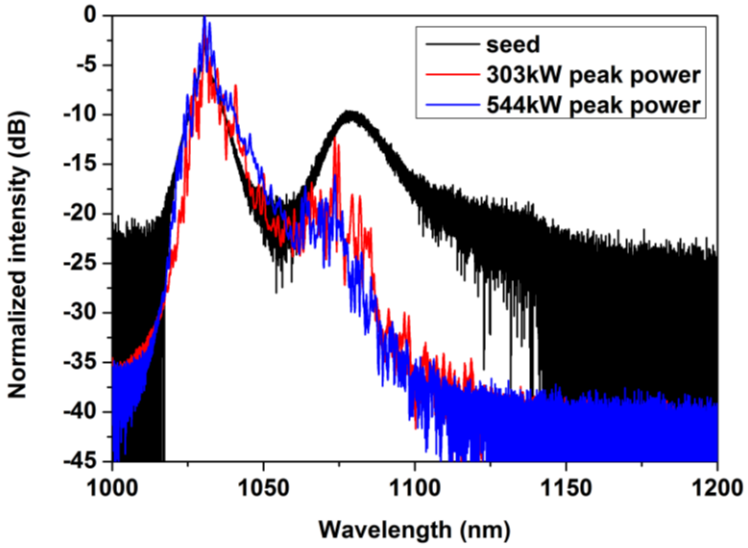

Figure 7.8 Optical spectrum of seed and amplified light

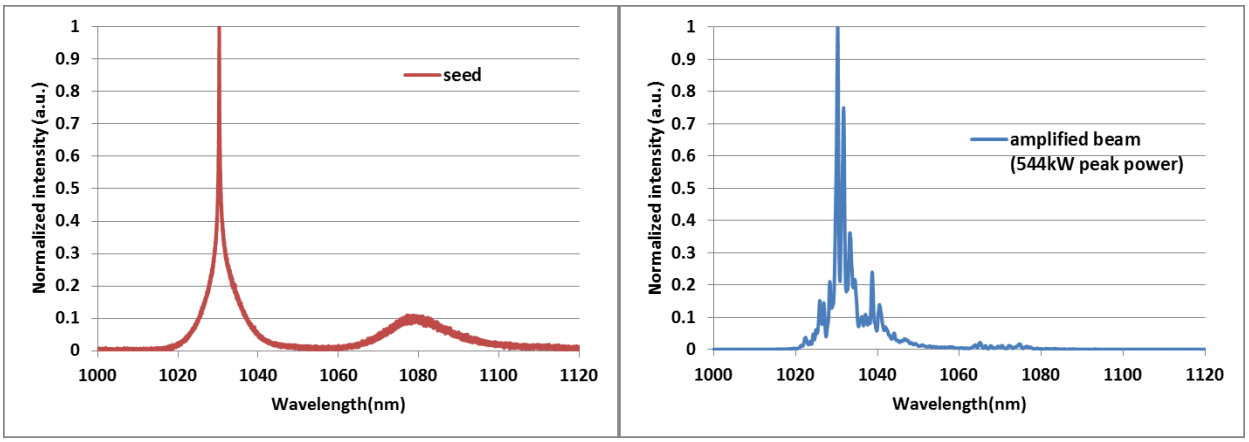

Figure 7.9 Comparison of the normalized linear spectra between seed and amplified light

The normalized spectrum of the amplified signal is shown in Figure 7.8. The stimulated Raman scattering (SRS) effect is observed around 1080nm wavelength where is the first Stokes peak. For the seed, the difference between the main signal peak and the SRS is less than 10dB difference. For the amplified signal with 544kW peak power, the difference between the main signal peak and the SRS peak is 18dB. The SRS effect is suppressed in the main amplifier due to the large MFD and short fiber length. During the amplification process, the gain of the signal wavelength (1030nm) is much larger than the gain of the laser light in Stokes peak (1080nm). The Raman gain value is very small and close to zero. The comparison of normalized spectrum in linear scale is shown in Figure 7.9. Roughly 41% of the power are in the seed spectrum and 6% of the power for the amplified laser beam are in the SRS region around 1080nm.

The normalized pulse shape of the amplified laser light is shown in Figure 7.10. Normally only a small portion of the output laser beam is coupled out, then the pulse shape is measured after it is attenuated to a safe power level. The saturation energy (see equation 3.14) of this type fiber (999c) is 0.242mJ at a wavelength of 1030nm theoretically. The pulse with 544kW peak power has a pulse energy of 1.4mJ which is much higher than the saturation energy. Therefore, the fiber amplifier is saturated as the pulse is amplified further. The saturation effect dominates the pulse shape, the leading edge of the pulse consumes the stored energy very quickly, while the tail edge cannot obtain the same gain. As a result, the pulse shape is distorted with a very sharp rise at the leading edge.

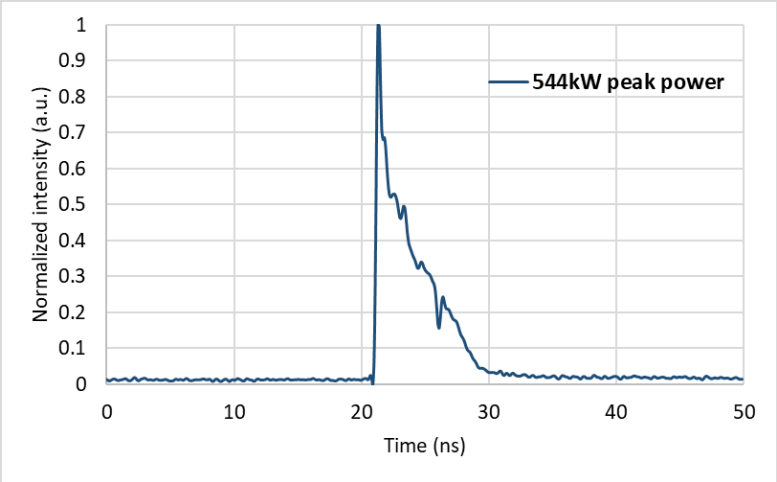

Figure 7.10 Pulse shape of amplified light with 544kW peak power

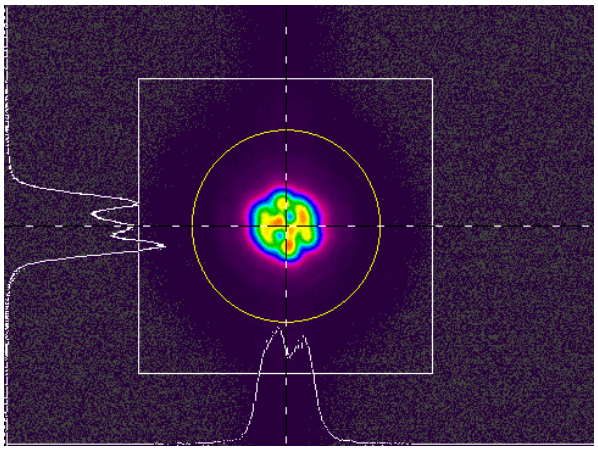

Figure 7.11 Beam pattern of the output light with 28W output power (544kW peak power).

Finally, the characterization of the beam quality was performed using a Spiricon M2-200s automated M^2 laser beam propagation analyzer. The measured beam quality (M^2 value) strongly

depends on the exact seed coupling condition for free space coupling. All measured results shown here are optimized values obtained by careful adjustment of the seed coupling. The figure 7.11 shows the beam pattern at the output power of 28W (corresponding to 544kW peak power) under 67W launched pump power which is highly multimoded with an M^2 value of 10.8 (x axis) and 11.4 (y axis).

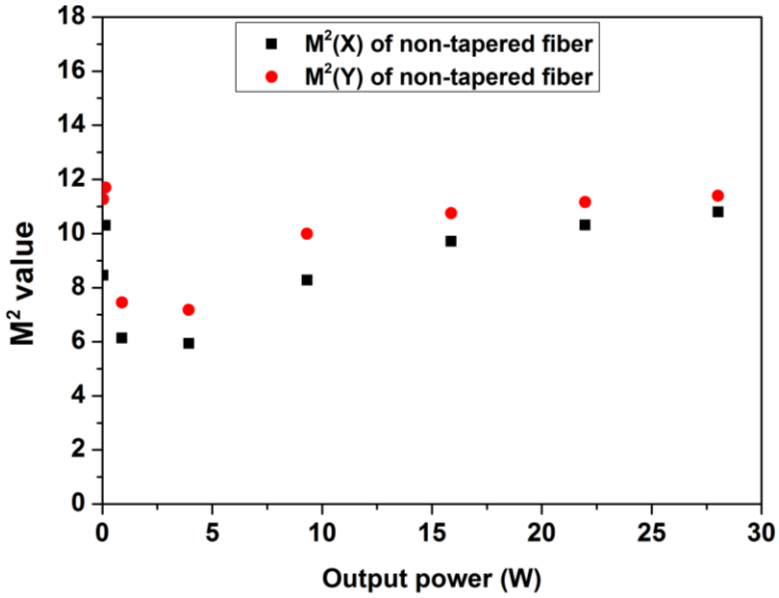

Figure 7.12 Measured beam quality for the non-tapered amplifier

The beam quality (M^2 value) of the amplified laser beam varies from 6 to 12 for different output powers (figure 7.12). At low output power, the beam quality is around 10. Some part of seed power is leaked into the pump cladding. The seed light in the fiber core is strongly absorbed and the seed light in the pump clad has a small loss which disturbs the beam quality measurement results. The seed light in fiber core can be absorbed and re-emitted again due to signal reabsorption which can also influence the beam quality. Above the amplifier threshold, the M^2 value decreases and achieves the best result of around 6 at 4W output power. In this power range, the FM and the HOMs can get similar gain due to the similar overlap factor with the active core. The beam quality (M^2 value) becomes worse again when further increasing the output power. The spatial hole burning effect appears and the gain shape in fiber active core is distorted due to the saturation effect. The excited atoms in the center region of fiber core are highly consumed by the FM, while the remaining excited atoms on the edge of fiber core provide higher gain for some HOMs, thereby spoiling the beam quality.

Despite the efforts in optimizing the seed coupling alignment, the best result of beam quality (M^2 value) at the highest output peal power (544kW) was between 10 to 12. The free space coupling of the seed laser light is not mode selective enough (i.e. HOMs are always excited with a certain percentage) which leads to this highly multi-HOMs operation in rod fiber amplifier.

7.2.3 Beam quality improvement with a tapered rod type fiber amplifier

7.2.3.1 Characterization of tapered rod fiber

(1) Adiabatic taper design and estimation

The coupling calculation of the fundamental mode to the next three higher order modes according to the adiabatic taper length criterion (equation 5.10) is shown in figure 7.13(a) which is also the boundary limitation of the taper angle according to different taper local diameters. Especially the coupling between LP01 and LP02 by conservation of azimuthal symmetry and the coupling between LP01 and LP11 through a broken azimuthal symmetry are calculated. The region below the curve of LP01 vs LP11 corresponds to the adiabatic region. The local real taper angle should always be contained in the adiabatic region.

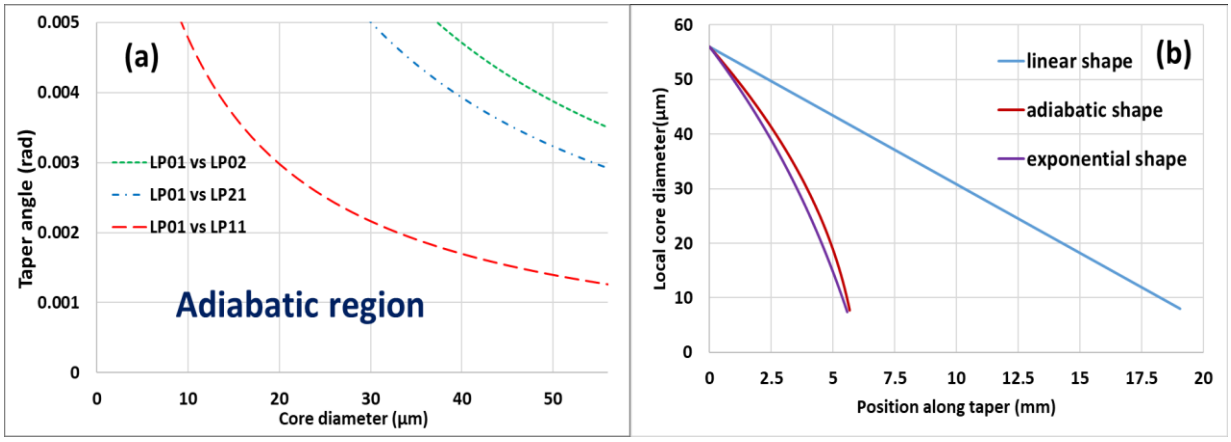

Figure 7.13 (a) Adiabatic region due to theoretical coupling calculation. (b) Theoretical calculation for different taper shape (999c)

The Figure 7.13(b) shows the theoretical calculation for different taper shapes of the local adiabatic taper. The minimum taper length for adiabatic shape is 5.7mm whose local taper angle satisfies the minimum critical adiabatic angle everywhere along the taper. If the taper shape is exponential shape, the minimum taper length is 5.8mm. The linear shape means the taper shape is linear and follows

the smallest taper local angle in adiabatic region. The minimum taper length for linear shape is 19.0mm. Normally it is good to have a local taper length longer than 19mm which has a safe margin for taper to keep the adiabatic property.

(2) Identification of local short taper

In order to maintain the diffraction limited beam quality while scale up the peak power, the rod-type fiber is tapered down to the single-mode region for seed coupling. The local adiabatic taper provides a monolithic signal path and should improve the beam quality significantly.

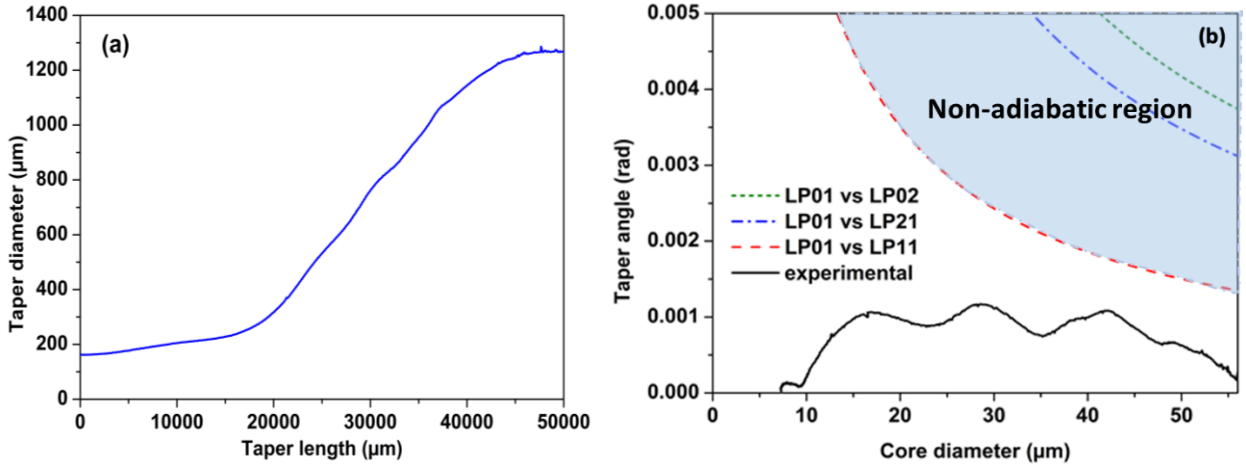

Figure 7.14. (a) Measurement of the outer taper radius as a function of the taper length. (b) Core taper angle as function of the core radius, including the adiabatic taper length scale criterion for coupling of the fundamental mode to the next three higher order modes.

Figure 7.14(a) shows the measured outer taper diameter against the taper length. On the whole, the taper shape is smooth. In order to check if the taper satisfies the adiabatic criterion or not, the angular profiles between the experimentally realized fiber taper and the adiabatic thresholds are compared. As shown in figure 7.14(b), the core taper angle is plotted as a function of the core radius. The black line is derived from the real taper shape (figure 7.14(a)), assuming that core diameter and outer taper diameter change proportionally. The other colored graph shows the adiabatic limit for coupling of the fundamental mode to the next three higher order modes according to the adiabatic taper length criterion. The experimentally realized taper angle is always smaller than the adiabatic threshold which means the taper shape should be smooth enough that the FM profile can

smoothly evolve inside the taper core, and no power coupling happens between FM and HOMs in theory. However, potential diffusion and bend effects are not considered here.

(3) Splice between taper and standard single mode fiber

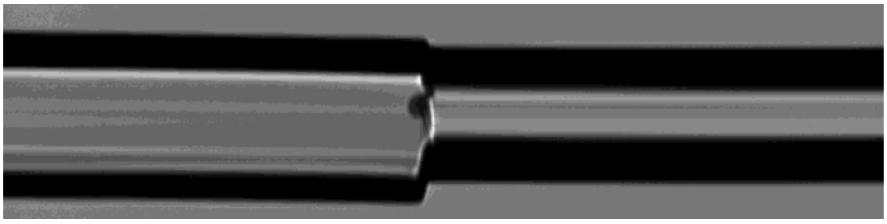

Figure 7.15. Splice between standard SM fiber (left) and the fiber taper waist (right).

The seed power is delivered by a standard SM fiber (10/125μm) which only guides the FM. The seed delivering fiber is directly spliced to the taper waist for seed coupling. The advantage of this technology is to provide a monolithic signal path for robust working environments. The splice point between the standard single mode fiber and the tapered fiber waist is shown in figure 7.15. The picture shows that the taper waist is a little smaller than the SM fiber. According to figure 7.23(b), the taper waist has a core diameter of 10μm and a core NA of 0.07 due to the diffusion. Then the V parameter of the taper waist is 2.14 (below 2.405) which is in single mode region. Figure 7.15 shows that the core diameter of taper waist is smaller than that of the seed delivery fiber. There are two reasons for this small core diameter of taper waist: 1. The rod fiber is tapered down to a smaller value than seed delivery fiber which brings it to single mode operation without HOMs due to the large core NA. 2. The diffusion phenomenon (figure 7.23) discussed in chapter 7.2.3.3 leads to a larger core diameter compared with the estimated core value of the taper waist. Therefore, it is good for mode matching if the fiber is tapered down to a smaller value.

(4) Schematic of tapered fiber amplifier

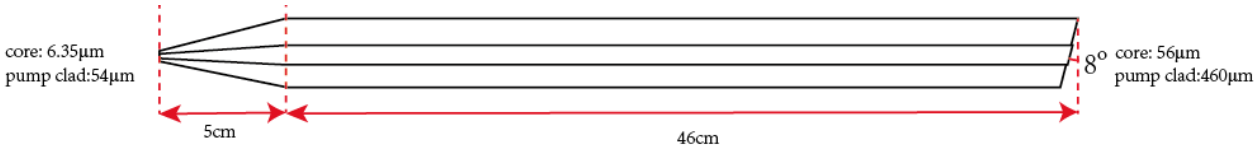

Figure 7.16 Schematic of the tapered rod fiber 999c

As is shown in figure 7.16, the non-tapered fiber sample which is discussed in section 7.1.1 is tapered down on the left side. The length of this tapered fiber sample is 51cm which includes a 5cm

taper length and a 46cm rod length. Several centimeters of fiber length are lost when preparing the taper on the rod fiber, therefore the tapered fiber is shorter than the original rod fiber. At the taper waist position, the core diameter is 6.35μm, the pump core diameter is 54μm, and the outer diameter is 143μm. The end facet of this tapered fiber (for pump coupling) is polished with an 8 degrees angle to avoid back reflections at the output facet. The pump with multi pump module (200μm core diameter and 0.22 core NA) is used to supply the pump power for the fiber amplifier. A pair of lenses with 30mm focus length each is used to couple the pump beam inside the rod fiber with free space coupling method.

(5) Near field and far field characterization

After splicing the taper with the standard SM fiber, the beam profile is measured in the near field and in the far field. The mean value of the beam pattern diameter calculated with 4σ method is 52μm according to the near field measurement. The divergence angle according to the far field measurement is 0.062rad. Notice that the wavelength of reference laser beam here is 1060nm. Then the BPP and the M^2 value can be estimated using the following equations to be 4.

$$BPP = (0{,}052mm/2) * 62mrad = 1.6mm\,mrad \tag{7.5}$$

$$M^2 = \pi * BPP/1{,}060\mu m = 4 \tag{7.6}$$

7.2.3.2 Results of tapered rod fiber amplifier

The ability of peak power scaling of the tapered fiber amplifier is tested first (see figure 7.17). The pump power was estimated based on a 90% pump coupling efficiency. The residual pump power cannot be directly measured. Therefore, it was estimated according to the analysis from the non-tapered amplifier assuming a constant absorption coefficient along the fiber. The tapered amplifier shows a slope efficiency of 60% vs. the absorbed pump power. The highest output power reached 10.3W under 44W of launched pump power, corresponding to a peak power of 230kW and a pulse energy of 0.5mJ which is still higher than the saturation energy of 0.242mJ. The efficiency of the tapered amplifier appears to be slightly lower, compared with the non-tapered fiber amplifier. However, the amplifier has not yet established a clear linear slope.

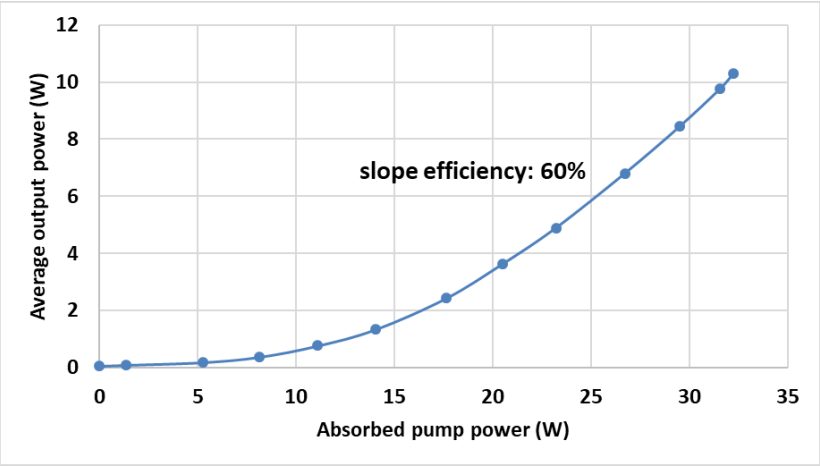

Figure 7.17 Average output power versus the absorbed pump power

As shown in figure 7.18, the direct and overall efficiencies under 44W launched pump power were 32% and 23% respectively. The estimated absorption of pump power drops from 81% to 73%. The fiber end face is burned already with lower pump power and at lower output power level compared with the non-tapered fiber amplifier. This is not very surprising, because the effective mode area of laser beam is smaller due to the improved beam quality which will be shown later. The power density is therefore higher and the fiber facet damage threshold is reached at a lower power level.

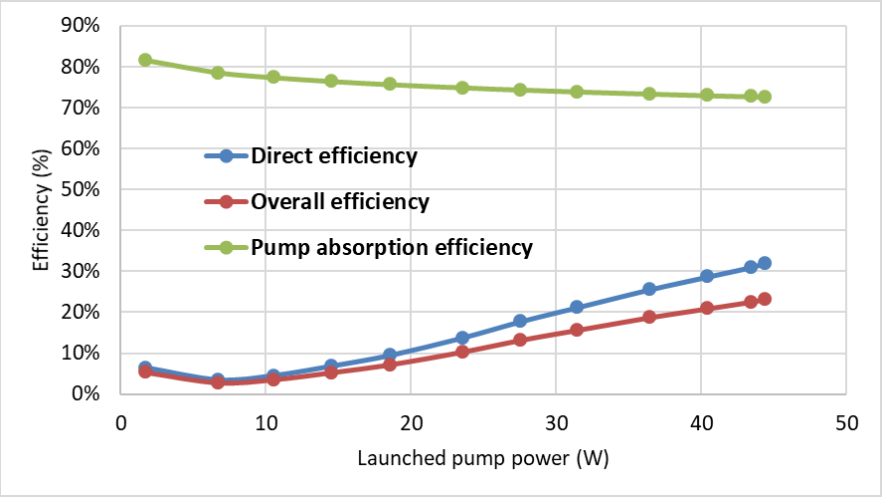

Figure 7.18 Direct efficiency, overall efficiency and pump absorption efficiency as a function of the launched pump power.

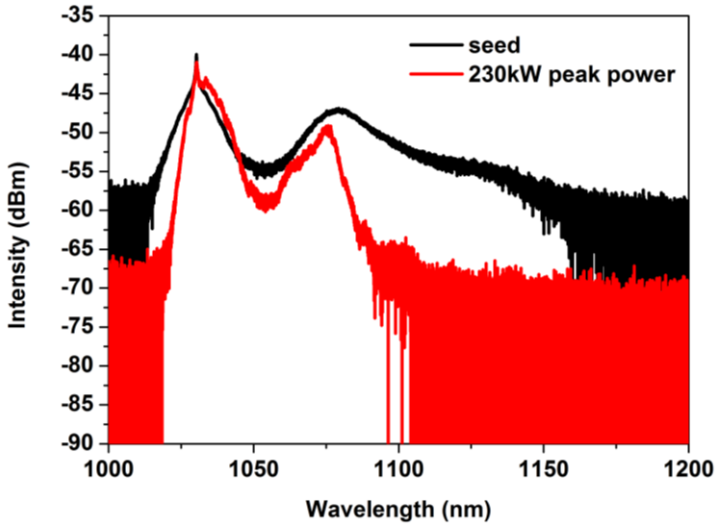

Figure 7.19 Optical spectrum of seed and amplified light

The spectrum of the amplified signal is shown in Figure 7.19. Compared to the seed spectrum, the difference between the main signal peak and the 1st Stokes peak is increasing. The SRS effect is suppressed in the main amplifier, but is still obvious. The comparison of the normalized spectrum in linear scale is shown in Figure 7.20. Roughly 41% of the power for seed spectrum and 22% of the power for amplified spectrum with 230kW peak power are in 1st Stokes region around 1080nm.

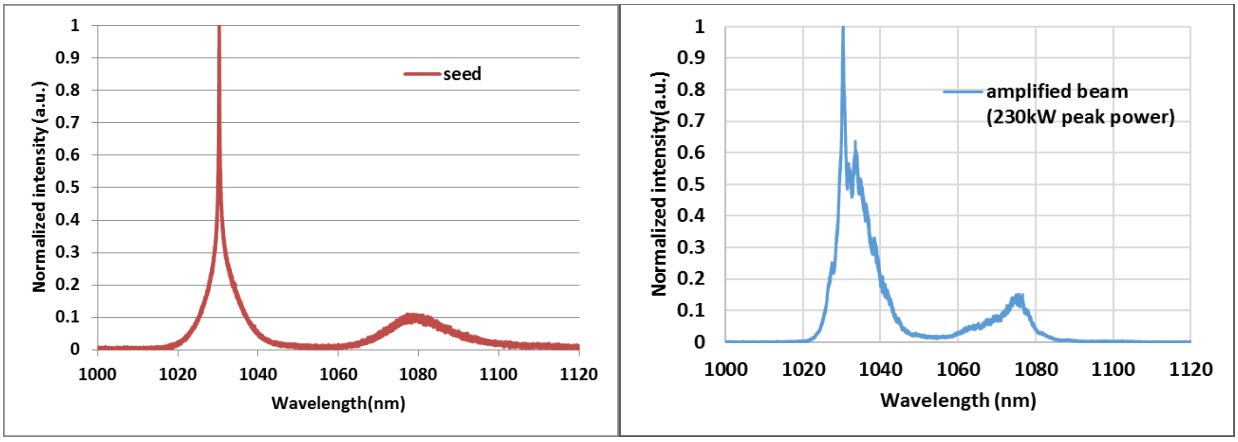

Figure 7.20 Comparison of the normalized linear spectra between seed and amplified light

The beam pattern at the highest output power (230kW) is shown in figure 7.21 with the corresponding beam quality (M^2 value) 3.2/3.5. The beam pattern is distorted due a few the excited HOMs.

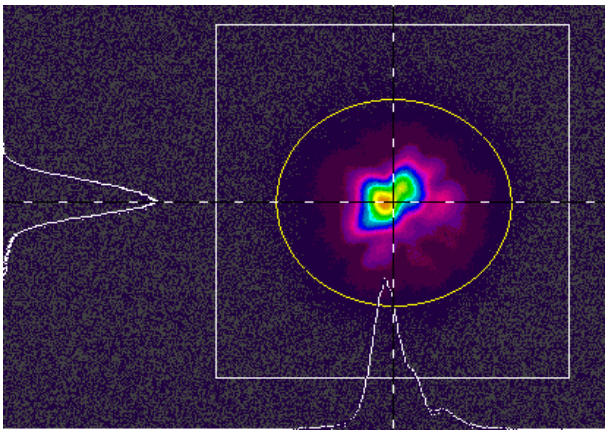

Figure 7.21 Beam pattern of the output light with 10.4W output power (230kW peak power)

In order to compare the results of the non-tapered and tapered fiber amplifiers, the beam quality (M^2 value) is plotted versus the average output power in Figure 7.22. The optimized beam quality of the non-tapered amplifier is between 6 and 12 and quite power dependent. The M^2 values for the tapered rod are between 2.5 to 4 with much higher stability compared to the free space coupling to the non-tapered fiber. For similar average output power of about 10W, the beam quality improves from values near 10 to approximately 3.5. The improvement of the beam quality depends critically on the suppression of coupling to HOMs and therefore on the quality of the taper and the splice to the seed fiber.

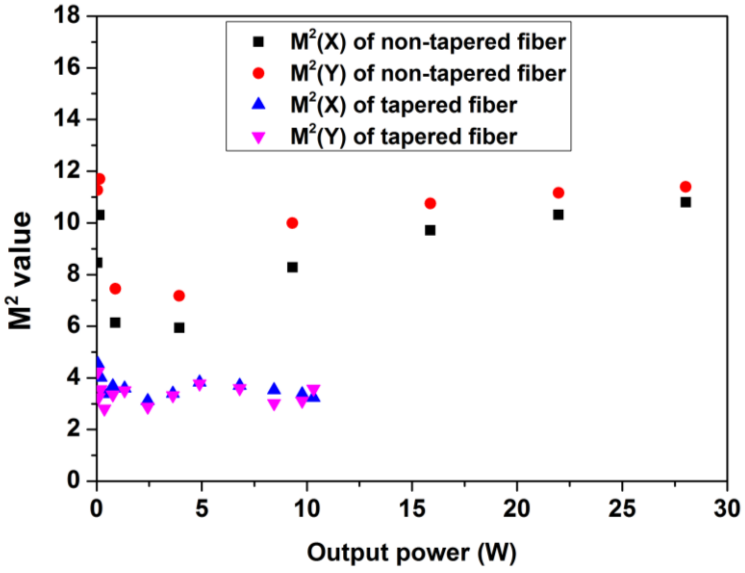

Figure 7.22 Measured beam quality for tapered fiber amplifier and non-tapered fiber amplifier

7.2.3.3 Investigation of dopants diffusion

Even though the beam quality is improved to 2.5 to 4 with use of a local adiabatic taper, the beam quality is still far away from the target value ($M^2 \leqq 1.5$). Some investigations have been done to find out the reasons behind. All theoretical calculation and estimation so far do not consider the possible change of the NA and the fiber core geometry (other than the direct taper reduction). For clarification, the following measurements were performed.

The Yb^{3+}-distribution of the taper waist was compared to that of the non-tapered rod (blue curve in figure 7.23(a), dimensions scaled down by taper ratio). It is clearly visible that the Yb_2O_3-distribution after the heat treatment (red curve in figure 7.23(a)) is characterized by strong diffusion. This is also indicated by the fact of that the core NA decreases from the initial value of 0.15 to 0.07, while the core radius is in the range of 10µm and larger than expected from the taper ratio (7µm). By excessive heating during the tapering, the fiber core can even vanish completely in the worst case.

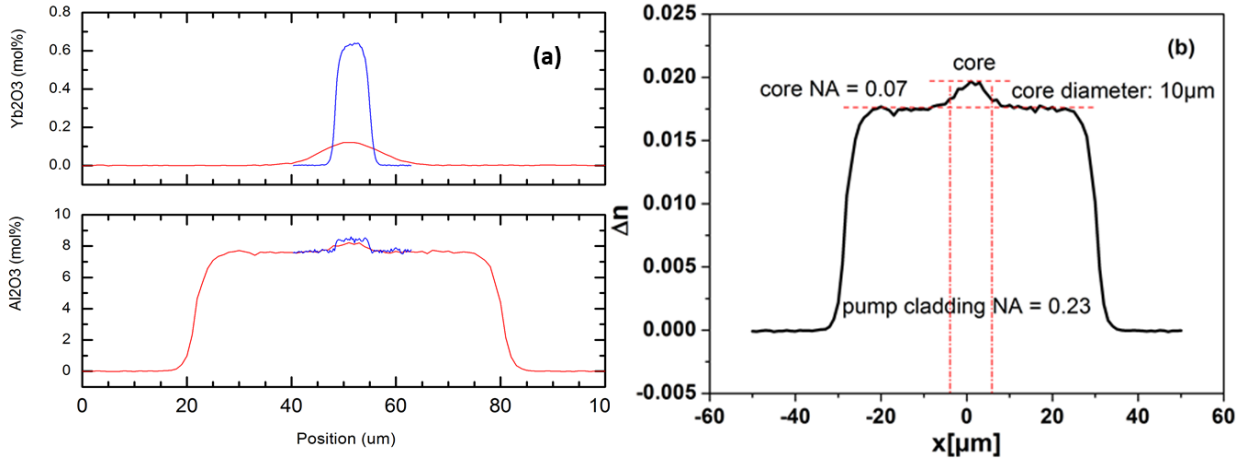

Figure 7.23 (a) Comparison of dopant concentration, blue line is the rod (dimensions scaled down by taper ratio) and red line is the taper waist. (b) Refractive index profile of the taper waist showing a reduced core NA

It is assumed that the main reason for the improvement of beam quality with the use of taper significantly depends on the quality of taper producing and the seed coupling with the splice. There always exists a certain amount of dopant diffusion during tapering process which can change the fiber properties. But the dopant diffusion can be effectively mitigated by optimizing the fiber design which is discussed in the following with a new designed LMA fiber.

7.3 Fully doped rod-type fiber with optimized fiber design (854b)

7.3.1 Improvement of fiber design and parameters of rod type fiber

(1) Theoretical calculation and improvement of fiber design

In order to mitigate the influence of diffusion according to the investigation of the fiber 999c, several improvements are made for a newly designed fiber which includes (1) Reduction of the Al^{3+}-content in the core and the inner clad to decrease the diffusion effect. (2) Reduction of the glass transition temperature of the outer clad to reduce the tapering process temperature. (3) Reduction of the core NA to that of the seed fiber to reduce the number of HOMs and allow mode matching and single-mode taper waist at the splice.

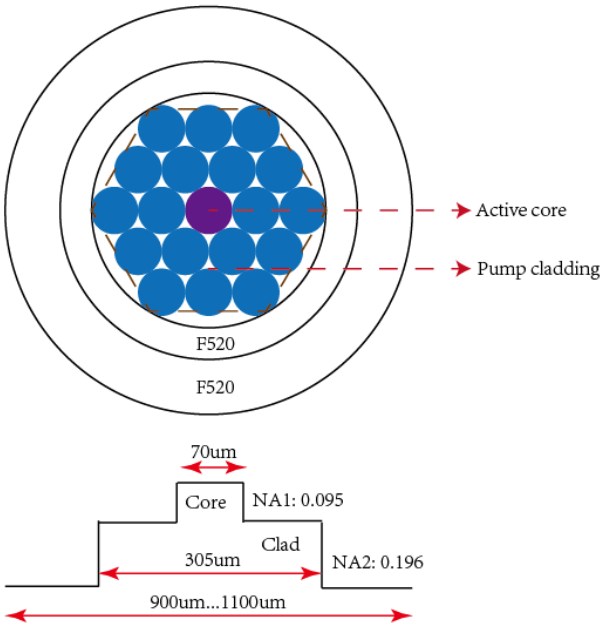

Figure 7.24 New fiber design: stacking geometry of the preform and refractive index profile of the drawn fiber.

The refractive index profile of the fiber is shown in figure 7.24. The Al^{3+}-content in the fiber components is the main factor which induces the diffusion during the tapering and splicing process. Because the Al^{3+} is a glass modifier in glass components, it dominates the dopants distribution and the homogeneity of glass. The reduction of the Al^{3+}-content can increase the transition temperature of the fiber core and inner cladding to suppress the diffusion of dopants. Therefore, the active core and the passive inner cladding rods adopt a lower Al^{3+} content compared with the fiber used in chapter 7.2. The outer tube glass uses F520 silica glass (Heraeus) which contains fluorine. The

F520 tube has a relatively low melting temperature which can help to decrease the process temperature during the tapering and the splice process to mitigate the diffusion phenomenon. The stacking profile of the preform is shown in figure 7.24. The central rod is active (Yb^{3+}-doped) which serves as fiber core. The two layers of passive rods will serve as the fiber inner cladding for the pump coupling. Two tubes with the same material F520 are used to over-clad the rods packing and serve as outer clad for fiber. The rods are stacked in a hexagonal shape and the core to clad diameter ratio is 1:4.3. On the basis of the composition of the fiber material, the estimated core NA is 0.095 while the estimated pump core NA is 0.196. Finally, the preform package is drawn to the desired fiber size.

(2) Parameters of rod type fiber (854b)

This rod-type double-clad fiber (fiber code: 854b) has a 45µm core, a 200µm inner cladding, and a 785µm outer diameter (see figure 7.25). The shape of the core and the inner cladding is hexagonal, because the preform of fiber is stacked in hexagonal shape with Repusil rods. This hexagonal shape can also help to improve the pump power absorption by suppressing helical pump modes. According to the calculation, the diameter of the effective mode area due to FM is 34µm. The theoretical power scaling (figure 7.2) is limited to 400kW according to the damage threshold and to 700kW according to the SRS limit of the fiber with a MFD of 34µm. An end cap for the fiber can be used to enhance the damage threshold.

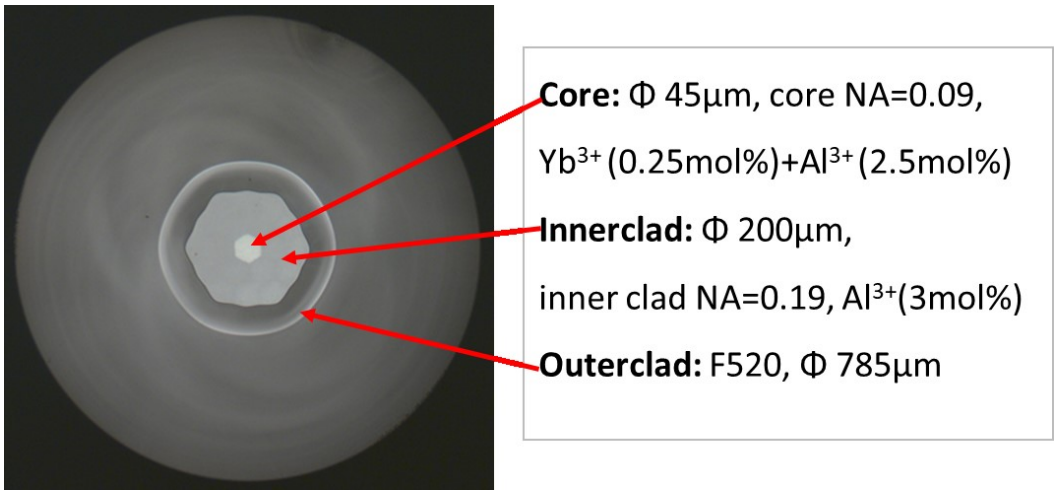

Figure 7.25. Cross-section of the LMA fiber.

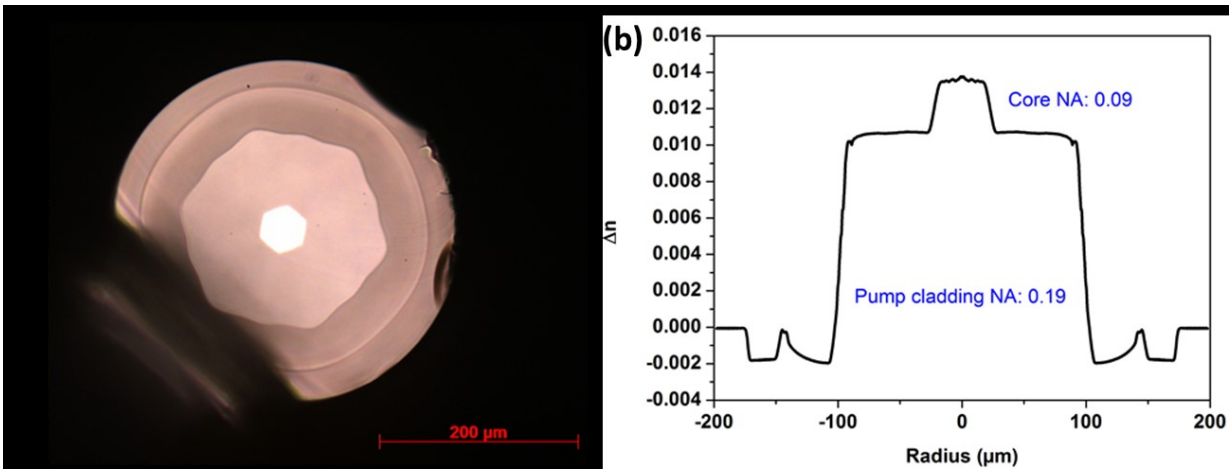

Figure 7.26 (a) End face of etched rod fiber. (b) Refractive index profile of the rod fiber.

The active core of the rod fiber contains 0.25mol% Yb_2O_3 and 2.5mol% Al_2O_3 and the passive inner cladding contains 3mol% Al_2O_3. The Al^{3+} dopants can help to elevate the refractive index of the inner cladding to decrease the core NA, because the Yb^{3+} concentration in the active core increases the refractive index of the core significantly. Compared to the fiber used in chapter 7.2, the Al^{3+} content is much lower and the Yb^{3+} also is relatively low, because the Al^{3+}-dopants dominate the solubility of the Yb^{3+}-ions. Even though this fiber has a lower Yb^{3+}-concentration, the unsaturated clad absorption at 976nm is 61dB/m in theory due to the high core to clad ratio. In order to measure the refractive index profile (figure 7.26(b)) using the index profilometer (Interfiber Analysis IFA-100 technology), the rod fiber is etched to 400µm outer diameter. The result shows that the fiber made by REPUSIL achieved a very homogenous step index profile with a core NA of 0.09 and a pump NA of 0.19.

7.3.2 Characterization of non-tapered reference fiber amplifier

(1) Fiber sample parameters

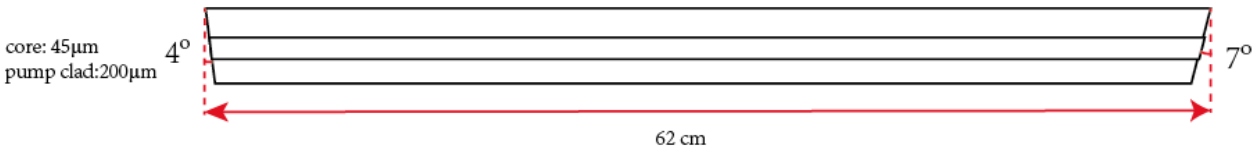

Figure 7.27 Schematic of rod fiber 854b

As is shown in figure 7.27, the non-tapered rod reference fiber has a length of 62cm. One end facet of the fiber (pump coupling) is polished with a 7 degrees angle while the other side of the fiber

(seed coupling) is polished at 4 degrees. The pump with single pump module (105μm core diameter and 0.16 core NA) is used to supply the pump power for the fiber amplifier. A pair of lenses with 7.5mm and 25mm focal length is used to couple the seed light while a pair of lenses with 25mm and 30mm focal length is used to couple the pump light inside the rod fiber with the free space coupling method.

(2) Experiment results

The slope efficiency was characterized first (Figure 7.28) and the output power and the peak power is plotted vs. the absorbed pump power. The absorbed pump power was estimated based on a 90% pump coupling efficiency and the measured residual pump power. The maximum output average power with this rod-type fiber is 13.8W with 30W launched pump power which is corresponding to a gain of 20dB based on average output power. The measured slope efficiency is 72% with respect to the absorbed pump power. The peak power of the pulses increases with increasing average output power. The highest peak power achieved with this rod-type fiber is 210kW with 0.69mJ pulse energy. The saturation energy of this type fiber is 0.175mJ at a wavelength of 1030nm theoretically which is much lower than the highest achieved pulse energy with this non-tapered fiber amplifier.

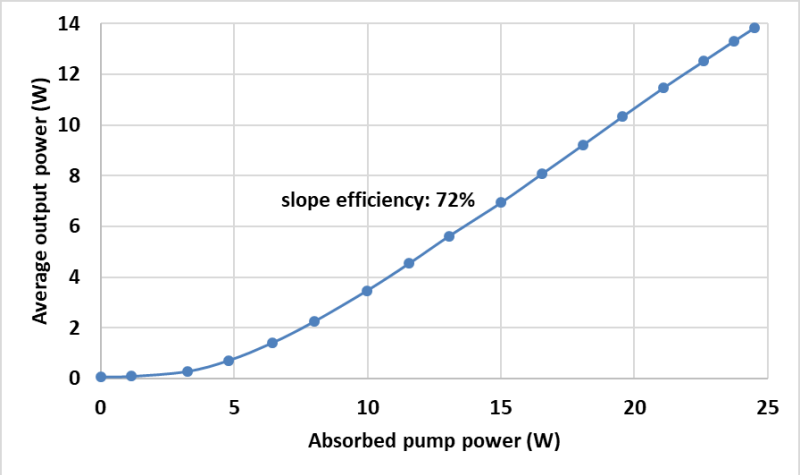

Figure 7.28 Average output power versus the absorbed pump power

The figure 7.29 shows the direct efficiency, the overall efficiency and the pump absorption efficiency. The absorption of the pump power drops from 88% to 82% due to the absorption saturation. Both, the direct efficiency and the overall efficiency are increasing with the increasing

pump power. The highest values are achieved with 30W of launched pump power and reached 56% and 46%, respectively. The clad absorption at 976nm based on the pump absorption efficiency in figure 7.29 varies between 28dB/m and 17dB/m which is lower than the theoretical calculation value of 61dB/m because of the pump saturation and the pump modes with low core overlap. This fiber gets much better beam quality (see figure 7.34) and the effective mode field area is much smaller, therefore the power density is much higher and the material damage threshold is reached at a lower peak power level.

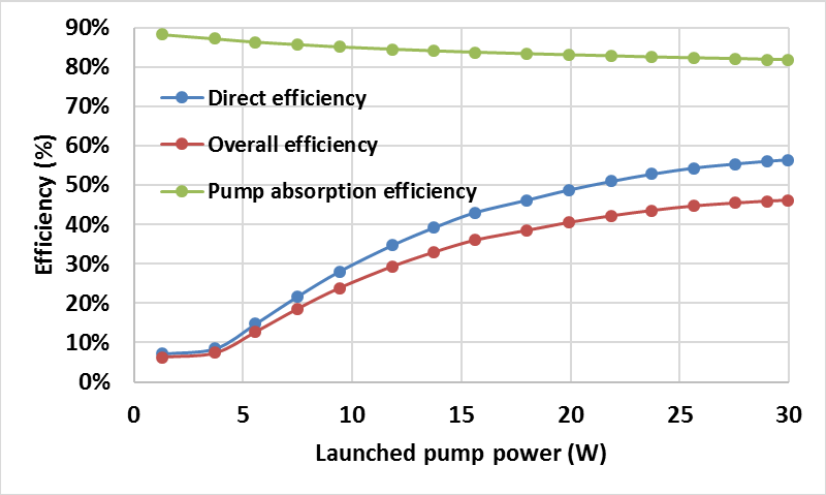

Figure 7.29 Direct efficiency, overall efficiency and pump absorption efficiency as a function of the launched pump power.

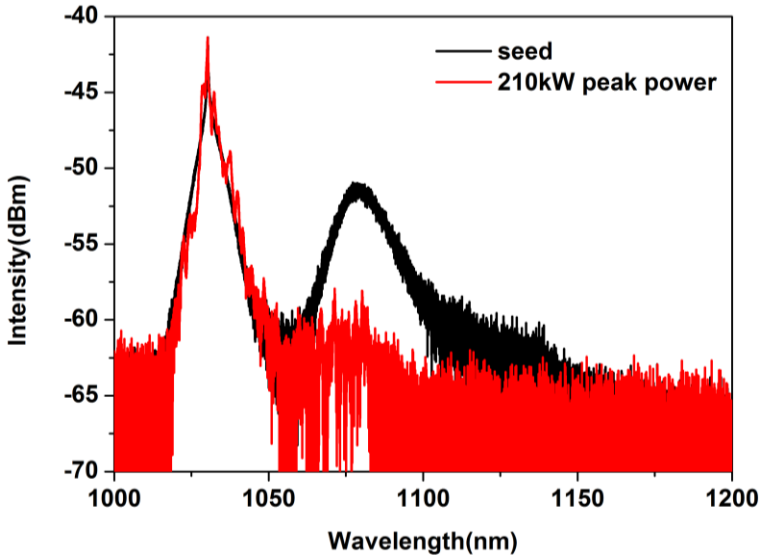

Figure 7.30 Optical spectrum of seed and amplified light

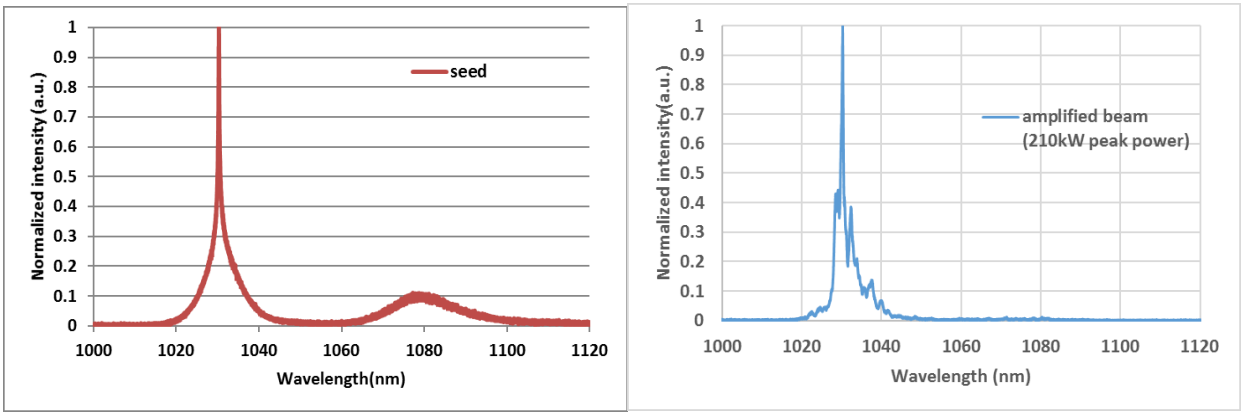

Figure 7.31 Comparison of the normalized linear spectra between seed and amplified light

The spectrum of the seed and amplified signal is shown in Figure 7.30. Compared to the seed, the SRS peak is diminished and suppressed during the amplification process with the highest output peak power. For the seed, the difference between the main signal peak and the SRS peak is less than 10dB. For the amplified laser beam with 210kW peak power, the difference between the main signal peak and the SRS peak is 20dB. The comparison of the normalized spectrum between seed and amplified signal in linear scale is shown in Figure 7.31. Roughly 41% power for seed spectrum and 6% power for amplified laser beam with 210kW peak power are in SRS region around 1080nm.

At last the beam quality was measured by Spiricon M2-200s automated M2 laser beam propagation analyzer. The figure 7.32 shows the beam pattern of the output power with 13.8W and 210kW peak power under 30W launched pump power which is multi-mode with an M^2 value of 3.7(x axis) and 3.4 (y axis).

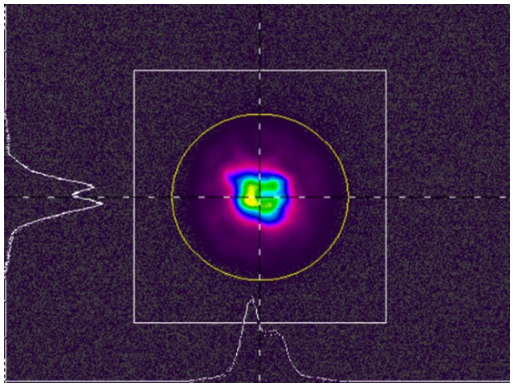

Figure 7.32 Beam pattern of the output light with 13.8W output power (210kW peak power).

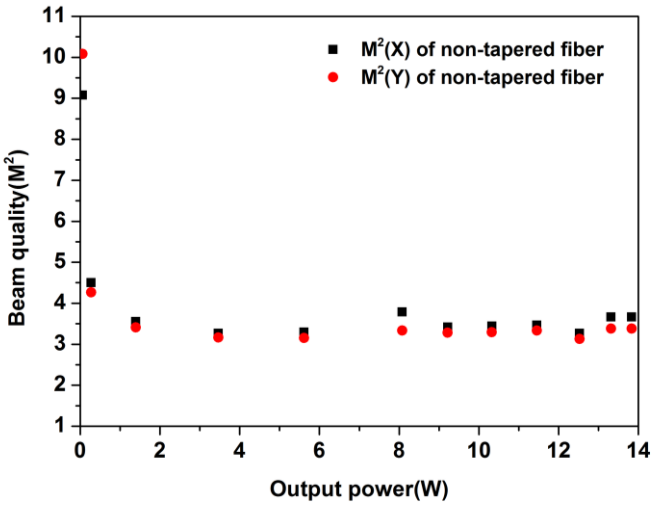

Figure 7.33 Measured beam quality for non-tapered reference fiber amplifier

The M^2 value varied from 3.1 to almost 4.5 when the output power increased from 0.5W to 13.8W (figure 7.33). The base line for this reference rod fiber is much lower than that for the fiber 999c due to a smaller core diameter and an optimized smaller core NA. Due to signal reabsorption, the beam quality is quite bad (M^2 near 10) without pump power. After applying pump power, the amplifier becomes transparent and the beam quality is improved.

7.3.3 Beam quality improvement with tapered rod type fiber amplifier

7.3.3.1 Characterization of the tapered amplifier

(1) Investigation of diffusion

In order to check if this fiber still exhibits significant diffusion, the refractive index (IR) of the down taper is measured (see figure 7.34) using Interfiber Analysis IFA-100 technology. When comparing this down taper IR profile with the IR profile of the rod fiber which is scaled down with taper ratio, there is little difference between them which means that the diffusion phenomenon is mitigated.

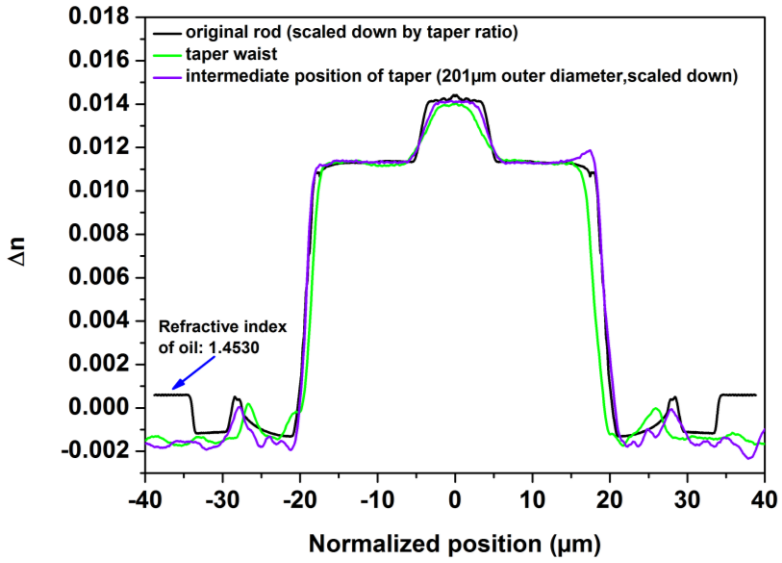

Figure 7.34 Refractive index profile of the down-taper and rod fiber

(2) Adiabatic taper design and estimation of properties

Figure 7.35(a) shows the calculated coupling condition of the fundamental mode to the next three higher order modes according to the adiabatic taper length criterion which is also the boundary limitation of the taper angle according to different taper local core diameter. The regions below the curve of LP01 vs LP11 are the adiabatic regions and the local real taper angle should not exceed the adiabatic limitation boundary.

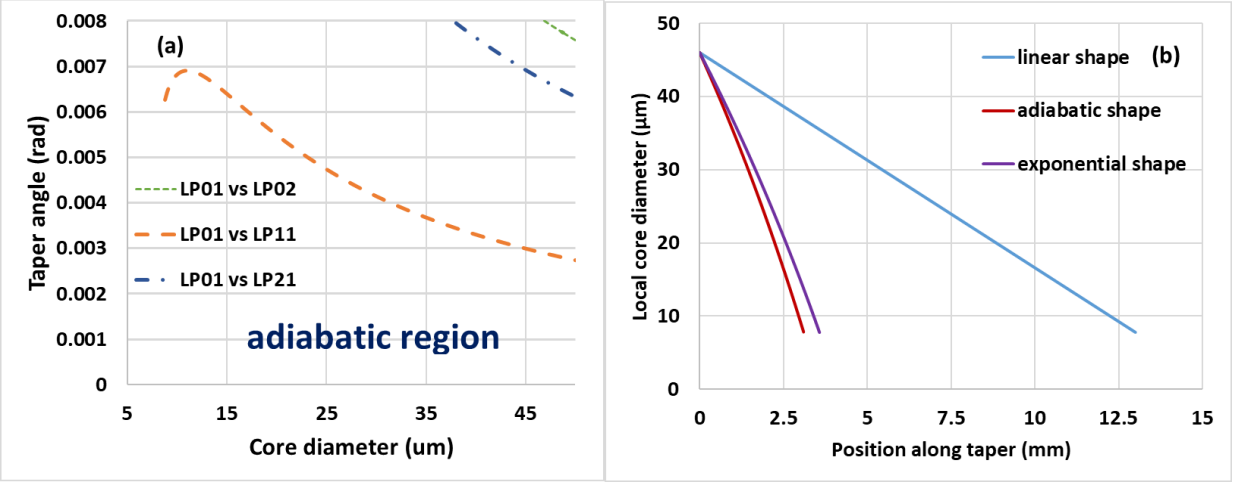

Figure 7.35 (a) Adiabatic region due to theoretical coupling calculation. (b) Theoretical calculation for different taper shape (854b)

Figure 7.35(b) shows the theoretical calculation of local core diameter for different taper shapes of this type fiber. The minimum taper length for linear shape is 13mm which is shorter than that of fiber discussed in figure 7.13 due to the smaller core NA and the smaller initial fiber core diameter.

(3) Characterization of local adiabatic taper

One piece of fiber with 72cm length was tapered down to the single-mode region. The tapering process was optimized. Figure 7.36(a) shows the measured taper diameter against the taper length.

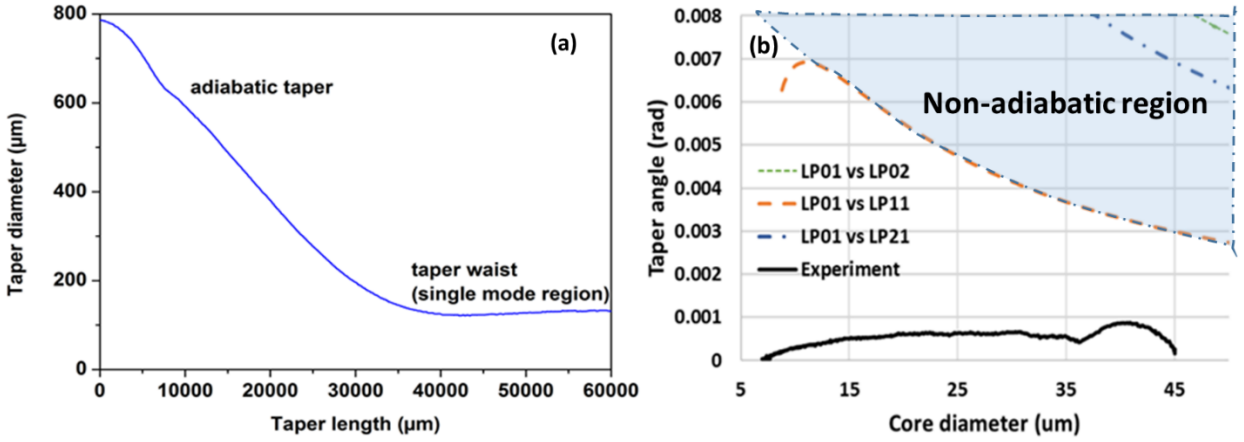

Figure 7.36 (a) Scanned taper length and outer diameter (b) Comparison of angular profiles between the experimentally realized fiber taper and the adiabatic thresholds

As is shown in figure 7.36(b), the black line is derived from the real taper shape, assuming the core diameter changes proportionally to the outer diameter. The experimentally realized taper angle is always smaller than the adiabatic threshold which means the taper shape should be smooth enough that the FM profile can smoothly evolve inside the taper core, and no power coupling happens between FM and HOMs in theory.

(4) Splice between seed delivery fiber and taper waist

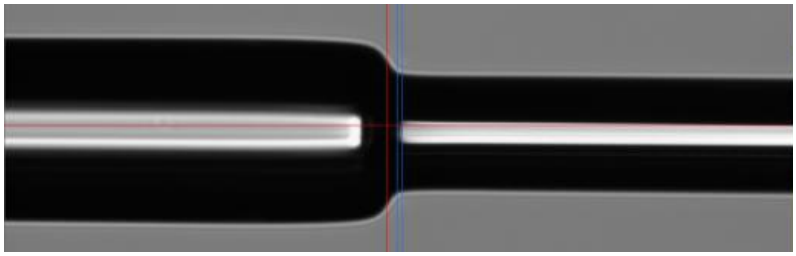

Figure 7.37 Splice point between standard SM fiber (left) and the fiber taper waist (right).

The seed beam is delivered by a standard single-mode fiber which only propagates the FM. The seed delivering fiber is directly spliced to the taper waist for seed coupling to provide a robust monolithic signal path even in harsh working environments.

(5) Schematic of tapered rod fiber

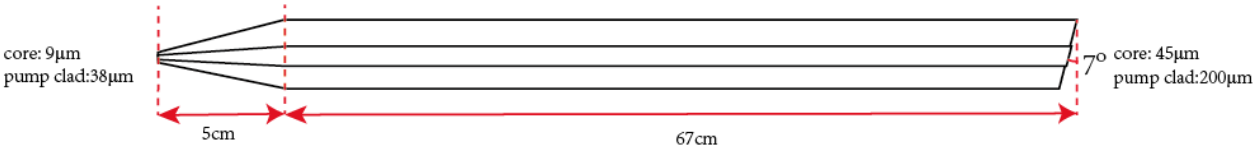

Figure 7.38 Schematic of the tapered rod fiber 854b

As is shown in figure 7.38, the rod fiber length is 67cm and the taper region length is 5cm for the tapered amplifier sample. At the taper waist, the laser core diameter is 9um, the pump core diameter is 38μm and the outer diameter is 157um. The end facet of this tapered fiber is polished at 7 degrees to avoid back-reflections of the laser beam. The pump with single pump module (105μm core diameter and 0.16 core NA) is used to supply the pump power for the fiber amplifier. A pair of lenses with 25mm and 30mm focal length is used to couple the pump light into the rod fiber with free space coupling method.

(6) Near field and far field characterization

The beam pattern (near field measurement) and divergence angle (far field measurement) of the laser beam is checked after the taper is spliced to the standard SM fiber. The mean diameter of the beam pattern which is calculated with the 4σ method according to the near field measurement is 32.2μm. The divergence angle of the laser beam which propagates in the tapered fiber is also checked with far field measurement. The divergence angle according to the far field measurement is 0.043rad for the laser beam at laser wavelength 1060nm. Then the BPP and the M^2 value can be calculated and the beam quality can be obtained which is estimated to be 1.36.

$$BPP = \left(\frac{0{,}0322mm}{2}\right) * 43mrad = 0.693mm\ mrad \quad (7.7)$$

$$M^2 = \pi * BPP/1{,}060\mu m = 1.36 \quad (7.8)$$

7.3.3.2 Results of tapered rod-type amplifier

The slope efficiency was characterized according to figure 7.39. In order to provide a better performance comparison, the output power is plotted vs. the absorbed pump power. This pump power was estimated based on a 90% pump coupling efficiency, the residual pump power is estimated according to a constant absorption coefficient along the fiber which is obtained from the non-tapered fiber amplifier. The slope of the tapered amplifier displays a slope efficiency of 70% vs. the absorbed pump power. The highest output power reached 8.38W under 20W of launched pump power, corresponding to a peak power of 140kW and a pulse energy of 0.42mJ. The efficiency of the tapered amplifier is similar to that of the non-tapered fiber amplifier.

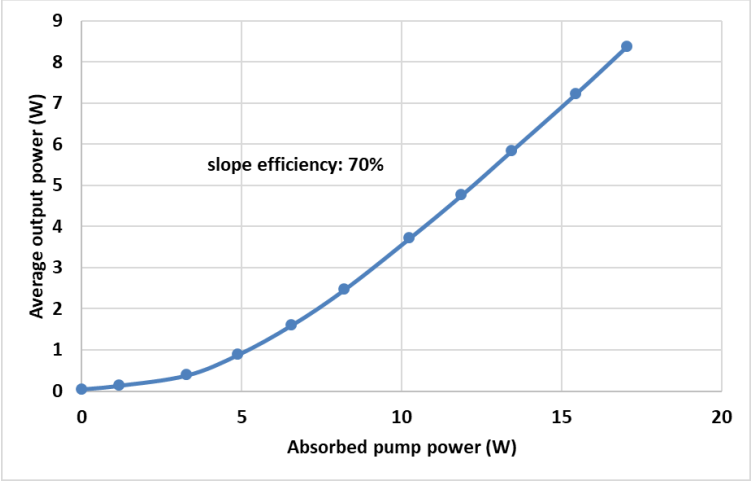

Figure 7.39 Average output power versus the absorbed pump power

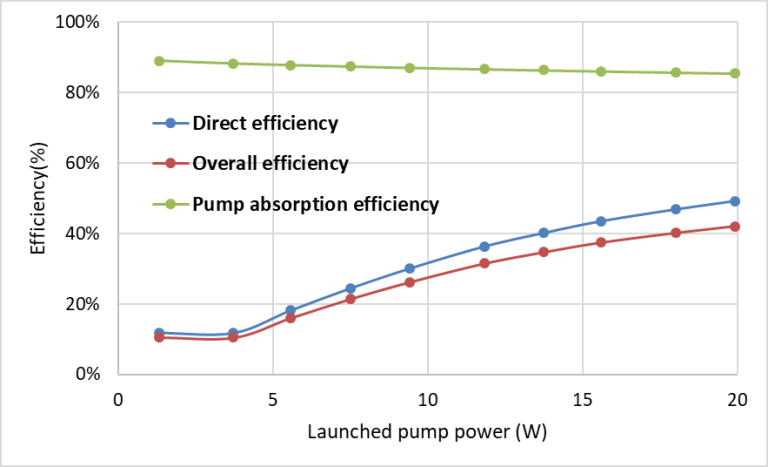

Figure 7.40 Direct efficiency, overall efficiency and pump absorption efficiency as a function of the launched pump power.

As is shown in figure 7.40, the direct and overall efficiency under 20W launched pump power was 49% and 42%, respectively. The estimated absorption of pump power drops from 89% to 86%.

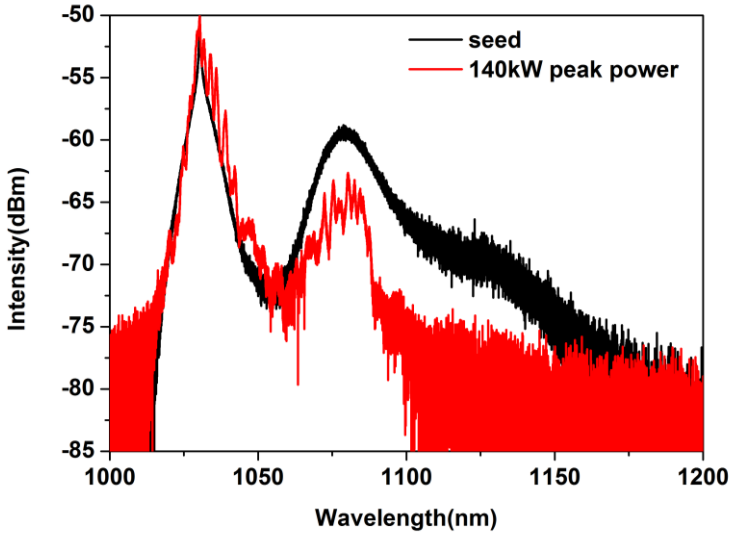

Figure 7.41 Optical spectrum of seed and amplified light

The spectrum of the amplified signal is shown in Figure 7.41 and compared to the seed spectrum. The seed spectrum already contains a significant first Stokes peak at 1080nm due to stimulated Raman scattering (SRS). Interestingly, this peak is suppressed in the tapered rod amplifier up to 140kW of peak power. This indicates that the laser gain strongly favors the 1030nm emission and drops sharply towards 1100nm. The comparison of the normalized spectrum in linear scale is shown in Figure 7.42. Roughly 41% power for seed spectrum and 14% power for amplified laser beam with 140kW peak power are in SRS region around 1080nm.

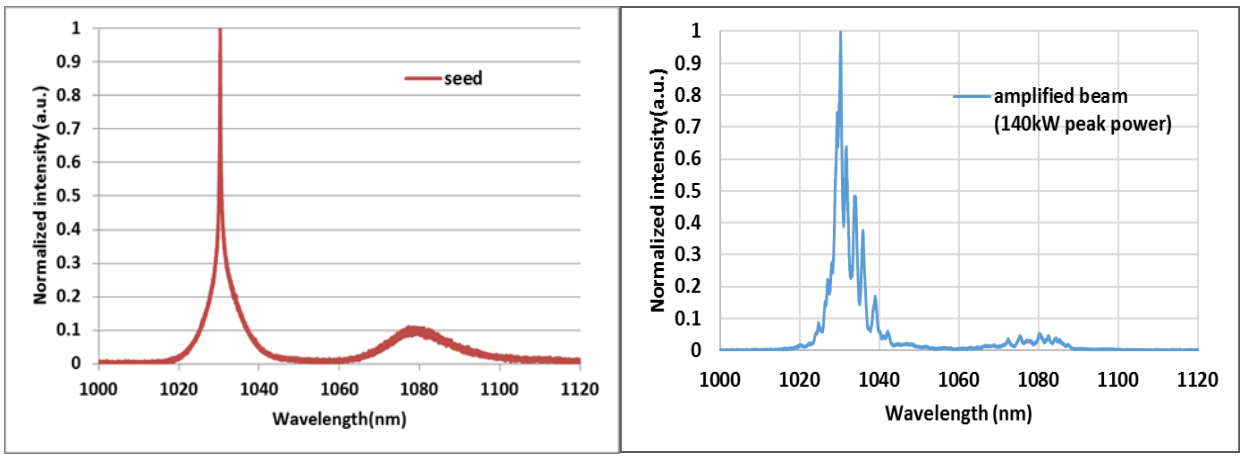

Figure 7.42 Comparison of the normalized linear spectra between seed and amplified light

The following experiments concentrated on the characterization of the beam quality improvement due to the local taper using a Spiricon M2-200s automated M2 laser beam propagation analyzer. The pattern of beam spot at the highest output power (140kW) is shown in figure 7.43. The corresponding beam quality (M^2 value) is 1.6/1.7 in x/y axis. The beam pattern is quite similar to a Gaussian shape.

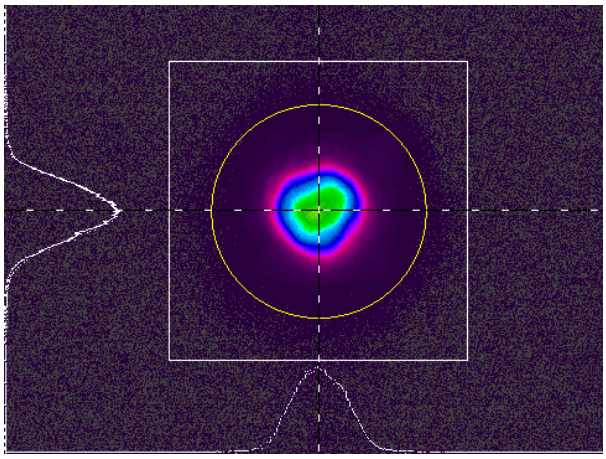

Figure 7.43 Beam pattern of the output beam with 8.38W output power (140kW peak power)

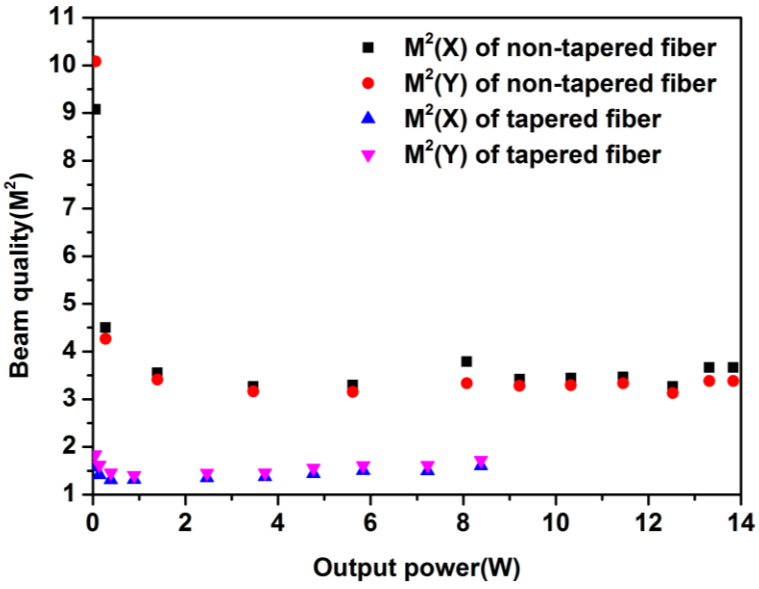

Figure 7.44 Measured beam quality for the non-tapered and the tapered fiber amplifier

The beam quality M^2 is plotted versus the average output power in Figure 7.44. The non-tapered rod amplifier serves again as a reference, even though the beam quality is very sensitive to the free space seed coupling conditions and therefore not very stable. All M^2 results presented here are

based on a carefully optimized coupling adjustment. The optimized beam quality of the non-tapered amplifier is between 3.1 and 4.5. The M^2 values for the tapered rod amplifier are between 1.3 to 1.7, but with much higher stability compared to the free space coupling to the non-tapered fiber. For a similar average output power of about 8W, the beam quality improves from values near 4 to 1.6/1.7. Even though the peak power is not scaled up to the megawatt level, the beam quality is good enough and quite stable with local adiabatic taper. The peak power scaling is limited by break down of the fiber end-face due to the material facet damage limit.

7.3.4 Peak power scaling of tapered rod-type fiber amplifier with endcap

7.3.4.1 Characterization of the endcap

In order to enhance the damage threshold and scale up the peak power of the tapered fiber amplifier as is discussed in chapter 7.3.3, an endcap is adopted to protect the fiber facet from facet damage. An endcap is a core-less pieces which is attached to fiber end tip in order to reduce the laser light intensity by expanding the laser beam [114]. The endcap is a useful method to enhance the laser damage threshold limit and to scale up the peak power. The choice of material for endcap is essential which at least should have a higher damage threshold than the doped fiber. A pure silica glass piece is the simplest choice due to the high melting temperature. A fusion splice is the most common way to attach an end cap to the fiber with low loss. The endcap length should be short enough, otherwise the laser beam can be blocked on the edge along the endcap. Limpert [115] has pointed out a simple equation to estimate the maximum endcap length, which can approximately expand the mode field to 3/4 of the end cap diameter:

$$L_{max} = \frac{d_{endcap}}{2n_{endcap}NA_{core}} \tag{7.9}$$

where d_{endcap} is the endcap diameter of and n_{endcap} is the endcap refractive index. NA_{core} is the numerical aperture of fiber core. L_{max} is the maximum length of the endcap.

The endcap material here uses F300 silica rod with 1000μm outer diameter. According the equation 7.9, the maximum length of an endcap is 3.8mm. The F300 silica rod was spliced to the tapered fiber amplifier (see figure 7.45), then was angle cleaved to avoid back-reflections into the MOPA system. Only a short 2mm long piece of F300 silica rod is left on the fiber amplifier as the endcap. Finally, the endcap is cleaved at an angle of 5.8 degrees. Because several parts of the rod type fiber

where used for several trials (cleaving on fiber end) of making the endcap, a tapered fiber amplifier with 50cm length (45cm rod and 5cm taper) was left for further investigations.

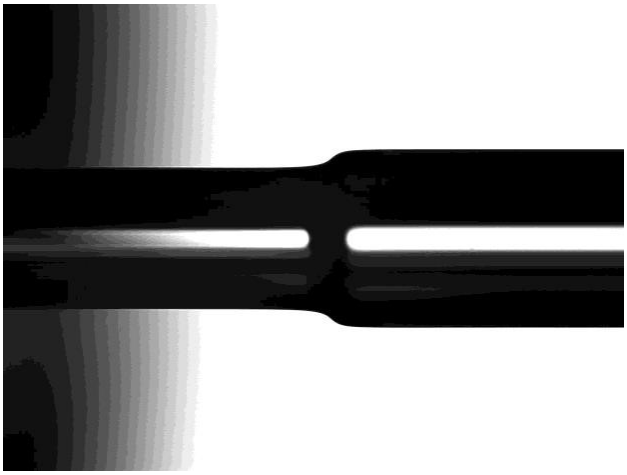

Figure 7.45 Endcap of tapered fiber amplifier: left side is the fiber amplifier and the right side is the endcap material (F300 with 1000μm outer diameter)

7.3.4.2 Results of tapered rod-type fiber amplifier with an endcap

The slope efficiency was characterized first which is shown in Figure 7.46. The absorbed pump power was estimated based on a 90% pump coupling efficiency, the residual pump power is estimated according to a constant absorption coefficient along the fiber, which is taken from the non-tapered fiber amplifier. The slope efficiency of this 50cm length tapered amplifier displays a value of 62% vs. the absorbed pump power. The highest output power reached 15.54W under 39.5W of launched pump power, corresponding to a peak power of 375kW and a pulse energy of 0.78mJ. The efficiency of this tapered amplifier with endcap is a little lower than the performance of the tapered fiber amplifier discussed in chapter 7.3.3, because the fiber length is 22cm shorter. In order to achieve the same output power, this shorter length fiber amplifier needs more pump power to get enough gain to compensate the reduced pump absorption efficiency. Because of the endcap, the peak power is significantly scaled up to 375kW which is 2.7 times higher than the achieved peak power of 140kW with the tapered fiber sample without endcap (see chapter 7.3.3).

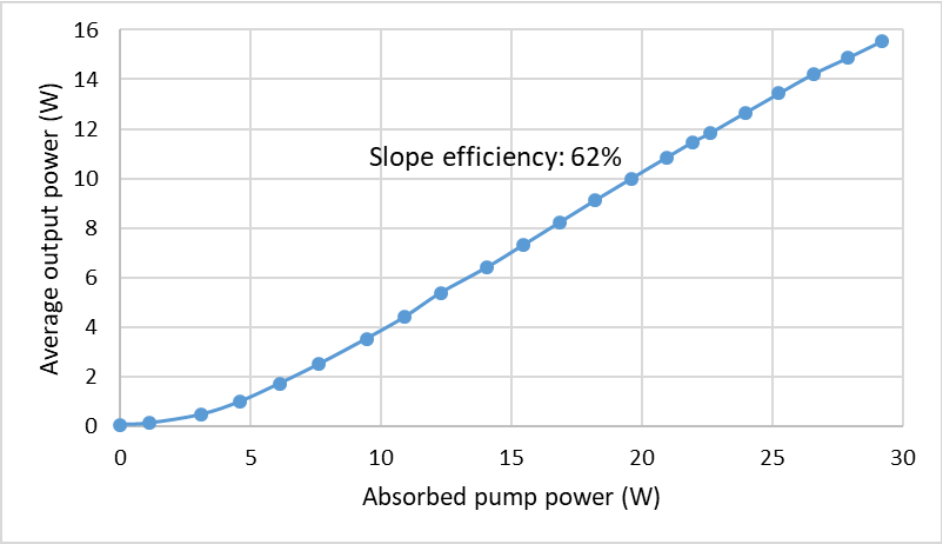

Figure 7.46 Average output power versus the absorbed pump power

Figure 7.47 shows the direct efficiency, the overall efficiency and the pump absorption efficiency. The absorption of the pump power drops from 86% to 74%. Both, the direct efficiency and the overall efficiency are increasing with the increasing pump power. The highest values with 39.5W of launched pump power are 53% and 39%, respectively.

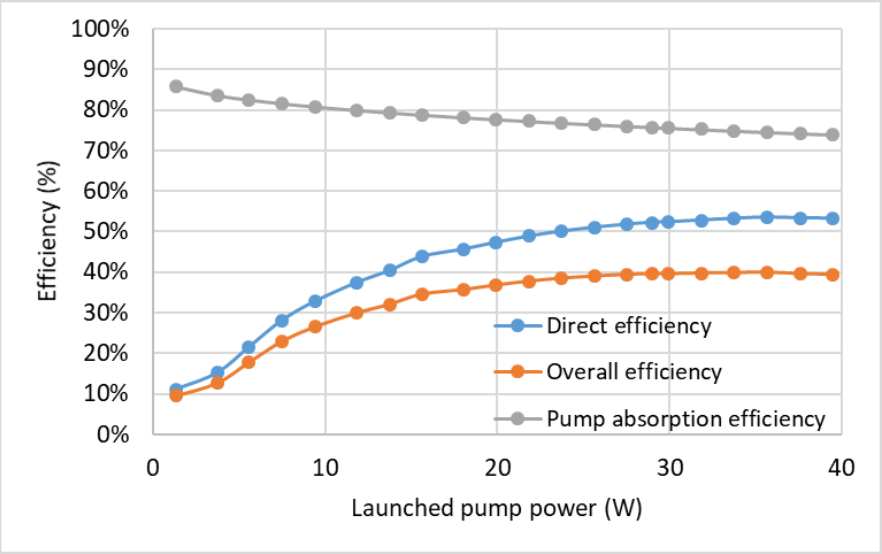

Figure 7.47 Direct efficiency, overall efficiency and pump absorption efficiency as a function of the launched pump power.

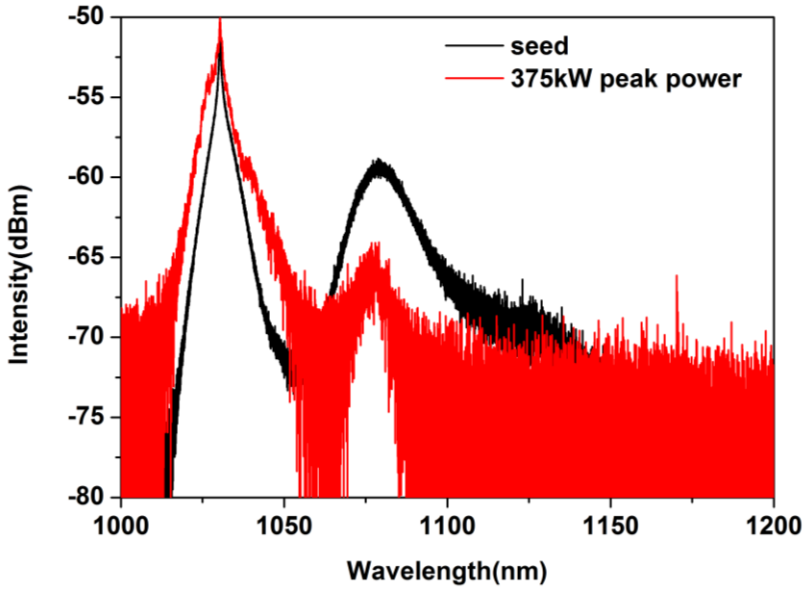

Figure 7.48 Optical spectrum of seed and amplified light

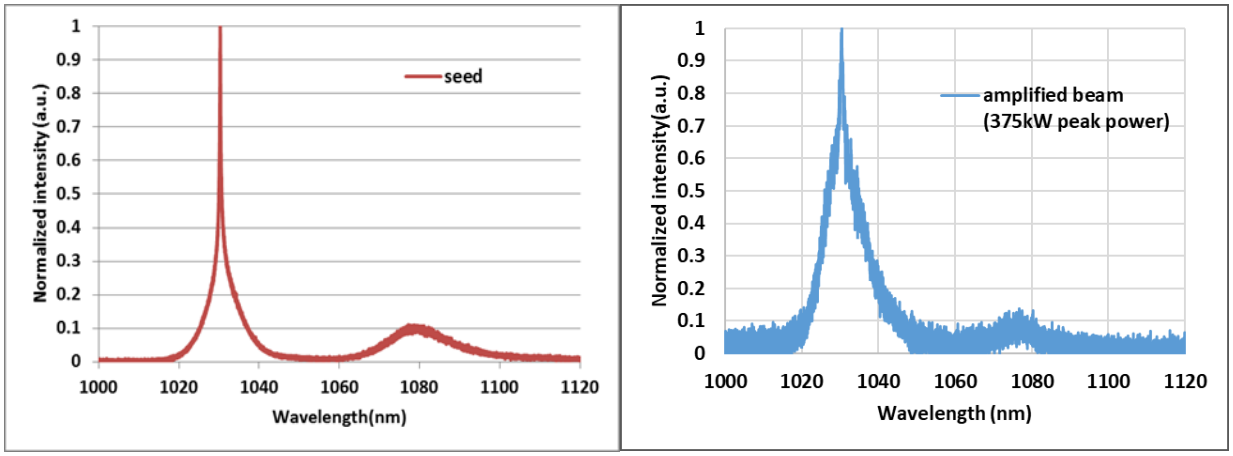

Figure 7.49 Comparison of the normalized linear spectra between seed and amplified light

The spectra of the amplified signals with 375kW peak power is shown in Figure 7.48 and is compared to the seed spectrum. The seed spectrum already contains a significant first Stokes peak at 1080nm due to stimulated Raman scattering (SRS). This SRS peak is efficiently suppressed in the tapered rod amplifier up to 375kW of peak power which indicates that the Raman gain is still very small while the laser gain strongly favors the 1030nm emission. The spectrum around 1030nm becomes broader than seed spectrum which is due to the non-linear broadening effect. The comparison of the normalized spectrum of seed light and amplified light in linear scale is shown in Figure 7.49. Roughly 41% power of seed spectrum and 12% power of amplified laser beam with 375kW peak power are in SRS region around 1080nm.

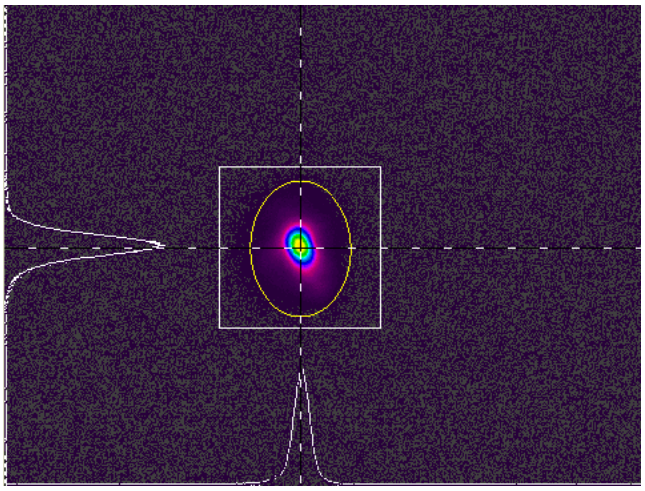

Figure 7.50 Beam pattern of the output light with 15.5W output power (375kW peak power)

The pattern of the beam spot at the highest output power with 15.5W average output power and 375kW peak power is shown in figure 7.50. The corresponding beam quality (M^2 value) is 1.58/1.64 in x/y axis which is nearly diffraction limited.

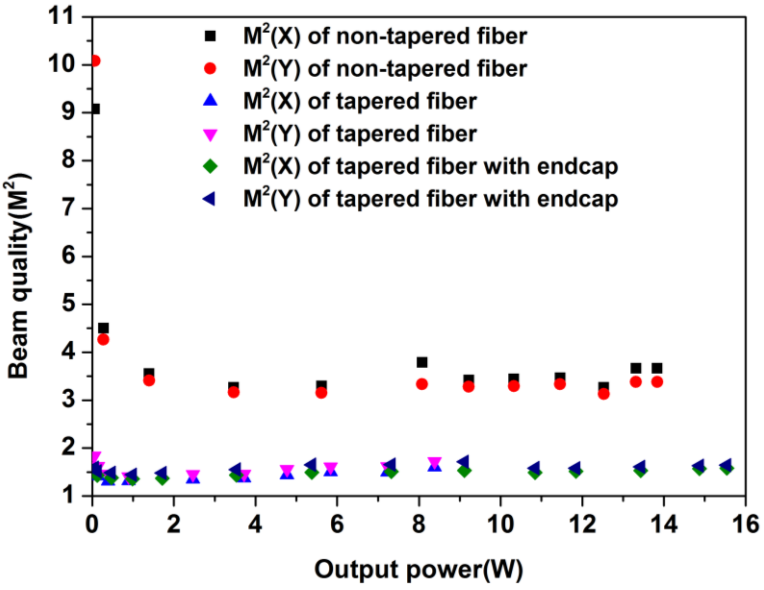

Figure 7.51 Measured beam quality for non-tapered reference fiber amplifier, tapered fiber amplifier and tapered fiber amplifier with endcap

The beam quality M^2 is plotted versus the average output power in Figure 7.51. The non-tapered rod amplifier and the tapered fiber amplifier without endcap serve as a reference. For this tapered fiber amplifier with endcap, the M^2 values are between 1.3 to 1.7 in the nearly diffraction limited

region which is in a similar range as the tapered fiber amplifier without endcap (chapter 7.3.3). For similar average output power of about 14W, the beam quality is improved from values near 4 with non-tapered fiber to 1.6 with tapered fiber.

7.4 Summary of rod-type fiber amplifiers

The fiber parameters and the main experimental results of the designed LMA fiber amplifiers are summarized in table 7.1.

Fiber code	Fiber 999c		Fiber 854b		
Core diameter	56µm		45µm		
Mode field diameter(MFD)	40µm		34µm		
Al^{3+} concentration	High (7mol% in core)		Low (2.5mol% in core)		
Outer cladding	F300 (pure silica)		F520 (Fluorine-doped silica)		
Temperature of tapering process	High		Low		
Diffusion problem	Serious		Almost no diffusion		
With or without taper	Non-tapered	Tapered fiber	Non-tapered	Tapered fiber	Tapered fiber with endcap
Seed coupling	Free space coupling	Splice	Free space coupling	Splice	Splice
Stability vs. seed coupling	Not stable	Stable	Not stable	Stable	Stable
End surface	Polished	Polished	Polished	Polished	Endcap
Average power (W)	28.0	10.3	13.8	8.4	15.5
Peak power (kW)	544	230	210	140	375
Beam quality (M^2)	6~12	2.5~4.0	3.1~4.5	1.3~1.7	1.3~1.7

Table 7.1 Summary of rod type fiber amplifiers

Above all, LMA fibers can efficiently scale up the peak power by increasing the mode field area and decreasing the laser power density. The use of a local short adiabatic tapers provides a robust seed coupling for fiber amplifiers compared to free space coupling, while maintaining the near diffraction limited beam quality by preferentially exciting the fundamental mode in a LMA step-index fiber amplifier. The dopant diffusion during the tapering process is successfully suppressed using an optimized fiber design (lower Al^{3+}-doping concentration in the core and inner cladding, and lower tapering process temperature with optimized outer cladding material). The use of an endcap can protect the fiber end facet and help to scale up the peak power of fiber amplifier. The peak power was scaled up to 375 kW with a near diffraction limited beam quality (M^2: 1.3~1.7). In summary, we have demonstrated a new type of REPUSIL-based rod amplifiers in the ns pulse regime with local short adiabatic tapers allowing high peak power in combination with near diffraction limited beam quality in a robust monolithic seed coupling setup.

8. Outlook: Confined doping for beam quality improvement

(1) Confined doping fiber parameter discussion

Beyond the use of a tapered seed coupling in a rod fiber amplifier, the REPUSIL method would also provide an option to prepare a confined doping amplifier core in a simple way. By this way a further improvement of amplification efficiency with diffraction limited beam quality could be expected. Therefore, as a method, a fiber design with such a confined doping is shortly discussed. Confined doping means the fiber core is only partially doped with active dopants to favor a particular mode in the amplification. In particular, the FM can get preferred gain due to the higher overlap coefficient between LP_{01} mode profile and active doping region.

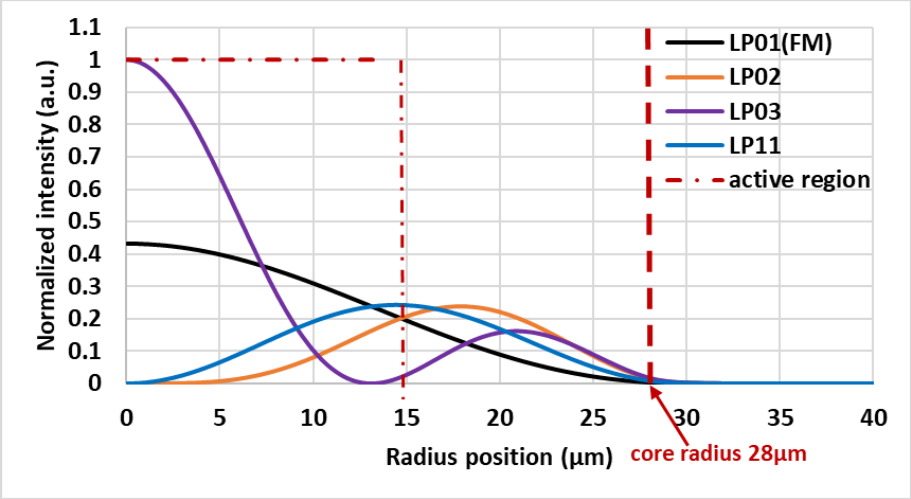

Figure 8.1 Illustration of the overlap between modes and the active region

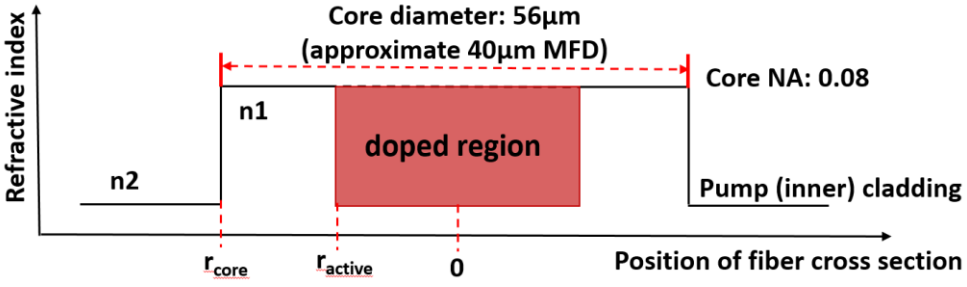

Figure 8.2 Refractive index profile of confine doped fiber for calculation

In the following we assume a core with a radius r_{core} where only a region with radius r_{active} is actively doped (figure 8.2). The design will be optimized for the seed delivery fibers as used in this work. The fiber core diameter is taken to be 56μm which approximately has a mode field diameter of 40

μm. This provides a peak power scaling potential up to 1MW with the use of endcaps (see figure 7.2). The fiber core NA is set to 0.08, which enables good mode matching to the seed delivery fiber and a single-mode operation at the taper waist. The refractive index of core and pump (inner) cladding are n1 and n2, respectively.

(2) Optimization of actively doped radius of the fiber core

In order to discriminate the gain (or mode overlap coefficient) between FM and HOMs, the optimized radius ratio between active core region radius and the total core radius should be investigated. The Radius ratio is the active core region radius r_{active} divided by the total core radius r_{core}. Figure 8.3 shows the overlap coefficient difference between the FM and the HOMs as a function of the radius ratio between the active core region and the fiber core. The overlap coefficient difference is calculated by subtracting the highest overlap coefficient value of HOMs from the overlap coefficient value of FM. The overlap coefficient of modes is calculated according to the equation 5.11. The optimized radius ratio between active region and the total fiber core is 0.68. This value corresponds to the best discrimination between the FM and the HOMs based on a high overlap and high modal gain for the FM and significantly smaller values for the other HOMs.

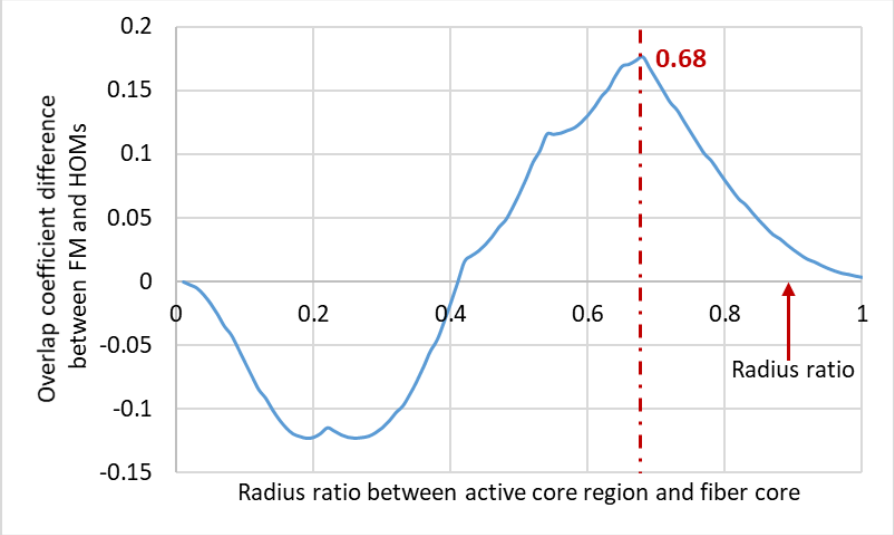

Figure 8.3 Investigation of the optimized radius ratio for the active (Yb^{3+}-doped) core region

The overlap coefficient between modes and the active core region is compared for the fully doped case and the confined doped case, respectively (see figure 8.4). The blue curve shows that the overlap coefficients for all modes are quite similar and approximate equal to 1 for fully doped fiber.

The red curve shows the overlap coefficients for different modes of confined doped core for the optimum radius ratio of 0.68 from Fig. 8.3. The overlap coefficient of FM is 0.835 while the overlap coefficients of the other HOMs are smaller than 0.658 with the radius ratio of 0.68. The gray curve corresponds to a stacked preform design with a radius ratio of 0.61 which represents a practical design with rods of uniform size as discussed in the next section.

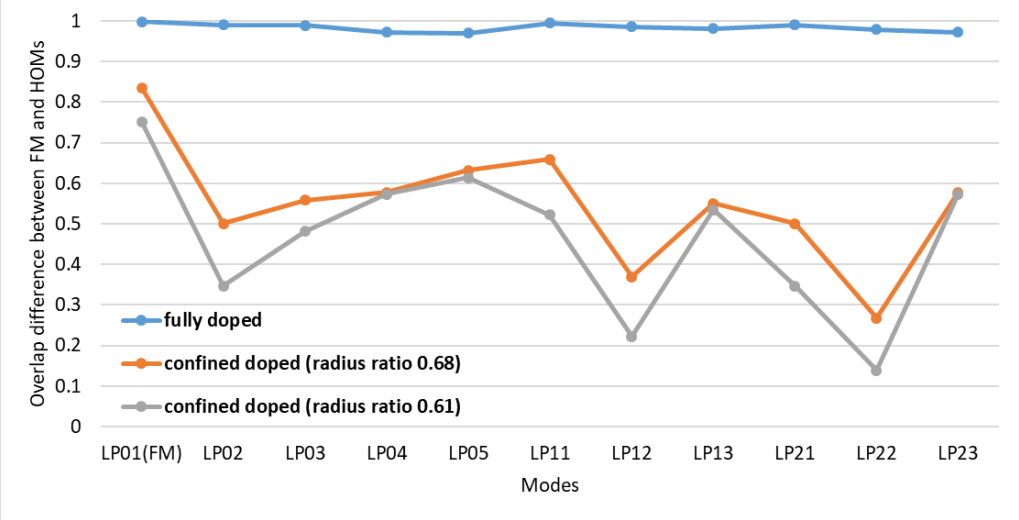

Figure 8.4 Overlap coefficients between guided modes and the active core region

(3) Preform preparation by stacking rods

Figure 8.5 shows the stacked preform for a confined doped fiber. The red rods will form the active core region, the yellow rods the passive core region, and the green rods the inner cladding region. All stacking rods of the preform are assumed to be of uniform size (diameter and length) which is typical for fiber preform produced by REPUSIL technology. The ratio between the active region and the total core area is 7:19 and therefore the ratio between the active region radius and the core radius is 0.61 due to the uniform size of stacking preform rods and limitation of choosing radius ratio. According to the calculation result in figure 8.4, the overlap coefficient of the FM is 0.75 while the overlap coefficients of the other HOMs are smaller than 0.61 with the radius ratio of 0.61. The FM still obtains the preferred gain and the gain of the HOMs is suppressed.

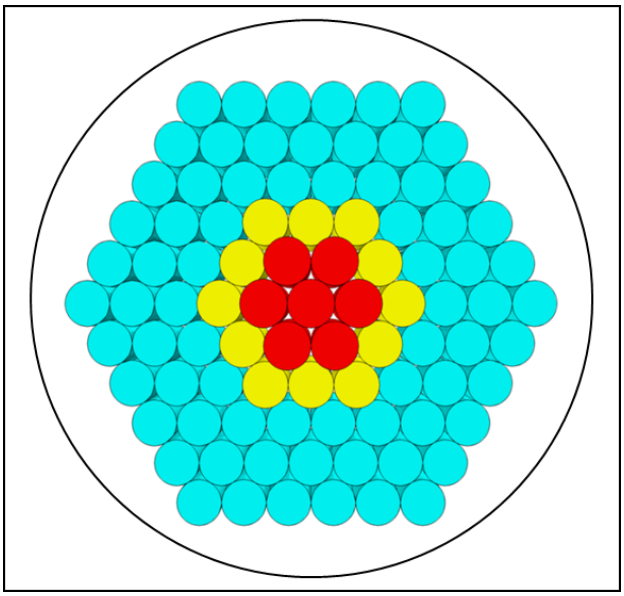

Figure 8.5 Preform preparation by stacking rods (red rods are for the active core, yellow rods are for the passive core, and green rods are for the inner cladding)

9. Conclusion

Large mode area (LMA) all-solid Yb^{3+}-doped double-clad fibers provide an economical and practical solution to mitigate the severe nonlinear effects while scaling up the peak power by mode area scaling. However, LMA step-index fibers also bear some problems such as bad beam quality in case of highly multi-moded excitation. The purpose of this research work incorporates three important parts: 1. achieve a monolithic signal path and robust fiber amplifier with an all-solid fiber. 2. explore an LMA step index fiber for peak power scaling. 3. explore a local short adiabatic taper to maintain the near diffraction limited beam quality. The aim is to achieve a high peak power with near diffraction limited beam quality and low Stimulated Raman Scattering (SRS) effect.

All fibers in this research work were prepared by the powder sintered technology (REPUSIL) which was developed by the IPHT and Heraeus Quarzglas and allows simple refractive index adjustment of the inner cladding and very homogeneous refractive index distributions. All designed LMA fibers were tested in a three-stage ns-pulsed fiber master oscillator power amplifier (MOPA) system. The two pre-amplifier stages provide the amplified seed signal with 3kW peak power and 138mW average power with 2ns pulse and a repetition rate of 20kHz which reaches the limitation of standard single mode amplifiers due to the SRS effect. The third stage is the main stage to test the designed LMA fibers to scale up the peak power and to maintain the good beam quality.

First experiments were performed with double-clad rod-type fibers with a core diameter of 56µm and an outer diameter of 1mm. A rod-type Yb-doped fiber was characterized before and after tapering the seed input section. While the non-tapered fiber amplifier was operated up to a peak power of 544kW and 1.4mJ pulse energy, the tapered amplifier reached 230kW and 0.5mJ. The limiting effect was damage to the output facet. The slope efficiency of non-tapered amplifier is 83% with respect to the absorbed pump light and slightly lower for the tapered amplifier. For comparable average powers of 10W, the taper improves the beam quality from M^2 values of about 10 to 3.5, while the monolithic seed coupling significantly improves the beam stability. It was observed that the dopants diffuse during the tapering process because of high temperature, possibly providing further sources for coupling to higher order modes. The amplifiers show that the SRS Stokes peak is suppressed up to peak powers of 544kW by preferential laser gain at the 1030nm seed wavelength, indicating further peak power scaling potential.

The second experiments were performed with optimized fibers with a core/clad diameter of 45µm/200µm and a core/clad numerical aperture of 0.09/0.19 which reduce the Al^{3+} content to mitigate the diffusion problem by lower glass melting temperature of the outer clad to decrease the tapering process temperature and reduce the core NA. While the non-tapered fiber amplifier was operated up to a peak power of 210kW, the tapered amplifier reached 140kW. Both fiber amplifiers show relatively low SRS levels and no remarkable photo-darkening. The optimized beam quality of the non-tapered amplifier is between 3.1 and 4.5 and quite power dependent. The M^2 values for the tapered rod are between 1.3 and 1.7 with much higher stability compared to the free space coupling of the non-tapered fiber. For similar average output powers of about 8W, the beam quality improves from values near 4 to approximately 1.6 which is close to a diffraction limited beam. An endcap was adopted for the tapered fiber amplifier. Because of an endcap the peak power is scaled up to 375kW in the nearly diffraction limited region with low SRS level.

For future work, the following improvements are envisioned: 1. Improve the beam quality by optimizing the tapering process and by the use of confined doped fibers according to the theoretically analysis in chapter 8. 2. A picosecond (ps) seed laser source could be considered to shorten the pulse width from nanosecond (ns) level to picosecond (ps) level which can help to scale up the peak power by increasing the laser induced damage threshold.

Finally, we can conclude that the new type of REPUSIL-based robust rod amplifier with index-adjusted inner cladding and local adiabatic tapers is successfully demonstrated. LMA fibers can efficiently scale up the peak power by increasing the mode field area and decreasing the laser power density. LMA short fibers provide an efficient solution to mitigate the nonlinear effects, especially the SRS effect for nanosecond pulsed amplifiers. The use of local short adiabatic tapers provides a robust seed coupling for fiber amplifiers compared to free space coupling, while maintaining the nearly diffraction limited beam quality by preferentially exciting the fundamental mode in LMA step-index fiber amplifiers. The dopant diffusion during the tapering process is successfully suppressed, resulting in a good beam quality. The peak power has been scaled up to 375 kW with good beam quality by adopting an endcap at the output of the tapered fiber amplifier.

A. Zusammenfassung

„All-solid“ Yb^{3+}-dotierte double-clad LMA-Fasern stellen eine sowohl ökonomische als auch praktische Lösung dar um die starken nichtlinearen Effekte bei der Leistungsskalierung mittels Vergrößerung des Modenfelds abzuschwächen. Dennoch zeigen LMA-Stufenindexfasern einige Probleme wie zum Beispiel die geringe Strahlqualität im Fall einer multimodalen Anregung. Das Ziel dieser wissenschaftlichen Arbeit beinhaltet drei wichtige Teile: 1. Realisierung eines monolithischen Signalweges und eines stabilen Faserverstärkers mittels einer „all-solid“ Faser; 2. Untersuchung einer LMA-Stufenindexfaser zur Spitzenleistungsskalierung; 3. Untersuchung eines lokalen adiabatischen Tapers zur Erhaltung einer nahezu beugungsbegrenzten Strahlqualität. Das gemeinsame Ziel ist es dabei, eine hohe Spitzenleistung mit nahezu beugungsbegrenzter Strahlqualität und niedriger stimulierte Ramanstreuung (SRS) zu erreichen.

Alle Fasern in dieser Forschungsarbeit wurden mit Hilfe der reaktiven Pulver Sinter-Technologie (REPUSIL) hergestellt, ein Verfahren welches in Zusammenarbeit von IPHT Jena und Heraeus Quarzglas entwickelt wurde und sowohl einfache Brechungsindexanpassungen des inneren Claddings als auch sehr homogene Brechzahlverteilungen erlaubt. Alle hergestellten LMA-Fasern wurden in einem dreistufigen Nanosekunden-gepulsten Faser-Masteroszillator-Leistungsverstärkersystem (MOPA) getestet. Die zwei Vorverstärkerstufen liefern das verstärkte Seedsignal mit 3 kW Spitzenleistung und 138 mW mittlerer Leistung mit 2 ns Pulsdauer und einer Repetitionsrate von 20 kHz, welche die Grenze von üblichen monomodalen Verstärkern aufgrund der SRS erreicht. Die dritte Stufe ist die Hauptstufe um die hergestellten LMA-Fasern hinsichtlich der Skalierung der Spitzenleistung und der Erhaltung der Strahlqualität zu testen.

Erste Experimente wurden an „Double-clad rod-type“ Fasern mit einem Kerndurchmesser von 56 µm und einem Faserdurchmesser von 1 mm durchgeführt. Eine „rod-type“ Yb-dotierte Faser wurde vor und nach dem Tapern der Eingangsseite charakterisiert. Während der ungetaperte Faserverstärker bis zu einer Spitzenleistung von 544 kW bei 1.4 mJ Pulsenergie betrieben werden konnte, erreichte der getaperte Verstärker 230 kW und 0.5 mJ. Der limitierende Faktor hierbei war die Zerstörung der ausgangsseitigen Faserendfläche. Der Wirkungsgrad bezüglich der absorbierten Pumpleistung liegt bei 83% für den ungetaperten Verstärker und etwas geringer für den getaperten Verstärker. Bei vergleichbaren mittleren Leistungen von 10 W verbessert der Taper die Strahlqualität M^2=10 auf M^2=3.5, wobei die monolithische Seed-Einkopplung zusätzlich auch die Strahlstabilität erheblich verbessert. Es wurde beobachtet, dass die Dotanden aufgrund der hohen

Temperatur während des Taper-Prozesses ausdiffundieren, was möglicherweise zu einer Kopplung zu Moden höherer Ordnung führen kann. Die Verstärker zeigen, dass das SRS Stokessignal bis zu einer Spitzenleistung von 540 kW mittels bevorzugter Laserverstärkung bei 1030 nm Seed-Wellenlänge unterdrückt werden kann, was auf weiteres Potenzial ind der Skalierung der Spitzenleistung hindeutet.

Die zweiten Experimente wurden mit optimierten Fasern mit einem Kern/Mantel-Durchmesser von 45µm/200µm und einer Kern/Mantel-NA von 0.09/0.19 durchgeführt. In diesen Fasern wurde der Al^{3+}-Gehalt verringert um das Diffusionsproblem aufgrund der niedrigeren Glasübergangstemperatur des äußeren Claddings abzuschwächen, die Temperatur beim Taperprozess zu verringern und die NA des Kerns abzusenken. Während der ungetaperte Faserverstärker bis zu einer Spitzenleistung von 210 kW betrieben werden konnte, erreichte der getaperte Verstärker 140 kW. Beide Faserverstärker zeigen relativ geringe SRS Signale und kein nennenswertes Photodarkening. Die optimierte Strahlqualität der ungetaperten „rod-type“ Fasern liegt zwischen M^2=3.1 und 4.5 und ist sehr leistungsabhängig. Die M^2-Werte der getaperten „rod-type“ Faser liegen zwischen 1.3 und 1.7 und zeigen eine sehr viel besser Stabilität im Vergleich zur Freistrahlkopplung der ungetaperten Faser. Für eine vergleichbare mittlere Ausgangsleistung von circa 8 W verbessert sich die Strahlqualität von M^2=4 auf ungefähr 1.6, was einen nahezu beugungsbegrenzten Strahl darstellt. Für den getaperten Faserverstärker wurde eine Endkappe verwendet. Aufgrund der Endkappe konnte die Spitzenleistung auf 375 kW, nahezu beugungsbegrenzt und mit niedrigem SRS Signal, skaliert werden.

Für zukünftige Arbeiten werden folgenden Verbesserungen angestrebt: (1). Verbesserung der Strahlqualität durch Optimierung des Taperprozesses und durch die Verwendung von „Confined doping“ Fasern entsprechend den theoretischen Überlegungen aus Kapitel 8. (2). Um die Pulsdauer von Nanosekunden auf Pikosekunden zu verkürzen könnte eine Pikosekunden Seed-Laserquelle in Betracht gezogen werden, wodurch eine Hochskalierung der Spitzenleistung durch Erhöhung der Laser-induzierten Zerstörschwelle möglich wäre.

Schlussendlich können wir zusammenfassen, dass die neuartigen REPUSIL-basierten „rod-type“ Faserverstärker mit Brechungsindex-angepasstem inneren Cladding und lokalen adiabatischen Tapern erfolgreich demonstriert werden konnten. Die Spitzenleistung kann mit Hilfe von LMA-Fasern auf effiziente Weise durch Vergrößerung des Modenfelddurchmessers und die

damit verbundene Verringerung der Laserleistungsdichte hochskaliert werden. Kurze LMA-Fasern stellen eine effiziente Lösung zur Verringerung nichtlinearer Effekte, insbesondere SRS für Nanosekunden-gepulste Verstärker, dar. Im Vergleich zur Freistrahleinkopplung ermöglicht die Verwendung kurzer lokaler adiabatischer Taper eine stabile Seed-Lasereinkopplung für Faserverstärker bei gleichzeitiger Erhaltung der nahezu beugungsbegrenzten Strahlqualität mittels bevorzugter Anregung des Grundmodes in LMA-Stufenindex-Faserverstärkern. Die Diffusion der Dotanden während des Taperprozesses wurde erfolgreich unterdrückt, was zu einer guten Strahlqualität führte. Durch die Verwendung einer Endkappe an der ausgangsseitigen Endfläche der Faser konnte die Spitzenleistung auf 375 kW mit guter Strahlqualität hochskaliert werden.

B. References

[1] T. H. Maiman, “Stimulated Optical Radiation in Ruby,” Nature 187, No. 4736, 493-494 (1960).

[2] H. Injeyan, G. D. Goodno, High-Power Laser Handbook (New York, 2011).

[3] D. J. Richardson, J. Nilsson and W. A. Clarkson, " High power fiber lasers: current status and future perspectives [Invited]," J. Opt. Soc. Am. B 27, B63-B92 (2010).

[4] F. J. Duarte, Tunable Laser Applications (New York, 2009).

[5] C. Jauregui, J. Limpert and A. Tünnermann, "High-power fibre lasers," Nature Photonics 7, 861-7 (2013).

[6] G. P. Agrawal, Nonlinear Fiber Optics (New York, 2013).

[7] R. L. Farrow, D. A. V. Kliner, G. R. Hadley, and A. V. Smith, “Peak power limits on fiber amplifiers imposed by self-focusing,” Opt. Lett. 31, 3423-3425 (2006).

[8] R. M. Wood, Laser-Induced Damage of Optical Materials (2003).

[9] F. Stutzki, F. Jansen, H. J. Otto, C. Jauregui, J. Limpert and A. Tünnermann, "Designing advanced very-large-mode-area fibers for power scaling of fiber-laser systems," Optica 1, 233-242 (2014).

[10] Oleg G. Okhotnikov, fiber laser (2012).

[11] V. Sudesh, T. McComb, Y. Chen, M. Bass, M. Richardson, J. Ballato and A. E. Siegman, "Diode-pumped 200 μm diameter core, gain-guided, index-antiguided single mode fiber laser," Appl. Phys. B 90, 369-72 (2008).

[12] G. Canat, S. Jetschke, S. Unger, L. Lombard, P. Bourdon, J. Kirchhof, V. Jolivet, A. Dolfi and O. Vasseur, "Multifilament-core fibers for high energy pulse amplification at 1.5 μm with excellent beam quality," Optics Letters 33, 2701-3 (2008).

[13] F. Kong, K. Saitoh, D. McClane, T. Hawkins, P. Foy, G. Gu and L. Dong, "Mode area scaling with all-solid photonic bandgap fibers," Opt. Express 20, 26363-72 (2012).

[14] C. H. Liu, G. Chang, N. Litchinitser, A. Galvanauskas, D. Guertin, N. Jabobson and K. Tankala, "Effectively Single-Mode Chirally-Coupled Core Fiber," in Advanced Solid-State Photonics, OSA Technical Digest Series (CD) (Optical Society of America, 2007), paper ME2.

[15] F. D Teodoro. and C. D. Brooks, "Multistage Yb-doped fiber amplifier generating megawatt peak-power, subnanosecond pulses," OPTICS LETTERS 30, 3299-3301 (2005).

[16] C. Gaida, F. Stutzki, F. Jansen, H. J. Otto, T. Eidam, C. Jauregui, O. de. Vries, J. Limpert and A. Tünnermann, "Triple-clad large-pitch fibers for compact high-power pulsed fiber laser systems," Optics Letters 39, 209-11 (2014).

[17] J. P. Koplow, D. A. V. Kliner and L. Goldberg, "Single-mode operation of a coiled multimode fiber amplifier," Optics Letters 25, 442-444 (2000).

[18] R. T. Schermer, " Mode scalability in bent optical fibers," Optics Express 15, 15674-15701 (2007).

[19] A. Galvanauskas, M. C. Swan, and C. Liu, "Effectively Single-Mode Large Core Passive and Active Fibers with Chirally Coupled-Core Structures," in Conference on Lasers and Electro-Optics/Quantum Electronics and Laser Science Conference and Photonic Applications Systems Technologies, OSA Technical Digest (CD) (Optical Society of America, 2008), paper CMB1.

[20] L. Dong, X. Peng, and J. Li, "Leakage channel optical fibers with large effective area," J. Opt. Soc. Am. B 24, 1689-1697 (2007).

[21] C. D. Brooks and F. Di. Teodoro, "Multimegawatt peak-power, single-transverse-mode operation of a 100mμ m core diameter, Yb-doped rod like photonic crystal fiber amplifier," Applied Physics Letters 89, 111119 (2006).

[22] M. Baumgart, F. Jansen, F. Stutzki, C. Jauregui, B. Ortaç, J. Limpert and A. Tünnermann, "High average and peak power femtosecond large-pitch photonic-crystal-fiber laser," Optics Letters 36, 244-246 (2011).

[23] M. Y. Cheng, Y. C. Chang, A. Galvanauskas, "High-energy and high-peak-power nanosecond pulse generation with beam quality control in 200-mm core highly multimode Yb-doped fiber amplifiers," Optics Letters 30, 358 (2005).

[24] Konstantin K. Bobkov, Maxim Yu. Koptev, Andrei E. Levchenko, Svetlana S. Aleshkina, Sergey L. Semenov, Alexander N. Denisov, Mikhail M. Bubnov, Denis S. Lipatov, Alexander Yu. Laptev, Alexey N. Guryanov, Elena A. Anashkina, Sergey V. Muravyev, Alexey V. Andrianov, Arkady V. Kim, Mikhail E. Likhachev, "MW peak power diffraction limited monolithic Yb-doped tapered fiber amplifier," Proc. SPIE 10083, Fiber Lasers XIV: Technology and Systems, 1008309 (2017).

[25]. A. Langner, G. Schötz, M. Such, T. Kayser, V. Reichel, S. Grimm, J. Kirchhof, V. Kraused, G. Rehmann, "A new material for high power laser fibers," Fiber Lasers V: Technology, Systems, and Applications 6873, 687311 (2008).

[26] R. Dauliat, D. Gaponov, R. Jamier, K. Schuster, S. Grimm, S. Valette, A. Benoit, F. Salin, P. Roy, "Powder technology and innovative fiber design enabling a new generation of high-power single-mode-fiber laser sources," Advanced Laser Technologies (2012).

[27] M. Leich, F. Just, A. Langner, M. Such, G. Schoetz, T. Eschrich and S. Grimm, "Highly efficient Yb-doped silica fibers prepared by powder sinter technology," Optics Letters 36, 1557-9 (2011).

[28] A. Langner, M. Such, G. Schötz, F. Just, M. Leich, S. Grimm, J. Dellith, M. Jäger, K. Schuster, H. Zimer, M. Kozak, B. Wedel, G. Rehmann, C. Bachert, V. Krause, "Design evolution, long term performance and application tests of extra-large mode area (XLMA) fiber lasers", Proc. SPIE 8601, Fiber Lasers X: Technology, Systems, and Applications, 86010G (2013).

[29] W. B. He, M. Leich, S. Grimm, J. Kobelke, Y. Zhu, H. Bartelt and M. Jäger, "Very large mode area ytterbium fiber amplifier with aluminum-doped pump cladding made by powder sinter technology," Laser Physics Letters 12, 015103 (2015).

[30] R. J. Mears, L. Reekie, I. M. Jauncey, and D. N. Payne, "Low-noise erbium-doped fiber amplifier operating at 1.54 m," Electron. Lett 23, 1026-1028 (1987).

[31] Delevaque, E, Georges, T, Monerie, M, Lamouler, P, and Bayon, J.F, "Modeling of pair-induced quenching in erbium doped silicate fibers," IEEE Photonic Technol. Lett. 5, 73–75(1993).

[32] D. C. Hanna, R. M. Percival, I. R. Perry, R. G. Smart, P. J. Suni, and A. C. Tropper, "An ytterbium-doped mono-mode fiber laser: broadband tunable operation from 1.010 m to 1.162 m and three-level operation at 974 nm," J. Mod. Opt, vol. 37,517-525(1990).

[33] H. M. Pask, R. J. Carman, D. C. Hanna, A. C. Tropper, C. J. Mackechnie, P. R. Barber, and J. M. Dawes, "Ytterbium-doped silica fiber lasers: versatile sources for the 1–1.2 m region," IEEE J. Select. Topics Quantum Electron., vol. 1, pp. 2–13 (1995).

[34] R. Paschotta, J. Nilsson, A. C. Tropper and D. C. Hanna, "Ytterbium-doped fiber amplifiers," Quantum Electronics, IEEE Journal of Quantum Electronics 33, 1049-56 (1997).

[35] F. Auzel, "On the maximum splitting of the (2F7/2) ground state in Yb3+-doped solid state laser materials," J. Lumin. 93, 129-135 (2001).

[36] Michalis N. Zervas, "High power ytterbium-doped fiber lasers — fundamentals and applications," Int. J. Mod. Phys. B 28, 1442009 (2014).

[37] E. Zhou, B. Zhao, X. Wang, Y. Wang, W. Wei, B. Peng, "Analysis of one-end-pumped Yb3+-doped gain guided and index antiguided fiber laser," Appl. Phys. B 99, 747-751(2010).

[38] Yonggang Zhu , Kailiang Duan, Hongmin Shao, Baoyin Zhao, Entao Zhang, Wei Zhao, "Theoretical analysis of output performance of GG–IAG fiber laser by multipoint distributed side pump," Optics Communications 285, Issue 24, 5359–5363(2012).

[39] Cyril C. Renaud, H. L. Offerhaus, J. A. Alvarez-Chavez, J. Nilsson, W. A. Clarkson, P. W. Turner, D. J. Richardson and A. B. Grudinin, "Characteristics of Q-switched cladding-pumped

ytterbium-doped fiber lasers with different high-energy fiber designs," IEEE JOUNRNAL OF QUANTUM ELECTRONICS 37(2), 199-206(2001).

[40] D. N. Schimpf, C. Ruchert, D. Nodop, J. Limpert, A. Tünnermann, F. Salin, "Compensation of pulse-shaping due to saturation in fiber-amplifiers," Proc. SPIE 7195, Fiber Lasers VI: Technology, Systems, and Applications, 71951E (2009).

[41] Andrew Malinowski, Khu Tri Vu, Kang Kang Chen, Johan Nilsson, Yoonchan Jeong, Shaiful Alam, Dejiao Lin, and David J. Richardson, "High power pulsed fiber MOPA system incorporating electro-optic modulator based adaptive pulse shaping," Opt. Express 17, 20927-20937 (2009).

[42] Carl G. Chen, Paul T. Konkola, Juan Ferrera, Ralf K. Heilmann, and Mark L. Schattenburg, "Analyses of vector Gaussian beam propagation and the validity of paraxial and spherical approximations," J. Opt. Soc. Am. A 19, 404-412 (2002).

[43] Saleh, B.E.A. and M.C. Teich, Fundamentals of Photonics (2007).

[44] Tae Moon Jeong and Jongmin Lee, "Accurate Determination of the Beam Quality Factor of an Aberrated High-power Laser Pulse," Journal of the Korean Physical Society 55(2), 488494(2009).

[45] ISO Standard 11146, "Lasers and laser-related equipment – Test methods for laser beam widths, divergence angles and beam propagation ratios" (2005)

[46] A. E. Siegman, "How to (Maybe) Measure Laser Beam Quality," in DPSS (Diode Pumped Solid State) Lasers: Applications and Issues, M. Dowley, ed., Vol. 17 of OSA Trends in Optics and Photonics (Optical Society of America, 1998), paper MQ1.

[47] V. V. Raman and K. S. Krishnan, "A new type of secondary radiation", Nature 121, 501 (1928).

[48] Jay W. Dawson, Michael J. Messerly, Raymond J. Beach, Miroslav Y. Shverdin, Eddy A. Stappaerts, Arun K. Sridharan, Paul H. Pax, John E. Heebner, Craig W. Siders, and C.P.J. Barty, "Analysis of the scalability of diffraction-limited fiber lasers and amplifiers to high average power," Opt. Express 16, 13240-13266 (2008).

[49] R. H. Stolen, E. P. Ippen, and A. R. Tynes, "Raman oscillation in glass optical waveguide," Appl. Phys.Lett. 20, 62-64 (1972).

[50] V. R. Supradeepa, "Stimulated Brillouin scattering thresholds in optical fibers for lasers linewidth broadened with noise," Opt. Express 21, 4677-4687 (2013).

[51] G. C. Valley, "A review of stimulated Brillouin scattering excited with a broad-band pump laser", IEEE J. Quantum Electron. 22 (5), 704 (1986).

[52] D. E. Laban, W. C. Wallace, R. D. Glover, R. T. Sang, and D. Kielpinski, "Self-focusing in air with phase-stabilized few-cycle light pulses," Opt. Lett. 35, 1653-1655 (2010).

[53] Gadi Fibich and Alexander L. Gaeta, "Critical power for self-focusing in bulk media and in hollow waveguides," Opt. Lett. 25, 335-337 (2000).

[54] Arlee V. Smith, Binh T. Do, G. Ronald Hadley, and Roger L. Farrow, "Optical Damage Limits to Pulse Energy from Fibers," IEEE JOURNAL OF SELECTED TOPICS IN QUANTUM ELECTRONICS 15(1), 153-158 (2009).

[55] Arlee V. Smith and Binh T. Do, "Bulk and surface laser damage of silica by picosecond and nanosecond pulses at 1064 nm," Appl. Opt. 47, 4812-4832 (2008).

[56] B. C. Stuart, M. D. Feit, A. M. Rubenchik, B. W. Shore, and M. D. Perry, "Laser induced damage in dielectrics with nanosecond to sub-picosecond pulses," Phys. Rev. Lett. 74,2248–2251 (1995).

[57] Alexandre Wetter, Mathieu Faucher, Benoit Sévigny, Nelson Vachon, "High core and cladding isolation termination for high-power lasers and amplifiers," Proc. SPIE 7195, Fiber Lasers VI: Technology, Systems, and Applications, 719521 (2009).

[58] J. Limpert, S. Höfer, A. Liem, H. Zellmer, A. Tünnermann, S. Knoke, H. Voelckel, "100-W average-power, high-energy nanosecond fiber amplifier," Appl Phys B 75, 477(2002).

[59] Sebastian Keppler, Alexander Savert, Jorg Korner, Marco Hornung, Hartmut Liebetrau, Joachim Hein and Malte Christoph Kaluza, "The generation of amplified spontaneous emission in high-power CPA laser systems",Laser & Photonics Reviews 10 (2), 264 (2016).

[60] Martin Blazek, Sébastien Hartmann, Andreas Molitor, and Wolfgang Elsaesser, "Unifying intensity noise and second-order coherence properties of amplified spontaneous emission sources," Opt. Lett. 36, 3455-3457 (2011).

[61] J. J. Koponen, M. J. Söderlund, S. K. T. Tammela, H. Po, "Photodarkening in ytterbium-doped silica fibers," Proc. SPIE 5990, Optically Based Biological and Chemical Sensing, and Optically Based Materials for Defence, 599008 (2005).

[62] J. J. Koponen, M. J. Söderlund, H. J. Hoffman, and S. K. T. Tammela, "Measuring photodarkening from single-mode ytterbium doped silica fibers," Opt. Express 14, 11539-11544 (2006).

[63] J. Jasapara, M. Andrejco, D. DiGiovanni, and R. Windeler, "Effect of Heat and H2 Gas on the Photo-Darkening of Yb+3 Fibers," in Conference on Lasers and Electro-Optics/Quantum Electronics and Laser Science Conference and Photonic Applications Systems Technologies, Technical Digest (CD) (Optical Society of America, 2006), paper CTuQ5.

[64] I. Manek-Hönninger, J. Boullet, T. Cardinal, F. Guillen, S. Ermeneux, M. Podgorski, R. Bello Doua, and F. Salin, "Photodarkening and photobleaching of an ytterbium-doped silica double-clad LMA fiber," Opt. Express **15** (4), 1606–1611 (2007).

[65] Sylvia Jetschke, Sonja Unger, Anka Schwuchow, Martin Leich, and Johannes Kirchhof, "Efficient Yb laser fibers with low photodarkening by optimization of the core composition," Opt. Express **16**, 15540-15545 (2008)

[66] Sylvia Jetschke, Sonja Unger, Anka Schwuchow, Martin Leich, and Matthias Jäger, "Role of Ce in Yb/Al laser fibers: prevention of photodarkening and thermal effects," Opt. Express 24, 13009-13022 (2016).

[67] Y. Jeong, J. Sahu, D. Payne, and J. Nilsson, "Ytterbium-doped large-core fiber laser with 1.36 kW continuous-wave output power," Opt. Express 12, 6088-6092 (2004).

[68] D. Brown and H. J. Hoffman, "Thermal, Stress, and Thermo-Optic Effects in High Average Power Double-Clad Silica Fiber Lasers," IEEE J. Sel. Top. Quantum Electron. 2, 207-217 (2001).

[69] Marc-André Lapointe, Stephane Chatigny, Michel Piché, Michael Cain-Skaff, Jean-Noël Maran, "Thermal effects in high-power CW fiber lasers," Proc. SPIE 7195, Fiber Lasers VI: Technology, Systems, and Applications, 71951U (2009).

[70] J. W. Kim, D. Y. Shen, Jayanta K. Sahu, Member, IEEE, and W. Andrew Clarkson, "Fiber-Laser-Pumped Er:YAG Lasers," IEEE JOURNAL OF SELECTED TOPICS IN QUANTUM ELECTRONICS 15(2), 361-371(2009).

[71] H. M. Presby, D. Marcuse, and H. W. Astle, "Automatic refractive-index profiling of optical fibers," Appl. Opt. 17, 2209-2214 (1978).

[72] Verkouteren JR, Steel EB, Windsor ES, Phelps JM, "Accuracy of the Double Variation Technique of Refractive Index Measurement," Journal of Research of the National Institute of Standards and Technology 97(6), 693-705 (1992).

[73] U. H. Manyam, B. Samson, V. Khitrov, D. P. Machewirth, N. Jacobson, J. Farroni, D. Guertin, J. Abrmczyk, A. Carter, and K. Tankala, "Laser fibers designed for single polarization output," in Advanced Solid-State Photonics, OSA Technical Digest (Optical Society of America, 2004), paper MA6.

[74] A. E. Siegman, "Gain-guided, index-antiguided fiber lasers," J. Opt. Soc. Am. B 24, 1677-1682 (2007).

[75] Jens Limpert, Fabian Roser, Damian N. Schimpf, Enrico Seise, Tino Eidam, Steffen Hadrich, Jan Rothhardt, Cesar Jauregui Misas, and Andreas Tunnermann," High Repetition Rate Gigawatt Peak Power Fiber Laser Systems: Challenges, Design, and Experiment," IEEE JOURNAL OF SELECTED TOPICS IN QUANTUM ELECTRONICS 15(1),159-169 (2009).

[76] Jens Limpert, Fabian Stutzki, Florian Jansen, Hans-Jürgen Otto, Tino Eidam, Cesar Jauregui and Andreas Tünnermann, "Yb-doped large-pitch fibres: effective single-mode operation based on higher-order mode delocalization," Light: Science & Applications 1, e8 (2012).

[77] Fabian Stutzki, Florian Jansen, Tino Eidam, Alexander Steinmetz, Cesar Jauregui, Jens Limpert, and Andreas Tünnermann, "High average power large-pitch fiber amplifier with robust single-mode operation," Opt. Lett. 36, 689-691 (2011).

[78] Kunimasa Saitoh, Yukihiro Tsuchida, Lorenzo Rosa, Masanori Koshiba, Federica Poli, Annamaria Cucinotta, Stefano Selleri, Mrinmay Pal, Mukul Paul, Debashri Ghosh, and Shyamal Bhadra, "Design of all-solid leakage channel fibers with large mode area and low bending loss," Opt. Express 17, 4913-4919 (2009).

[79] P. Wang, L. J. Cooper, J. K. Sahu, and W. A. Clarkson, "Efficient single-mode operation of a cladding-pumped ytterbium-doped helical-core fiber laser," Opt. Lett. 31, 226-228 (2006).

[80] Ron Spittel, Adrian Lorenz, Sylvia Jetschke, Matthias Jäger, Hartmut Bartelt, " Equivalent step-index model of multifilament core fibers, " Proc. SPIE 8627, Integrated Optics: Devices, Materials, and Technologies XVII, 862714 (2013).

[81] Y. Huo, P. Cheo, and G. King, “Fundamental mode operation of a 19-core phase-locked Yb-doped fiber amplifier,” Opt. Express 12, 6230-6239 (2004).

[82] L. Li, A. Schülzgen, S. Chen, V. L. Temyanko, J. V. Moloney, and N. Peyghambarian, “Phase locking and in-phase supermode selection in monolithic multicore fiber lasers,” Opt. Lett. 31, 2577-2579 (2006).

[83] R. F. Cregan, B. J. Mangan, J. C. Knight, T. A. Birks, P. St. J. Russell, P. J.Roberts, and D. C. Allan, “Single-mode photonic band gap guidance of light in air,” Science 285, 1537 (1999).

[84] J. R. Marciante, “Gain Filtering for Single-Spatial-Mode Operation of Large- Mode-Area Fiber Amplifiers,” IEEE J. Sel. Topics in Quantum Electron. 15,30-36 (2009).

[85] J. A. Alvarez-Chavez, H. L. Offerhaus, J. Nilsson, P. W. Turner, W. A. Clarkson, and D. J. Richardson, "High-energy, high-power ytterbium-doped Q-switched fiber laser," Opt. Lett. 25, 37-39 (2000).

[86] Yongmin Jung, Yoonchan Jeong, Gilberto Brambilla, and David J. Richardson, "Adiabatically tapered splice for selective excitation of the fundamental mode in a multimode fiber," Opt. Lett. 34, 2369-2371 (2009).

[87] U. Griebner, R. Koch, H. Schönnagel, and R. Grunwald, “Efficient laser operation with nearly diffraction-limited output from a diode-pumped heavily Nd-doped multimode fiber,” Opt. Lett. 21, 266−268 (1996).

[88] S. Ramachandran, J. W. Nicholson, S. Ghalmi, M. F. Yan, P. Wisk, E. Monberg, and F. V. Dimarcello, “Light propagation with ultralarge modal areas in optical fibers,” Opt. Lett. 31, 1797-1799 (2006).

[89] S. Ramachandran, J.M. Fini, M. Mermelstein, J.W. Nicholson, S. Ghalmi, M.F. Yan, “Ultra-large effective-area, higher-order mode fibers: a new strategy for high-power lasers,” Laser & Photonics Reviews 2(6), 429-448(2008).

[90] J. A. Alvarez-Chavez, A. B. Grudinin, J. Nilsson, P. W. Turner and W. A. Clarkson, "Mode selection in high power cladding pumped fibre lasers with tapered section," Lasers and Electro-Optics,247-248(1999).

[91] Juho Kerttula, Valery Filippov, Vasily Ustimchik, Yuri Chamorovskiy, and Oleg G. Okhotnikov, "Mode evolution in long tapered fibers with high tapering ratio," Opt. Express 20, 25461-25470 (2012).

[92] Libo Yuan, Zhihai Liu, and Jun Yang, "Coupling characteristics between single-core fiber and multicore fiber," Opt. Lett. 31, 3237-3239 (2006).

[93] J. D. Love, W. M. Henry, W. J. Stewart, R. J. Black, S. Lacroix, F. Gonthier," Tapered single-mode fibres and devices", IEE PROCEEDINGS-J 138, 343-354 (1991).

[94] M. Sumetsky, "Theory of Adiabatic Optical Fiber and Microfiber Tapers," in Optical Fiber Communication Conference and Exposition and The National Fiber Optic Engineers Conference, Technical Digest (CD) (Optical Society of America, 2006), paper OTuH2.

[95] Tajamal Bhutta, Jacob I. Mackenzie, David P. Shepherd, and Raymond J. Beach, "Spatial dopant profiles for transverse-mode selection in multimode waveguides," J. Opt. Soc. Am. B 19, 1539-1543 (2002).

[96] Mali Gong, Suying Liao, Yanyang Yuan and Haitao Zhang, “High-order modes suppression in large-mode-area fiber amplifiers and lasers by controlling the mode power allocations,” Journal of Optics A: Pure and Applied Optics 11(1), 015701(2009).

[97] Mircea Hotoleanu, Miko Söderlund, Dahv Kliner, Jeffrey Koplow, Simo Tammela, Valery Philipov, “High-order modes suppression in large mode area active fibers by controlling the radial distribution of the rare earth dopant,”. Proc. SPIE 6102, Fiber Lasers III: Technology, Systems, and Applications, 61021T (2006).

[98] Teemu Kokki ; Joona Koponen ; Marko Laurila and Changgeng Ye, "Fiber amplifier utilizing an Yb-doped large-mode-area fiber with confined doping and tailored refractive index profile", Proc. SPIE 7580, Fiber Lasers VII: Technology, Systems, and Applications, 758016(2010).

[99] Mali Gong, Yanyang Yuan, Chen Li, Ping Yan, Haitao Zhang, and Suying Liao, "Numerical modeling of transverse mode competition in strongly pumped multimode fiber lasers and amplifiers," Opt. Express 15,3236-3246(2007).

[100] John R. Marciante, Richard G. Roides, Vladimir V. Shkunov, and David A. Rockwell, "Near-diffraction-limited operation of step-index large-mode-area fiber lasers via gain filtering," Opt. Lett. 35, 1828-1830 (2010).

[101] C. Ye, J. Koponen, T. Kokki, J. Montiel i Ponsoda, A. Tervonen and S. Honkanen, "Near-diffraction-limited output from confined-doped ytterbium fibre with 41 μm core diameter," in Electronics Letters 47(14), 819-821(2011).

[102] S.R. Nagel, J.B. Mac.Chesney, K.L. Walker, "An overview of the modified chemical vapor deposition (MCVD) process and performance," IEEE Transactions on Microwave Theory and Techniques, 30(4), 305-322(1982).

[103] Anirban Dhar, Mukul Ch. Paul, Mrinmay Pal, Ashok Kr. Mondal, Suchitra Sen, Himadri Sekhar Maiti, and Ranjan Sen, "Characterization of porous core layer for controlling rare earth incorporation in optical fiber," Opt. Express 14, 9006-9015 (2006).

[104] Schuster, K, Unger, S, Aichele, C, et al. "Material and technology trends in fiber optics," Advanced Optical Technologies 3(4), 447-468 (2014).

[105] S. Unger, A. Schwuchow, S. Jetschke, V. Reichel, A. Scheffel, J. Kirchhof, "Optical properties of Yb-doped laser fibers in dependence on codopants and preparation conditions," Proc. SPIE 6890, Optical Components and Materials V, 689016 (2008).

[106] Pochi Yeh, Amnon Yariv and Emanuel Marom, "Theory of Bragg fiber," J. Opt. Soc. Am. 68, 1196-1201 (1978).

[107] A.W. Snyder, J.D. Love, Optical waveguide theory (London, New York, 1983).

[108] KATSUNARI OKAMOTO, Fundamentals of optical waveguides (2000).

[109] Shahraam Afshar V. and Tanya M. Monro, "A full vectorial model for pulse propagation in emerging waveguides with subwavelength structures part I: Kerr nonlinearity," Opt. Express 17, 2298-2318(2009).

[110] T.A. Birks, Y.W. Li, "The shape of fiber tapers, " Journal of Lightwave Technology 10, Issue4(1992).

[111] S.W. Harun, K.S. Lim, C.K. Tio, K. Dimyati, H. Ahmad, "Theoretical analysis and fabrication of tapered fiber," Optik - International Journal for Light and Electron Optics 124, Issue 6, 538–543(2013).

[112] A. E. Siegman, "Propagating modes in gain-guided optical fibers," J. Opt. Soc. Am. A 20, 1617-1628 (2003).

[113] D. Marcuse, "Loss analysis of single-mode fiber splices," Bell Syst. Tech. J. 56, 703 (1977).

[114] Alexandre Wetter, Mathieu Faucher, Benoit Sévigny, Nelson Vachon, “High core and cladding isolation termination for high-power lasers and amplifiers,” Proc. SPIE 7195, Fiber Lasers VI: Technology, Systems, and Applications, 719521 (2009).

[115] J. Limpert, S. Höfer, A. Liem, H. Zellmer, A. Tünnermann, S. Knoke, H. Voelckel, “100-W average-power, high-energy nanosecond fiber amplifier,” Appl Phys B 75, 477(2002).

C. Abbreviations

YDFA: Yb^{3+}-doped fiber amplifier

MOPA: Master Oscillator Power Amplifier

SRS: Stimulated Raman Scattering

SBS: Stimulated Brillouin Scattering

FM: fundamental mode

HOMs: higher order modes

LMA: large mode area

MFD: mode field diameter

NA: numerical aperture

PCF: photonic crystal fiber

CCC: Chirally coupled core fiber

REPUSIL: reactive powder sinter technology

CW: continue wave

MW: megawatt

ASE: amplified spontaneous emission

BPP: beam parameter product

PD: Photodarkening

MCVD: Modified Chemical Vapor Deposition

ns: nanosecond

ps: picosecond

D. Acknowledgement

This dissertation is on the basis of the work in Leibniz Institute of Photonic Technology (IPHT) Jena, in the group of Active Fiber Modules of Fiber Optics (FAG2.2). I would like to show my grate respect to all my dear colleagues who offers me such nice working environment and much kindness help.

First of all, I would like to thank Prof. Dr. Hartmut Bartelt, who gives me this opportunity to pursue my PhD work in the group of Fiber Optics in IPHT and at Friedrich Schiller University Jena. I emphasize my thankful for the great effort from Prof. Dr. Hartmut Bartelt who paid large amount of time in supervising me and discussing with me for all the problems I had met during my PHD study period.

I also want to present my sincere acknowledgement to Dr. Jaeger Matthias who provides me the resources of research work and gives many pertinent comments on my work.

I would also like to give my special thanks to Tina Eschrich, Martin Leich and Martin Lorenz for their devotion in discussion during my research process and provide me many useful suggestion and help when I experience difficulties and problems. It was pleasant for me to have intense discussions with them and to learn from them. Moreover, I would like to thank Tina Eschrich and Martin Lorenz again for preparation and passive characterization of fibers and tapers

I am also grateful to my colleague Ron Fatobene for his help in building up my simulation models. Ron Fatobene gives me lots of help and suggestion for my PHD study, especially in the beginning of my PHD study.

I would like to appreciate the help of my dear colleagues. My sincere thanks also go to Wenbin He for the assistance during my experiment work at the beginning, Matthias Arnz for polishing of fibers, Tobias Tiess for introducing me to use the various devices and components in the lab, the fiber technology group (i.e. Kay Schuster, Jens Kobelke, Claudia Aichele, et al) for production of rod fibers.

I would also like to thank all researchers in IPHT and Friedrich Schiller University Jena who have given me help for my research work during my PHD study period.

At last, I would like to thank my dear husband, my parents and my little baby for the help and support. Their love gives me security, their support and understand gives me great consolation.

E. Curriculum vitae

Personal information:

Name:	Yuan Zhu	Gender:	Female
Nationality：	P.R. China	Date of Birth:	07.04.1986
Location of birth:	Shanxi, China	E - mail：	zhuyuan37@live.cn
Phone：	015123046194		
Address:	Boegeholdstraße 7, 07745, Jena, Deutschland		

Education:

(1) Bachelor study in Sun Yat-Sen University (Guangzhou, China)

- Major: Optical Information Science and Technology
- Period of study: 09.2005 – 08.2009
- Bachelor degree achieved on 25 JUNE 2009

(2) Master study in Sun Yat-Sen University (Guangzhou, China)

- Major: Optics
- Period of study: 09.2009 – 08.2012
- Master Science degree achieved on 25 JUNE 2012
- Thesis: Simulation of three-dimensional growth of micro-structured Copper Sculpture Film by Monte-Carlo Method

(3) PHD Study in Friedrich-Schiller-University Jena

- Faculty: Faculty of Physics and Astronomy / Leibniz Institute of Photonic Technology (IPHT) Jena
- Research area: Fiber optics
- Period of study: 10.2012 – now
- Thesis: Laser peak power scaling and beam quality improvement with Ytterbium rod-type fiber amplifiers made by Powder Sinter Technology

Location, Date Signature

F. Ehrenwörtliche Erklärung

Ich erkläre hiermit ehrenwörtlich, dass ich die vorliegende Arbeit selbständig, ohne unzulässige Hilfe Dritter und ohne Benutzung anderer als der angegebenen Hilfsmittel und Literatur angefertigt habe. Die aus anderen Quellen direkt oder indirekt übernommenen Daten und Konzepte sind unter Angabe der Quelle gekennzeichnet.

Bei der Auswahl und Auswertung folgenden Materials haben mir die nachstehend aufgeführten Personen in der jeweils beschriebenen Weise entgeltlich/unentgeltlich geholfen:

1. Arbeitsgruppe Optische Fasertechnologien des IPHT Jena (Jens Kobelke, Claudia Aichele…) : Herstellung der Laserspezialfasern

2. Tina Eschrich und Martin Lorenz (IPHT Jena): Herstellung und passive Charakterisierung von Fasertapern

3. Matthias Arnz: Polieren der Faserendflächen

Weitere Personen waren an der inhaltlich-materiellen Erstellung der vorliegenden Arbeit nicht beteiligt. Insbesondere habe ich hierfür nicht die entgeltliche Hilfe von Vermittlungs- bzw. Beratungsdiensten (Promotionsberater oder andere Personen) in Anspruch genommen.

Niemand hat von mir unmittelbar oder mittelbar geldwerte Leistungen für Arbeiten erhalten, die im Zusammenhang mit dem Inhalt der vorgelegten Dissertation stehen.

Die Arbeit wurde bisher weder im In- noch im Ausland in gleicher oder ähnlicher Form einer anderen Prüfungsbehörde vorgelegt.

Die geltende Promotionsordnung der Physikalisch-Astronomischen Fakultät ist mir bekannt.

Ich versichere ehrenwörtlich, dass ich nach bestem Wissen die reine Wahrheit gesagt und nichts verschwiegen habe.

Ort, Datum Unterschrift d. Verfassers